UCLA
UCLA Electronic Theses and Dissertations

Title

Extending the Limits of Hydrodynamics to Dense Plasmas and High Mach Number Cavitation in Compressible Fluids

Permalink

https://escholarship.org/uc/item/63n7z0vd

Author

Krimans, Daniels

Publication Date

2024

Peer reviewed|Thesis/dissertation

eScholarship.org Powered by the California Digital Library
University of California

UNIVERSITY OF CALIFORNIA

Los Angeles

Extending the Limits of Hydrodynamics to Dense Plasmas and High Mach Number Cavitation in Compressible Fluids

A dissertation submitted in partial satisfaction
of the requirements for the degree
Doctor of Philosophy in Physics

by

Daniels Krimans

2024

© Copyright by
Daniels Krimans
2024

ABSTRACT OF THE DISSERTATION

Extending the Limits of Hydrodynamics to Dense Plasmas and High Mach Number Cavitation in Compressible Fluids

by

Daniels Krimans
Doctor of Philosophy in Physics
University of California, Los Angeles, 2024
Professor Seth J. Putterman, Chair

In this dissertation, I investigate the limits of the hydrodynamic approach to many-body systems. Due to the impracticality of solving equations of motion for individual particles, hydrodynamics provides an effective description, reducing complex systems to a few macroscopic variables, such as density, entropy, and velocity. However, the validity of hydrodynamic equations has to be carefully assessed when applied to small length scales comparable to the average interparticle distance. I explore this limitation by analyzing systems under extreme physical conditions in two scenarios.

First, I study strongly coupled plasmas, where traditional hydrodynamic methods fail. In such plasmas, the electrostatic interaction is sufficiently strong to influence their equilibrium and out-of-equilibrium behavior. I use a variational approach to derive generalized hydrodynamic equations from first principles, where the effects of strong coupling are included using nonlocal terms. The obtained results are compared in the linear regime to numerical experiments, showing excellent agreement for a wide range of coupling strengths. This suggests exploring the developed framework for nonlinear problems and other long-range systems in the future.

Second, I examine extreme bubble collapse when the bubble is surrounded by a compressible fluid. The goal is to evaluate the response of the compressible fluid when its motion

reaches high Mach numbers. This is challenging to describe with existing numerical methods due to the presence of large gradients within the fluid. I implement a uniform density and pressure approximation inside the bubble, which allows for quick and accurate computations that include the effects of compressibility of the surrounding fluid. To check the accuracy of the created solver, I derive an asymptotic analytic benchmark for late stages of the collapse. This key limit was achieved in the simulations. The obtained results in the future can be coupled with molecular dynamics for the gas inside the cavity to estimate the possibility of thermal fusion in such collapses.

The dissertation of Daniels Krimans is approved.

Stuart Brown

Troy A. Carter

Gary A. Williams

Seth J. Putterman, Committee Chair

University of California, Los Angeles

2024

"The sciences do not try to explain, they hardly even try to interpret, they mainly make models. By a model is meant a mathematical construct which, with the addition of certain verbal interpretations, describes observed phenomena. The justification of such a mathematical construct is solely and precisely that it is expected to work."

- John von Neumann

Table of Contents

List of Figures

Acknowledgments

I am deeply grateful to my advisor, Seth Putterman, who has been an invaluable mentor throughout my journey. He taught me so much in physics, mathematics, and many aspects of science and life in general. I thank him for inspiring me and giving me interesting research projects, where he encouraged me to explore my own ideas, making me feel like a colleague rather than a student. He always found time to support me when I was confused or discouraged, and showed genuine concern for my well-being. I will always cherish our walks around campus, coffee hangouts, and our engaging discussions.

I also want to thank my collaborators: Steven Ruuth from Simon Fraser University and the group at Michigan State University consisting of Michael Murillo, Zachary Johnson, Luciano Silvestri, Thomas Chuna. Their shared knowledge and valuable insights made our collaborations fruitful. I am thankful for their friendly attitude and feeling welcome to express my opinions in our discussions.

To the UCLA Acoustics and Low Temperature Group consisting of Gary Williams, Rhyan Ghosh, Yotam Ofek, Alex Stensen, and others, I owe many stimulating physics discussions.

My gratitude goes to the people and friends I met during graduate school for their support and for the memories we shared.

I want to express my deepest appreciation to my family and friends, especially my best friend and wife, Alise, for their unconditional love and support throughout my graduate school journey. Their encouragement made the challenges easier to overcome and added joy to the experience. Thanks to them, I was able to maintain focus while also exploring life beyond graduate school, leading to countless amazing new experiences and personal growth.

Several parts of this dissertation are based on published papers co-authored by my advisor, Seth Putterman, who is also the Principal Investigator for the awards funding this line of study. Chapter 2 is a modified version of a published paper and is reproduced from D. Krimans and S. Putterman, "Variational principles for the hydrodynamics of the clas-

sical one-component plasma," Phys. Fluids **36**, 037131 (2024), https://doi.org/10.1063/5.0194352, with the permission of AIP Publishing. Section 3.2 is reproduced from D. Krimans and S. Putterman, "Power law singularity for cavity collapse in a compressible Euler fluid with Tait–Murnaghan equation of state," Phys. Fluids **35**, 086114 (2023), https://doi.org/10.1063/5.0160469, with the permission of AIP Publishing. I thank Zoltan Donkó and Ihor Korolov for the provided numerical data from the molecular dynamics simulations, discussed in Chapter 2.

The work discussed in Chapter 2 has been funded by the AFOSR (No. FA9550-21-1-0295), while the research discussed in Chapter 3 has been funded by AFOSR (No. FA9550-22-1-0425) and DoD (No. HQ0034-20-1-0034). The views, opinions, and/or findings expressed are those of the authors and should not be interpreted as representing the official views or policies of the Department of Defense or the U.S. Government.

Curriculum Vitae

2015 – 2018	B.S. in Physics, University of Latvia.
2018 – Present	Ph.D. student in Physics, University of California, Los Angeles (UCLA).

Publications

[1] D. Krimans and S. Putterman, "Variational principles for the hydrodynamics of the classical one-component plasma," Physics of Fluids **36**, 037131 (2024).

[2] D. Krimans and S. Putterman, "Power law singularity for cavity collapse in a compressible Euler fluid with Tait–Murnaghan equation of state," Physics of Fluids **35**, 086114 (2023).

CHAPTER 1

Introduction and summary

In this dissertation, I explore a theoretical problem of formulating and understanding the limits of a physics theory. To approach such a general issue, I concentrate my attention on many-body systems consisting of a large number of particles, which are interesting because the naive approach of solving equations of motion for each of the individual particles forming the system is not practically feasible. Because of this difficulty, the question of deriving and understanding an appropriate theory arises. To avoid the issue of considering each of the many particles individually, one of the widely used approaches is to create an effective description using hydrodynamics, where the full description of a many-body system is given in terms of just a few smooth macroscopic variables, such as density, entropy, and velocity [1]. Such an approach has been explored using, for example, Euler, Navier-Stokes, elasticity and two-fluid plasma equations [1, 2, 3, 4], and has been demonstrated to be successful for problems in gases, liquids, solids, and also plasmas, where particles interact using long-range forces. Indeed, this approach allows the investigation of linear problems, such as the propagation of longitudinal and transverse waves, but also more complicated nonlinear problems, such as rapid bubble collapse in liquids. The goal of this dissertation is to explore hydrodynamic approaches and their limits when applied to problems with extreme physical conditions.

When discussing the limits of hydrodynamic equations, it is claimed that such an averaged macroscopic description can be valid only when the length scales in the problem are much greater than the average distance between the particles forming the system [1, 2]. For example, in the case of low amplitude wave propagation, the characteristic length scale for changes in hydrodynamic variables is the wavelength of a wave. In nonlinear problems,

the mentioned criterion is particularly important, as large gradients for the hydrodynamic profiles might develop, in which case the macroscopic properties change over a small length scale. An extreme case of that is a shock wave, having a boundary across which the hydrodynamic functions are discontinuous [1]. In such cases, the predictions based on hydrodynamics must be carefully assessed. I am interested in understanding to which extent hydrodynamic methods can be accurate in the limit where the length scales in the problem are small, and to understand whether it is possible to improve and extend them beyond this limit.

An interesting aspect to note is that typically hydrodynamic equations are written in terms of local differential equations. So, even if the particles forming the system interact using long-range forces, such as charged particles in a plasma, the hydrodynamic equations describing their interaction are written for macroscopic, averaged electric and magnetic fields, which reduces the problem to local equations. Therefore, not much is explored and understood in using nonlocal differential equations to describe hydrodynamic motion. This opens up an alternative pathway to extend the hydrodynamic description beyond the previously mentioned limitations.

In this dissertation, I analyze two problems where extreme physical conditions can be attained, and the validity of hydrodynamic approaches can be probed. The first of these is a description of a strongly coupled one-component plasma, which is discussed in detail in Chapter 2. Such a plasma is relevant in astrophysical applications but has recently been created and described in a laboratory setting. In a strongly coupled plasma, the electrostatic interaction between the charged particles is so strong that it significantly influences its thermodynamic and out-of-equilibrium properties, leading to the plasma exhibiting solid-like behavior. This happens because the plasma has a sufficiently high density, which forces particles to be closer to each other and experience stronger interaction, while the temperature is sufficiently low, which decreases the random thermal motion of particles, making it more difficult for them to escape the interaction. In such a system, it is claimed that the hydrodynamic description in the manner of Navier-Stokes is not valid at any coupling strength [5]. In my work, I argue that the hydrodynamic methods can be very successful

in explaining the properties of a strongly coupled plasma, even at small length scales. The issue is that the correct equations are not Navier-Stokes equations but rather they have to be extended. To do so, I derived from first principles a set of generalized hydrodynamic equations, which include the effects of strong coupling. Such equations were formulated with the help of nonlocal terms, which are commonly omitted in hydrodynamic descriptions. These nonlocal terms were key to accurately capture the effects of long-range electrostatic interaction in the regime of strong coupling. The success of the derived hydrodynamic equations was shown by computing longitudinal and transverse dispersion laws, where the agreement with the molecular dynamics data is excellent even up to wavelengths of the same order of magnitude as the average interparticle distance, showing that for a strongly coupled plasma the common view on the limits of validity of the hydrodynamic approach does not apply.

In particular, I discuss:

- how to formulate a variational principle for hydrodynamic motion, including nonlocal terms that represent long-range interaction,
- how to derive equations of motion, momentum and energy conservation laws for actions that include nonlocal terms,
- how to ensure the consistency of nonlocal variational principles with the thermodynamics of strong coupling by using the derived energy conservation law,
- what the difficulties are in uniquely specifying the nonlocal action for the out-of-equilibrium motion of a strongly coupled plasma and what the key additional assumptions are needed to obtain the correct hydrodynamic equations,
- how to derive longitudinal and transverse dispersion laws when nonlocal terms are included,
- that the obtained dispersion laws agree excellently with the data available from molecular dynamics simulations, even when the wavelength is comparable to the average interparticle distance.

The agreement of the developed general theoretical framework with numerical experiments suggests considering more complicated problems in strongly coupled plasmas, which are experimentally relevant but where numerical data are not yet available, such as the motion of vortices, adiabatic expansion, and shock waves. Additionally, it also motivates applying the nonlocal hydrodynamic approach to other long-range systems, such as Yukawa fluids, two-component plasmas, and fluids consisting of electric and magnetic dipoles.

The second problem analyzed in this dissertation is the extreme bubble collapse in compressible fluids, which is discussed in detail in Chapter 3. Experimentally, during a single collapse, the bubble's radius can decrease by a factor of a hundred [6], and so the pressure, number density, and temperature for the gas in the bubble can increase by many orders of magnitude. In fact, the temperature achieved could be so high as to allow for thermal fusion [7]. Due to the extreme conditions and the large gradients developed in the hydrodynamic profiles at late stages of such rapid collapses, it is not clear to what degree the hydrodynamic equations can describe them. Therefore, the goal is to explore the results obtained from hydrodynamics and compare them to the experimental data. Even though the bubble starts from rest, by the end of the collapse, it achieves a velocity larger than the ambient speed of sound of the outside fluid, showing the necessity of including the effects of compressibility. To do so, local Euler equations are used together with the Tait-Murnaghan equation of state [2]. Nevertheless, due to the multiple length and time scales involved in the collapse, even the numerical solvers that were recently developed just for this problem are not able to accurately compute the rapid collapses with the parameters found in experiments. To resolve this issue, I implemented an approximation where the pressure and density inside the bubble are assumed to be uniform. Such a simplification is unable to capture all the complicated phenomena for the gas in the bubble, such as shock wave formation, but it allows, for the first time, the exploration of the effects of compressibility for the experimentally relevant parameters. Additionally, I extended an asymptotic analytic result for the late stages of collapse, which was previously discussed in the context of water, to a wide range of liquids. In the rapid collapses investigated numerically, such an asymptotic result was indeed

achieved, showing both the accuracy of our approach and the possibility of attaining such an asymptotic regime in real experiments.

In particular, I discuss:

- the issues with currently available numerical solvers for the problem of bubble collapse, which show limitations for sufficiently strong collapses and cannot be used to address the problem within the available computational resources,
- how to numerically implement the uniform bubble approximation for the gas in the cavity, allowing for quick and accurate computation of the problem,
- how to perform analytic computations for the asymptotic behavior of the outside fluid during the late stages of the collapse, which creates a benchmark to test the numerical solvers,
- the obtained solution of the problem with relevant experimental parameters for water and liquid lithium, where the collapse was shown to achieve the predicted asymptotic behavior.

The obtained numerical results, with their excellent numerical convergence properties and agreement with the asymptotic behavior, motivate coupling them to molecular dynamics simulations for the gas in the bubble [8, 9, 10]. In that case, it should be possible to observe the effects of compressibility of the outside fluid on the motion within the gas. This would allow to predict the optimal combination of the gas inside the cavity and the outside fluid for achieving thermal fusion, which could then be suggested for experimental investigation. Such experimental data would then determine whether the predictions based on hydrodynamic models are appropriate in such extreme scenarios.

CHAPTER 2

Variational principles for the hydrodynamics of the classical one-component plasma

This chapter is a modified version of a published paper and is reproduced from D. Krimans and S. Putterman, "Variational principles for the hydrodynamics of the classical one-component plasma," Phys. Fluids **36**, 037131 (2024), with the permission of AIP Publishing.

2.1 Introduction

We are interested in formulating and analyzing variational approaches to obtain hydrodynamic equations for classical systems with long-range interactions and considerable coupling strength. In our analysis, the variational principles should be understood in the sense of the mechanical least action principle, as discussed in classical mechanics [11] and classical field theory [12], where such an approach is very successful. This can be contrasted with variational approaches that focus on obtaining thermodynamic properties of a system, for example, by minimizing the Helmholtz free energy [13]. One of the simplest and best-known examples of a system with long-range interactions and strong coupling effects is the one-component plasma (OCP), which we utilize as a basis for our analysis. It consists of two types of charged particles, with all particles interacting pairwise via the Coulomb potential $\phi(r) = q_1 q_2 / 4\pi\varepsilon_0 r$, where q_1 and q_2 represent the charges of any two particles, and r denotes the distance between them. However, in this plasma, only one component moves, while the other forms a stationary neutralizing background.

The OCP is important for understanding white dwarfs in astrophysics [14, 15]. The linear

regime can be probed using scattering experiments on molten salts [16, 17], as molten salts are believed to be strongly coupled plasmas [18]. Nonlinear effects can be experimentally tested using plasma expansion during laser breakdowns [19], expansion of ultracold neutral plasma [20], and by considering photoelectron sources, where the emitted electrons are strongly coupled immediately after emission [21]. Additionally, the OCP can be thought of as a limit of more complicated Yukawa fluids, where particles interact using Yukawa potential. Such Yukawa fluids can be experimentally realized as dusty plasmas [22]. Therefore, insights from the variational hydrodynamics of the OCP might be used to understand variational principles for Yukawa fluids.

The OCP has been numerically investigated in thermal equilibrium [23, 24]. Due to the long-range interaction, in addition to the ideal gas terms, there are nonlocal contributions to the energy and pressure that depend not only on the interaction potential but also on the pair distribution function $g(r)$, which gives the probability of two particles being distance r apart. For the OCP, thermodynamic properties depend on the coupling parameter, which is the ratio of the average potential energy due to the Coulomb interaction and the thermal energy due to temperature T. It is given for the moving particles as $\Gamma = q^2/4\pi\varepsilon_0 a k_B T$, where q is the charge of the moving particles, and a is the average distance between moving particles. This average distance can be estimated using the number density n as $4\pi a^3/3 = 1/n$. We will be especially interested in cases where the coupling between particles is significant, and thus, $\Gamma \geq 1$. From numerical experiments, the pair distribution function [25] and nonlocal contributions to energy and pressure [26, 27] are known as functions of Γ. These results are used in our variational approach to ensure that the conserved energy of our theory correctly matches the known result in thermal equilibrium, ensuring the consistency of our calculations with thermodynamics. Additionally, numerical experiments have shown that the OCP experiences a phase transition at around $\Gamma = 172$ between the fluid and body-centered cubic crystalline phases [28]. As we are specifically interested in the fluid phase, we will only examine the region with $\Gamma < 172$.

Using numerical simulations, one can investigate the linear behavior of the OCP close to

equilibrium by computing dispersion curves [29, 30]. For example, one can find that there is an onset of negative dispersion for longitudinal waves after reaching some critical value of Γ [31], and propagating transverse waves are observed at sufficiently short wavelength [32]. The extensive available data on the dispersion curves provide a perfect opportunity to test our general theoretical framework.

To theoretically analyze dispersion curves, one can, for example, use the generalized Langevin equation with memory functions [33] or the quasilocalized charge approximation (QLCA) [34, 35]. Both of these approaches yield excellent results compared to numerical simulations [31, 36]. However, they rely on the approximation of strong coupling, $\Gamma \gg 1$, and are not able to produce predictions for nonlinear effects. Moreover, QLCA does not include thermodynamic effects that would result in the usual speed of sound term at weak coupling [35]. While it is possible to add such a term phenomenologically [37, 38], we believe it lacks rigorous justification. In contrast, our variational approach is consistent with thermodynamics, capable of predicting nonlinear effects, and does not rely on the assumption of a very strong coupling.

Additionally, it is possible to use molecular dynamics simulations to numerically analyze the nonlinear effects of the OCP on short time scales [39, 40]. However, to an even greater extent than in the case of linear behavior, accurate numerical simulations of nonlinear problems require vast computational resources, especially for large systems and long observation times. In comparison, hydrodynamic equations are independent of the number of particles in the plasma, and the equations are usually quickly solved numerically. This is evident for some nonlinear problems, such as the expansion of the ultracold neutral plasma [20]. Other examples of nonlinear phenomena that interest us are solid body rotation, vortex motion, and shock waves. Finally, working in terms of a few macroscopic hydrodynamic variables provides a clearer physical picture. The goal of the proposed variational approach is to generate equations for reversible hydrodynamics analogous to Euler equations, which would generalize the equilibrium state of the OCP to motion that depends on both space and time.

Both the linear and nonlinear dynamics of the OCP can be analyzed using the frame-

work of kinetic theory and generalized hydrodynamics [41, 42, 43]. Such an approach has the advantage of including effects of heat transfer, viscosity, and relaxation. However, the challenge is to find an appropriate closure to the hierarchy of equations that would make them simple enough for computations and, at the same time, consistent with thermodynamics. In the development of our variational approach, our closure assumption is that a general description of the OCP can be expressed in terms of a few macroscopic hydrodynamic variables. Then, the variational principle guarantees that the equations are closed and have the conservation laws and symmetries built-in. We hope that such an alternative would, in some cases, provide simpler and more practical results. Even though our approach does not include heat transfer, viscosity, or relaxation, one can later introduce these effects, as in the case of Navier-Stokes equations [1], generalized hydrodynamics [44, 43], or by considering linear in velocity drag force between moving particles and the stationary background, as in the case of two-fluid plasma equations [4].

The range of validity of hydrodynamic equations, such as the Euler and Navier-Stokes equations, is generally determined by the transport processes, which are characterized by the mean free path of the collisions of the particles forming the system [1]. Motions on a shorter length scale fall outside the regime of classical hydrodynamics' validity. In the case of the strongly coupled OCP, we propose that the range of validity for the continuum equations is even greater than that for classical fluids. In particular, we conjecture that the stresses introduced by strong coupling lead to hydrodynamic equations at the level of description of the Euler equations that are valid even when the length scale for the motion under consideration is smaller than a. This is confirmed by comparing our obtained results to molecular dynamics simulations and will be determined in the future through experiments testing our theory.

In hydrodynamics, there are two ways of describing the fluid: the Eulerian approach, where the hydrodynamic quantities depend on the position in the laboratory frame, and the Lagrangian approach, where the hydrodynamic quantities depend on reference positions in some reference state. For example, the reference positions can be initial or equilibrium

positions of particles forming the fluid. It is known that Euler equations of hydrodynamics, which are successful in explaining many hydrodynamic phenomena, can be obtained from variational principles in both Eulerian and Lagrangian approaches [45, 46, 47, 48], but we are not aware of generalizations to the case of systems with nonlocal interaction, where the effects of strong coupling are included. In our work, we present variational principles for the classical OCP for both Eulerian and Lagrangian approaches. Although they only differ by a choice of coordinates, different assumptions about the out-of-equilibrium behavior of the pair distribution function are more natural in each of them. This leads to different equations of motion with different properties. This will be shown to be crucial in understanding the hydrodynamics of strongly coupled systems. For example, assuming that the out-of-equilibrium behavior of the pair distribution function depends on reference positions rather than on laboratory positions is what permits the propagation of small amplitude transverse waves, as observed in numerical simulations.

We start by postulating a nonlocal Lagrangian field density from which we derive well-defined equations of motion and conservation laws for energy and momentum. The chosen complete set of variables for the variational principle is exactly the same as in the case of Euler equations. In the Eulerian approach, it is given by number density n, velocity $\vec{v}$, and specific entropy s, while in the Lagrangian approach, it is given by the displacement field $\vec{x}$. To analyze the obtained equations of motion, the expression for the conserved energy is evaluated at equilibrium and then matched to the results of thermal equilibrium, making our variational principles consistent with thermodynamics.

Three distinct variational principles are analyzed, differing in the assumed behavior of the pair distribution function, g, out of equilibrium. In the Eulerian action, we assume $g(n, s, |\vec{x} - \vec{x}'|)$, where $\vec{x}, \vec{x}'$ are positions in the laboratory frame. In the Lagrangian action, we assume $g(n, s, |\vec{a} - \vec{a}'|)$, where the dependence on positions is instead to be understood with respect to the reference positions $\vec{a}, \vec{a}'$. Finally, motivated by the obtained results, the Lagrangian action is improved by considering the modified Lagrangian action, where $g(n^{\mathrm{ref}}, T(n, s), |\vec{a} - \vec{a}'|)$ is assumed. The difference arises from working in terms of number

density and temperature instead of number density and specific entropy, and assuming that the temperature is evaluated at a given laboratory position, while the independent number density variable, n^{ref}, is evaluated at the reference state.

We then linearize the equations of motion and obtain expressions for both longitudinal and transverse dispersion laws, and discuss the difficulties of relating coefficients in the dispersion relation to the thermodynamic parameters due to nonlocal effects. To have simple and practical expressions for the dispersion laws and due to insufficient numerical data, we use a simple step function approximation for the pair distribution function, as has been done for QLCA [36]. This also gives a better physical understanding of the different terms appearing in the linearized equations. Such calculations are performed for all of the different variational principles discussed, and the differences between them are analyzed. The results are also compared to the theoretical calculations using QLCA [36] and to the numerical results of molecular dynamics [30, 31, 32].

The key results can be seen in Figs. 2.1 and 2.2, which show that different variational principles with varying assumptions on the out-of-equilibrium behavior of the pair distribution function yield significantly different results. For example, it can be observed that in the Eulerian approach, there are no transverse modes, unlike in the modified Lagrangian approach. Furthermore, the modified Lagrangian variational principle provides excellent results for both longitudinal and transverse dispersion curves for all equilibrium values of the coupling parameter, Γ_0, and the results remain accurate even at wavelengths comparable to the average distance between particles. It correctly predicts that the onset of negative dispersion occurs at $\Gamma_0 = 9.5$, consistent with the values estimated by the molecular dynamics calculations ranging from $\Gamma_0 = 9.5$ to $\Gamma_0 = 10.0$ [30, 31]. Moreover, it was checked numerically that in the strong coupling limit, where $\Gamma_0 \to \infty$, the results of the modified Lagrangian variational principle tend towards the QLCA result. Thus, it accurately predicts the finite values of both longitudinal and transverse frequencies as the wavelength tends to zero [36].

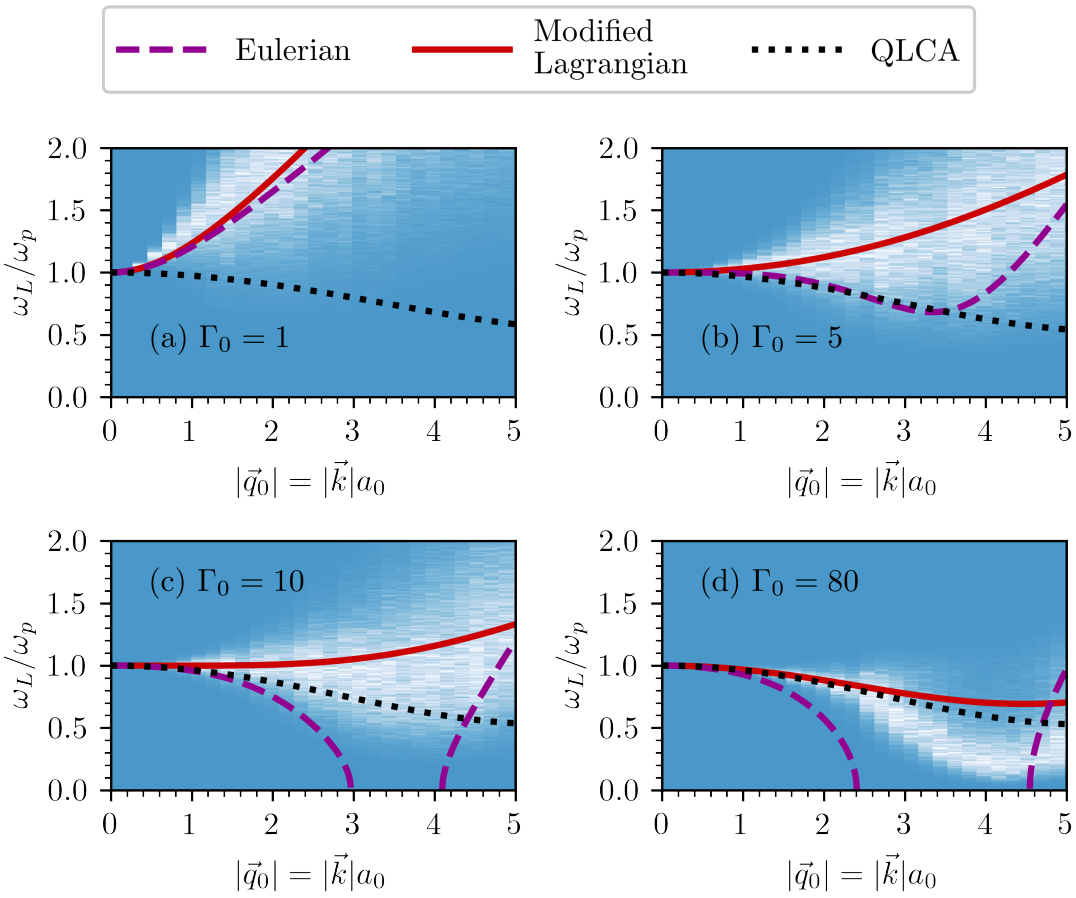

Figure 2.1: The longitudinal dispersion law is shown in normalized variables for various values of Γ_0. The results from the variational approaches are as follows: Eulerian (dashed purple line, as discussed in Section 2.2.3) and modified Lagrangian (solid red line, as described in Section 2.3.4). The step function approximation for the pair distribution function is assumed, and $u(\Gamma) = -0.9\Gamma + 0.5944\Gamma^{1/3} - 0.2786$ is defined in Eq. (2.30) and taken from Ref. [27]. For comparison, we include the result from QLCA [36] (dotted black line) and values of the longitudinal current fluctuation spectrum obtained from molecular dynamics simulations provided by the authors of Ref. [30] (colored background with large values being white and small values being blue), where the dispersion law is identified by the peaks of the spectrum. Note that the QLCA dispersion law shows negative dispersion for all Γ_0, while the proposed modified Lagrangian and simulations show a transition to negative dispersion around $\Gamma_0 = 9.5$. Additionally, the purely Eulerian theory shows instability, where $\omega_L^2 < 0$, for $\Gamma_0 \geq 7.9$.

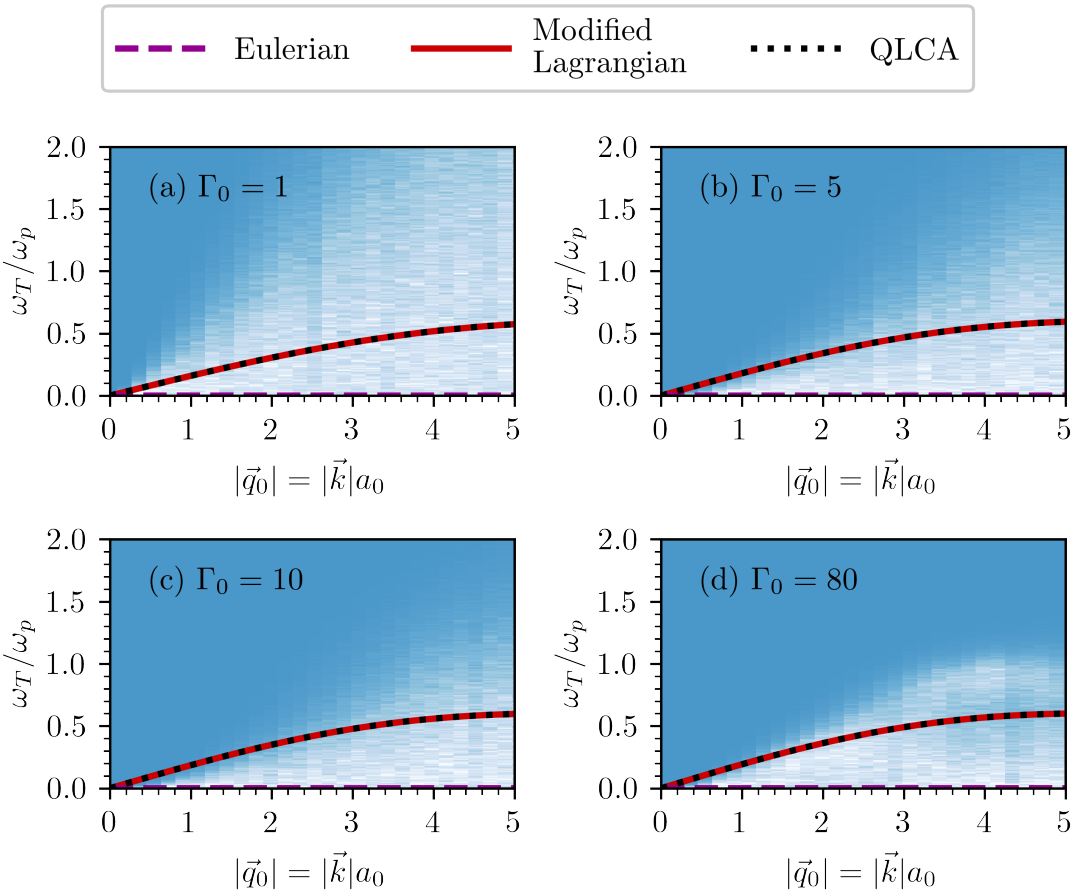

Figure 2.2: The transverse dispersion law is shown in normalized variables for different values of Γ_0. The results from the variational approaches are as follows: Eulerian (dashed purple line, as discussed in Section 2.2.3) and modified Lagrangian (solid red line, as described in Section 2.3.4). The step function approximation for the pair distribution function is assumed, and $u(\Gamma) = -0.9\Gamma + 0.5944\Gamma^{1/3} - 0.2786$ is defined in Eq. (2.30) and taken from Ref. [27]. For comparison, we include the result from QLCA [36] (dotted black line) and values of the transverse current fluctuation spectrum obtained from molecular dynamics simulations provided by the authors of Ref. [30] (colored background with large values being white and small values being blue), where the dispersion law is identified by the peaks of the spectrum.

2.2 Eulerian approach

2.2.1 Equations of motion

Let us assume that we are working with the OCP consisting of two species of charged particles. The particles that move have a charge q_+, while the particles forming a stationary neutralizing background have a charge q_-. In the Eulerian approach, each of the hydrodynamic functions is assumed to depend on the position in the laboratory frame, $\vec{x}$, and time, t. Similar to the case of Euler equations [45, 46, 47], we assume that the complete set of variables for the hydrodynamic motion of moving particles consists of velocity, $\vec{v}$, number density, n, and specific entropy, s. The latter two satisfy continuity equations.

$$\frac{\partial n}{\partial t} + \vec{\nabla} \cdot (n\vec{v}) = 0, \quad \frac{\partial s}{\partial t} + \vec{v} \cdot \vec{\nabla} s = 0. \tag{2.1}$$

Therefore, our goal is to write a variational principle with a nonlocal Lagrangian density for the OCP that would include the effects of strong coupling, from which the equation of motion for $\vec{v}$ could be found.

To satisfy the continuity equations given by Eq. (2.1), we introduce additional Lagrange multiplier fields α and β, as in the case of usual Euler equations. In general, one should also introduce an additional Lagrange multiplier field to ensure that the initial coordinates of fluid particles do not change along a particle's path [46, 47, 48]. However, we do not explicitly consider it in our calculations, as it does not change the obtained results.

Next, we propose the following Lagrangian for the generalized model of the OCP in the Eulerian approach, where the variation is performed for $n, \vec{v}, s$, and also for the functions α, β. The local terms, which are integrated only over $\vec{x}$, correspond exactly to the Lagrangian for Euler equations. The first local term, including the mass m of a single moving particle, represents kinetic energy, and the second local term represents the local internal energy that generates the local pressure.

On the other hand, the nonlocal terms, which are integrated over both $\vec{x}$ and $\vec{x}'$, represent nonlocal interaction between the particles. The first nonlocal term describes the interaction

between the moving particles and, without any loss of generality, is written as an arbitrary function $F(n, n', s, s', |\vec{x} - \vec{x}'|)$, where we use the notation n', s' to indicate that the functions are evaluated at $\vec{x}'$ instead of $\vec{x}$. For this term, we assume that the dependence on coordinates is solely through the combination $|\vec{x} - \vec{x}'|$, ensuring conservation laws for both linear and angular momentum.

The second nonlocal term represents the interaction between oppositely charged particles, which is necessary to ensure that the equations have an equilibrium solution. The third nonlocal term represents the interaction between the particles that form the stationary neutralizing background, necessary to ensure that the expression for the energy of the OCP is well-defined in the thermodynamic limit. Here, we assume that the interaction between charged species is due to the Coulomb potential, $\phi_{ij}(r) = q_i q_j / 4\pi\varepsilon_0 r$, where i, j correspond to the species of the particles, and r is the distance between particles. Additionally, n_- represents the time-independent number density of the particles forming the neutralizing background.

$$\begin{aligned} L &= \int \mathcal{L}_1 \mathrm{d}\vec{x} + \iint \mathcal{L}_2 \mathrm{d}\vec{x}\mathrm{d}\vec{x}' \\ &= \int \left(\frac{1}{2} m n \vec{v}^2 - n f(n, s) + \alpha \left(\frac{\partial n}{\partial t} + \vec{\nabla} \cdot (n\vec{v}) \right) + \beta \left(\frac{\partial s}{\partial t} + \vec{v} \cdot \vec{\nabla} s \right) \right) \mathrm{d}\vec{x} \\ &\quad + \iint \Big(- n n' F(n, n', s, s', |\vec{x} - \vec{x}'|) - n n'_- \phi_{+-}(|\vec{x} - \vec{x}'|) \\ &\quad - \frac{1}{2} n_- n'_- \phi_{--}(|\vec{x} - \vec{x}'|) \Big) \mathrm{d}\vec{x}\mathrm{d}\vec{x}' \end{aligned} \tag{2.2}$$

Performing variations with respect to fields α, β gives the continuity equations in Eq. (2.1), as intended. However, for variations with respect to the remaining functions, one must be careful when analyzing the nonlocal terms. To perform the variations, change variables under the integral from $(\vec{x}, \vec{x}')$ to $(\vec{x}', \vec{x})$, which has a unit Jacobian.

It is useful to introduce, for each function f, the notation f^T to mean taking f but replacing all occurrences of $\vec{x}$ with $\vec{x}'$ and all occurrences of $\vec{x}'$ with $\vec{x}$. For example, $f^T(n, n') = f(n', n)$. In that case, for any field that is being varied, denoted as Ψ, and any functions f, g, we have that $(fg)^T = f^T g^T$, and $(\partial_{\Psi'} f)^T = \partial_\Psi (f^T)$.

Using these results, we obtain the following equations of motion from the variational

principle.

$$\begin{aligned}\delta n: \quad & \frac{1}{2}m\vec{v}^2 - f(n,s) - n\frac{\partial f}{\partial n}\Big|_s - \frac{\partial \alpha}{\partial t} - \vec{v}\cdot\vec{\nabla}\alpha \\ = \int & \left(n'(F+F^T) + nn'\frac{\partial(F+F^T)}{\partial n}\Big|_{n',s,s',|\vec{x}-\vec{x}'|} + n'_-\phi_{+-}(|\vec{x}-\vec{x}'|)\right) \mathrm{d}\vec{x}',\end{aligned} \tag{2.3}$$

$$\delta\vec{v}: \quad mn\vec{v} + \beta\vec{\nabla}s - n\vec{\nabla}\alpha = \vec{0}, \tag{2.4}$$

$$\delta s: \quad n\frac{\partial f}{\partial s}\Big|_n + \frac{\partial \beta}{\partial t} + \vec{\nabla}\cdot(\beta\vec{v}) = -\int nn'\frac{\partial(F+F^T)}{\partial s}\Big|_{n,n',s',|\vec{x}-\vec{x}'|}\mathrm{d}\vec{x}'. \tag{2.5}$$

Our goal with the variational principle is to understand the equation of motion for $\partial\vec{v}/\partial t$. However, when examining the obtained Eqs. (2.3), (2.4), (2.5), one can see one of the disadvantages of the Eulerian formulation of variational principles. In this formulation, the resulting equations depend on the constraint fields α, β, which then must be solved by using clever manipulations in terms of $n, s, \vec{v}$. To achieve this, we repeat computations similar to those for Euler equations [45].

From Eq. (2.4), one can solve for $\vec{\nabla}\alpha$ and not for α itself. Therefore, one takes the gradient of Eq. (2.3), expands the gradients of $f, (F+F^T)$ using the chain rule, and substitutes the expression for $\vec{\nabla}\alpha$. Then, the resulting equation does not depend on α anymore, but depends on derivatives of $(\beta\vec{\nabla}s)/n$. The time derivative of $(\beta\vec{\nabla}s)/n$ can be simplified by using the product rule and then using the time derivatives of n, s, β as given in Eqs. (2.1), (2.5). The remaining terms with β can be simplified by using the product rule and the identity $\vec{a}\times(\vec{b}\times\vec{c}) = (\vec{a}\cdot\vec{c})\vec{b} - (\vec{a}\cdot\vec{b})\vec{c}$ with $\vec{a} = n\vec{v}, \vec{b} = \vec{\nabla}(\beta/n), \vec{c} = \vec{\nabla}s$. Finally, to simplify the terms with cross products and curls, use the mathematical identity $\vec{\nabla}(\beta/n)\times\vec{\nabla}s = \vec{\nabla}\times(\beta\vec{\nabla}s/n)$, and use Eq. (2.4) to obtain $\vec{\nabla}\times(\beta\vec{\nabla}s/n) = -m\vec{\nabla}\times\vec{v}$. Finally, use the following identity for derivatives of the velocity field.

$$\frac{\partial\vec{v}}{\partial t} + (\vec{v}\cdot\vec{\nabla})\vec{v} = \frac{\partial\vec{v}}{\partial t} + \vec{\nabla}\left(\frac{\vec{v}^2}{2}\right) - \vec{v}\times(\vec{\nabla}\times\vec{v}) \tag{2.6}$$

The final equation of motion for $\vec{v}$ is as follows, but at this point, functions f, F are still

arbitrary.

$$mn\left(\frac{\partial\vec{v}}{\partial t}+(\vec{v}\cdot\vec{\nabla})\vec{v}\right)=-\vec{\nabla}\left(n^2\frac{\partial f}{\partial n}\Big|_s+\int n^2n'\frac{\partial(F+F^T)}{\partial n}\Big|_{n',s,s',|\vec{x}-\vec{x}'|}\mathrm{d}\vec{x}'\right)$$
$$-\int\left(nn'\frac{\partial(F+F^T)}{\partial\vec{x}}\Big|_{n,n',s,s',\vec{x}'}+nn'_-\frac{\partial\phi_{+-}}{\partial\vec{x}}\Big|_{\vec{x}'}\right)\mathrm{d}\vec{x}' \tag{2.7}$$

2.2.2 Conservation laws

Let us consider the momentum and energy conservation laws of our theory in the Eulerian approach. In particular, energy conservation will be important because the expression for the conserved energy coming from the variational principle that depends on functions f, F can be computed in equilibrium and compared to the expression found in thermodynamics. This ensures both the consistency of our theory with thermodynamics and allows us to identify what functions f, F should be in terms of the thermodynamic quantities.

We now examine the momentum conservation law in each of the directions $i = 1, 2, 3$. The momentum conservation law relies on the observation that in Eq. (2.2), the local part of the Lagrangian density, $\mathcal{L}_1$, does not depend explicitly on $\vec{x}$, and the term with F in the nonlocal part of this Lagrangian density, $\mathcal{L}_2$, as well as ϕ_{+-}, ϕ_{--}, all depend explicitly on $\vec{x}, \vec{x}'$ only in a translationally invariant combination $\vec{x} - \vec{x}'$. It is important to note that it is not true that $\mathcal{L}_2$ depends explicitly on $\vec{x}, \vec{x}'$ in a translationally invariant way, as the number density of the stationary neutralizing background, n_-, might depend on $\vec{x}$.

To compute the momentum conservation law for our nonlocal variational principle, we use an approach analogous to that used in the case of local variational principles [12, 49]. We apply the chain rule to expand the full derivatives of $\mathcal{L}_1$ and, motivated by the equation of motion in Eq. (2.7), $(1/2)\int(\mathcal{L}_2 + \mathcal{L}_2^T)\mathrm{d}\vec{x}'$ with respect to x_i. Due to nonlocality, we also use the chain rule to expand the full derivative of $(\mathcal{L}_2+\mathcal{L}_2^T)/2$ with respect to x_i'. It is important to note that the integral over $\vec{x}'$ of the latter is zero, as can be shown by integration by parts. We add these calculations and simplify terms using all of the equations of motion obtained from the variational principle, and then apply the product rule. Finally, to simplify the obtained equation in our particular case, we use the chain rule, integration by parts, and

our assumptions regarding $\mathcal{L}_1, F, \phi_{+-}, \phi_{--}$ to obtain the following equation that nearly has the form of a conservation law.

$$\begin{aligned}\frac{\partial}{\partial t}\left(\alpha\frac{\partial n}{\partial x_i}+\beta\frac{\partial s}{\partial x_i}\right)-\frac{\partial}{\partial x_i}\left(\frac{1}{2}mn\vec{v}^2-nf\right)+\sum_{j=1}^{3}\frac{\partial}{\partial x_j}\left(\alpha\frac{\partial(nv_j)}{\partial x_i}+\beta v_j\frac{\partial s}{\partial x_i}\right)\\ =-\int n'_-\frac{\partial n}{\partial x_i}\phi_{+-}\mathrm{d}\vec{x}'-\int n'\Bigg(\frac{\partial n}{\partial x_i}(F+F^T)\\ +n\frac{\partial n}{\partial x_i}\frac{\partial(F+F^T)}{\partial n}\Big|_{n',s,s',|\vec{x}-\vec{x}'|}+n\frac{\partial s}{\partial x_i}\frac{\partial(F+F^T)}{\partial s}\Big|_{n,n',s',|\vec{x}-\vec{x}'|}\Bigg)\mathrm{d}\vec{x}'\end{aligned} \tag{2.8}$$

Similar to the equations of motion obtained from the variational principle, the resulting momentum conservation law depends on the constraint fields α, β, which highlights a disadvantage of Eulerian formulation. We will now rewrite it so that it is expressed solely in terms of $n, s, \vec{v}$.

As α is only given in the equations of motion in Eqs. (2.3), (2.4) through its derivatives, we use the product rule to introduce an additional spatial derivative to α in all of the terms containing it. This enables us to employ Eqs. (2.3), (2.4), along with the continuity equation for number density given in Eq. (2.1), to eliminate all of the terms containing α. After this simplification, all of the terms with β also disappear. Finally, to simplify the nonlocal terms that contain F, ϕ_{+-}, we expand the derivatives using the chain rule, and then use assumptions about the explicit dependence of $\vec{x}, \vec{x}'$ in F, ϕ_{+-}, and apply integration by parts. The final result is given next.

$$\begin{aligned}\frac{\partial(mnv_i)}{\partial t}+\vec{\nabla}\cdot(mnv_i\vec{v})+\frac{\partial}{\partial x_i}\left(n^2\frac{\partial f}{\partial n}\Big|_s+\int n^2n'\frac{\partial(F+F^T)}{\partial n}\Big|_{n',s,s',|\vec{x}-\vec{x}'|}\mathrm{d}\vec{x}'\right)\\ =-\int\left(nn'\frac{\partial(F+F^T)}{\partial x_i}\Big|_{n,n',s,s',\vec{x}'}+nn'_-\frac{\partial\phi_{+-}}{\partial x_i}\Big|_{\vec{x}'}\right)\mathrm{d}\vec{x}'\end{aligned} \tag{2.9}$$

Notice that this equation could also be obtained directly by adding the equation of motion for $\vec{v}$ given by Eq. (2.7) to the continuity equation for number density in Eq. (2.1) and using the product rule. However, this method requires the knowledge that the correct expression for the momentum density in our theory is indeed $mn\vec{v}$.

The momentum conservation law given by Eq. (2.9) allows us to define the full momentum $\vec{P}$ of the particles that move in the OCP and consider how it changes over time. In particular,

we integrate Eq. (2.9) with respect to $\vec{x}$ and use integration by parts. To further simplify nonlocal terms, we use the properties that for all functions f, g, we have $(f^T)^T = f, (f+g)^T = f^T + g^T, (fg)^T = f^T g^T$. Additionally, we note that the integral of f over $\vec{x}, \vec{x}'$ is the same as the integral of f^T. We also use the following identity.

$$\left(\frac{\partial(F+F^T)}{\partial x_i}\Big|_{n,n',s,s',\vec{x}'}\right)^T = \frac{\partial((F+F^T)^T)}{\partial x_i'}\Big|_{n,n',s,s',\vec{x}} \tag{2.10}$$

These identities together with the assumption that F depends explicitly on $\vec{x}, \vec{x}'$ only through the combination $\vec{x} - \vec{x}'$ are used to show the following integral is zero.

$$\iint nn' \frac{\partial(F+F^T)}{\partial x_i}\Big|_{n,n',s,s',\vec{x}'} \mathrm{d}\vec{x}\mathrm{d}\vec{x}' = 0 \tag{2.11}$$

Finally, the time evolution for the momentum $\vec{P}$ in each direction is given as follows. It can be observed that the momentum of moving particles is not necessarily conserved and can change due to the force from the stationary neutralizing background.

$$\frac{\mathrm{d}P_i}{\mathrm{d}t} = \frac{\mathrm{d}}{\mathrm{d}t}\left(\int mnv_i \mathrm{d}\vec{x}\right) = -\iint nn'_- \frac{\partial\phi_{+-}}{\partial x_i}\Big|_{\vec{x}'} \mathrm{d}\vec{x}\mathrm{d}\vec{x}' \tag{2.12}$$

Notice that the momentum of moving particles is conserved in the case when the neutralizing background is both uniform and infinite, as can be shown by Eq. (2.12) by using that ϕ_{+-} depends on $\vec{x}, \vec{x}'$ only through combination $\vec{x} - \vec{x}'$, and by integrating by parts.

Let us now explore the energy conservation law that will be used to match functions in the variational principle to the thermodynamic quantities. Energy conservation law relies on the observation that in the proposed Lagrangian in Eq. (2.2) both the local part of the Lagrangian density, $\mathcal{L}_1$, and the nonlocal part, $\mathcal{L}_2$, do not depend explicitly on time t.

To compute the energy conservation law for our nonlocal variational principle, we employ an analogous approach as in the case of local variational principles [12, 49]. We use the chain rule to expand the full derivatives of $\mathcal{L}_1$ and, motivated by the equation of motion in Eq. (2.7), $(1/2)\int(\mathcal{L}_2 + \mathcal{L}_2^T)\mathrm{d}\vec{x}'$ with respect to t. We add these calculations and simplify terms using all of the equations of motion obtained from the variational principle and the product rule. To further simplify the obtained equation in our particular case, we rewrite time derivatives

of n, s and n', s' in the nonlocal terms using the continuity equations given in Eq. (2.1), and then apply integration by parts to the nonlocal terms with derivatives with respect to $\vec{x}'$.

$$\begin{aligned}
&\frac{\partial}{\partial t}\Bigg(-\frac{1}{2}nm\vec{v}^2 + nf - \alpha\vec{\nabla}\cdot(n\vec{v}) - \beta\vec{v}\cdot\vec{\nabla}s + \int\Bigg(\frac{nn'}{2}(F+F^T) + \frac{nn'_-}{2}\phi_{+-} \\
&\quad + \frac{n'n_-}{2}\phi_{+-} + \frac{n_-n'_-}{2}\phi_{--}\Bigg)\mathrm{d}\vec{x}'\Bigg) + \sum_{j=1}^{3}\frac{\partial}{\partial x_j}\left(\alpha\frac{\partial(nv_j)}{\partial t} + \beta v_j\frac{\partial s}{\partial t}\right) \\
&= \int\Bigg(\frac{n'}{2}(F+F^T)\vec{\nabla}\cdot(n\vec{v}) + \frac{nn'}{2}\frac{\partial(F+F^T)}{\partial n}\Big|_{n',s,s',|\vec{x}-\vec{x}'|}\vec{\nabla}\cdot(n\vec{v}) \\
&\quad + \frac{nn'}{2}\frac{\partial(F+F^T)}{\partial s}\Big|_{n,n',s',|\vec{x}-\vec{x}'|}\vec{v}\cdot\vec{\nabla}s + \frac{nn'}{2}\vec{v}'\cdot\frac{\partial(F+F^T)}{\partial\vec{x}'}\Big|_{n,n',s,s',\vec{x}} \\
&\qquad - \frac{n(n')^2}{2}\frac{\partial(F+F^T)}{\partial n'}\Big|_{n,s,s',|\vec{x}-\vec{x}'|}\vec{\nabla}'\cdot\vec{v}'\Bigg)\mathrm{d}\vec{x}' \\
&\quad + \int\left(\frac{n'_-}{2}\phi_{+-}\vec{\nabla}\cdot(n\vec{v}) + \frac{n'n_-}{2}\vec{v}'\cdot\frac{\partial\phi_{+-}}{\partial\vec{x}'}\Big|_{\vec{x}}\right)\mathrm{d}\vec{x}'
\end{aligned} \tag{2.13}$$

As before, we observe a disadvantage of the Eulerian formulation of the variational principles, as the obtained energy conservation law depends on the constraint fields α, β. We now rewrite it so that it is given only in terms of $n, s, \vec{v}$, using a similar strategy as when analyzing the momentum conservation law.

As α appears in the equations of motion in Eqs. (2.3), (2.4) only through its derivatives, we use the product rule to introduce an additional spatial derivative to α in all terms containing it. This allows to utilize Eqs. (2.3), (2.4), together with the continuity equation for specific entropy in Eq. (2.1), to eliminate all terms that include α. Following this simplification, all terms with β also vanish. Finally, for simplifying nonlocal terms, we employ the chain rule and integration by parts. The final result is provided next.

$$\frac{\partial\mathcal{E}}{\partial t} + \sum_{j=1}^{3}\frac{\partial J_j}{\partial x_j} = \sigma, \tag{2.14}$$

$$\mathcal{E} = \frac{1}{2}mn\vec{v}^2 + nf + \int\left(\frac{nn'}{2}(F+F^T) + \frac{nn'_-}{2}\phi_{+-} + \frac{n'n_-}{2}\phi_{+-} + \frac{n_-n'_-}{2}\phi_{--}\right)\mathrm{d}\vec{x}', \tag{2.15}$$

$$
\begin{aligned}
J_j = v_j \Bigg(& \frac{1}{2} mn\vec{v}^2 + nf + n^2 \frac{\partial f}{\partial n}\Big|_s \\
& + \int \left(\frac{nn'}{2}(F + F^T) + n^2 n' \frac{\partial (F + F^T)}{\partial n}\Big|_{n',s,s',|\vec{x}-\vec{x}'|} + \frac{nn'_-}{2}\phi_{+-} \right) \mathrm{d}\vec{x}' \Bigg),
\end{aligned} \tag{2.16}
$$

$$
\begin{aligned}
\sigma = & \int \frac{nn'}{2} \left(n(\vec{\nabla} \cdot \vec{v}) \frac{\partial (F + F^T)}{\partial n}\Big|_{n',s,s',|\vec{x}-\vec{x}'|} - n'(\vec{\nabla}' \cdot \vec{v}') \frac{\partial (F + F^T)}{\partial n'}\Big|_{n,s,s',|\vec{x}-\vec{x}'|} \right) \mathrm{d}\vec{x}' \\
& + \int \frac{nn'}{2} \left(\vec{v}' \cdot \frac{\partial (F + F^T)}{\partial \vec{x}'}\Big|_{n,n',s,s',\vec{x}} - \vec{v} \cdot \frac{\partial (F + F^T)}{\partial \vec{x}}\Big|_{n,n',s,s',\vec{x}'} \right) \mathrm{d}\vec{x}' \\
& + \int \left(\frac{n'n_-}{2} \vec{v}' \cdot \frac{\partial \phi_{+-}}{\partial \vec{x}'}\Big|_{\vec{x}} - \frac{nn'_-}{2} \vec{v} \cdot \frac{\partial \phi_{+-}}{\partial \vec{x}}\Big|_{\vec{x}'} \right) \mathrm{d}\vec{x}'.
\end{aligned} \tag{2.17}
$$

Notice that this equation could also be obtained by directly computing the time derivative of the correct energy density as given in the energy conservation law. Then, one can use the product rule and time derivatives found in the equations of motion given by Eqs. (2.1), (2.7). To simplify, one employs the product rule, the chain rule, integration by parts, and the identity $\vec{v} \cdot (\vec{v} \cdot \vec{\nabla})\vec{v} = \vec{v} \cdot \vec{\nabla}(\vec{v}^2/2)$. This approach avoids issues with constraint fields α, β but requires knowledge of the correct expression for the energy density in our theory.

The energy conservation law, given by Eq. (2.14), allows us to define the energy E of the OCP and consider how it changes over time. To achieve this, we integrate Eq. (2.14) with respect to $\vec{x}$ and use integration by parts. To further simplify nonlocal terms, we employ the following properties: for all functions f, g, we have $(f^T)^T = f, (f + g)^T = f^T + g^T, (fg)^T = f^T g^T$, and the integral of f over $\vec{x}, \vec{x}'$ is the same as the integral of f^T. To simplify nonlocal terms involving ϕ_{+-}, we use the fact that $(\partial \phi_{+-}/\partial \vec{x})^T = \partial(\phi_{+-}^T)/\partial \vec{x}'$, and that $\phi_{+-}^T = \phi_{+-}$ due to the assumption that it depends on $\vec{x}, \vec{x}'$ through $|\vec{x} - \vec{x}'|$. To simplify nonlocal terms with F, we use the identity in Eq. (2.10), and analogous identities, where in Eq. (2.10), x_i, x_i' are replaced by n, n' and s, s', respectively.

$$
\begin{aligned}
\frac{\mathrm{d}E}{\mathrm{d}t} = \frac{\mathrm{d}}{\mathrm{d}t} \Bigg(& \int \left(\frac{1}{2} mn\vec{v}^2 + nf \right) \mathrm{d}\vec{x} + \iint \Bigg(\frac{nn'}{2}(F + F^T) + \frac{nn'_-}{2}\phi_{+-} \\
& + \frac{n'n_-}{2}\phi_{+-} + \frac{n_-n'_-}{2}\phi_{--} \Bigg) \mathrm{d}\vec{x}\mathrm{d}\vec{x}' \Bigg) = 0
\end{aligned} \tag{2.18}
$$

Now, we would like to consider the expression for the energy, E, in the thermodynamic equilibrium. In terms of our variational principle, this means that we consider the hydrodynamic functions $n, s, \vec{v}$ to be uniform and time-independent with values $n = n_0, s = s_0, \vec{v} = \vec{0}$, which correspond to no macroscopic motion. To fully specify the value of the energy, we also assume that the number density of the stationary neutralizing background is uniform, with a value $n_- = n_{-,0}$. To relate $n_0, n_{-,0}$, we use an assumption that the total charge of the OCP is zero. This assumption is relevant to strongly coupled plasma experiments [14, 15, 16, 17, 19, 20, 22]. In terms of equilibrium number densities, this charge neutrality condition becomes $q_+ n_0 + q_- n_{-,0} = 0$.

In the thermodynamic limit, where the number of moving particles $N \to \infty$ and the volume of the system $V \to \infty$ while the number density is fixed, the equilibrium energy of the OCP diverges. Therefore, instead, we consider the equilibrium energy per particle, E_0/N. From Eq. (2.18), we obtain the following expression, where we change variables inside the integrals to $\vec{R} = (\vec{x} + \vec{x}')/2, \vec{r} = \vec{x} - \vec{x}'$, which has a unit Jacobian. This change of variables allows us to simplify the integrals, as we assume that F, ϕ_{+-}, ϕ_{--} depend explicitly on $\vec{x}, \vec{x}'$ only through the combination $\vec{x} - \vec{x}'$. Finally, we can further simplify the expression using the assumed form of the potential $\phi_{ij}(r) = q_i q_j / 4\pi\varepsilon_0 r$, where i, j are the corresponding species of the particles, and r is the distance between the particles.

$$\frac{E_0}{N} = f(n_0, s_0) + \frac{n_0}{2} \int \left((F + F^T)(n_0, n_0, s_0, s_0, |\vec{r}|) - \frac{q_+^2}{4\pi\varepsilon_0 |\vec{r}|} \right) \mathrm{d}\vec{r} \tag{2.19}$$

This expression can be compared to the expression from the thermodynamics of the thermodynamic equilibrium energy of the OCP per moving particle, E_{th}/N [23, 24], where T is the temperature and g is the equilibrium pair distribution function.

$$\frac{E_{\mathrm{th}}}{N} = \frac{3}{2} k_B T(n_0, s_0) + \frac{n_0}{2} \int \frac{q_+^2}{4\pi\varepsilon_0 |\vec{r}|} \left(g(n_0, s_0, |\vec{r}|) - 1 \right) \mathrm{d}\vec{r} \tag{2.20}$$

By comparing Eqs. (2.19) and (2.20), we have the following constraints on functions f, F. Here, we use that $F^T(n_0, n_0, s_0, s_0, |\vec{r}|) = F(n_0, n_0, s_0, s_0, |\vec{r}|)$ directly from the definition.

$$f(n_0, s_0) = \frac{3}{2} k_B T(n_0, s_0), \quad F(n_0, n_0, s_0, s_0, |\vec{r}|) = \frac{q_+^2}{8\pi\varepsilon_0 |\vec{r}|} g(n_0, s_0, |\vec{r}|). \tag{2.21}$$

This constraint uniquely determines function f, but not F. This is because F is specified by this constraint only for values when n is equal to n', and when s is equal to s'. To resolve this issue, from now on we replace Lagrangian in Eq. (2.2) with a less general Lagrangian, where F is assumed to be a function of only $n, s, |\vec{x} - \vec{x}'|$. Notice that this is not a unique choice as one could also take, for example, $F = F((n+n')/2, (s+s')/2, |\vec{x} - \vec{x}'|)$ or $F = F(\sqrt{nn'}, \sqrt{ss'}, |\vec{x} - \vec{x}'|)$. However, in some sense, our choice is the simplest possible, and then F is uniquely determined from the constraint in Eq. (2.21). Therefore, we have the following result.

$$f(n,s) = \frac{3}{2} k_B T(n,s), \quad F(n,s,|\vec{r}|) = \frac{q_+^2}{8\pi\varepsilon_0 |\vec{r}|} g(n,s,|\vec{r}|). \tag{2.22}$$

Such identification allows us to rewrite the equation of motion for velocity given by Eq. (2.7) in the following way in terms of thermodynamic functions. Here, we use $\phi_{ij}(r) = q_i q_j / 4\pi\varepsilon_0 r$, where i, j are the corresponding species of the particles, and r is the distance between the particles.

$$\begin{aligned} mn\left(\frac{\partial \vec{v}}{\partial t} + (\vec{v}\cdot\vec{\nabla})\vec{v}\right) &= -\vec{\nabla}\left(\frac{3}{2} k_B n^2 \frac{\partial T}{\partial n}\Big|_s + \frac{q_+^2}{8\pi\varepsilon_0}\int \frac{n^2 n'}{|\vec{x}-\vec{x}'|}\frac{\partial g}{\partial n}\Big|_{s,|\vec{x}-\vec{x}'|} \mathrm{d}\vec{x}'\right) \\ -\frac{q_+ n}{4\pi\varepsilon_0}\int &\left(q_+ n' \frac{\partial}{\partial \vec{x}}\left(\frac{1}{|\vec{x}-\vec{x}'|}\frac{(g+g^T)}{2}\right)\Big|_{n,n',s,s',\vec{x}'} + q_- n'_- \frac{\partial}{\partial \vec{x}}\left(\frac{1}{|\vec{x}-\vec{x}'|}\right)\Big|_{\vec{x}'}\right)\mathrm{d}\vec{x}' \end{aligned} \tag{2.23}$$

2.2.3 Dispersion laws

While discussing the energy conservation law, we considered equilibrium solutions in which hydrodynamic functions, $n, s, \vec{v}$, are uniform and time-independent, with values $n = n_0, s = s_0, \vec{v} = \vec{0}$. In this context, the stationary neutralizing background has a uniform number density with the value $n_- = n_{-,0}$, which is related to n_0 by using the charge neutrality assumption, $q_+ n_0 + q_- n_{-,0} = 0$.

Now, we would like to examine the linearized equations of motion that correspond to the OCP being close to thermodynamic equilibrium. In this case, we assume the following form for the time-dependent functions, where $n_1, s_1, \vec{v}_1$ denote first-order corrections.

$$n = n_0 + n_1(\vec{x}, t), \quad s = s_0 + s_1(\vec{x}, t), \quad \vec{v} = \vec{v}_1(\vec{x}, t). \tag{2.24}$$

With such assumptions regarding $n, s, \vec{v}$, we will expand equations of motion given by Eqs. (2.1), (2.23) up to the first order. However, let us first consider these equations of motion and determine whether our proposed equilibrium solutions satisfy them. The continuity equations in Eq. (2.1) are satisfied since all hydrodynamic functions do not depend on either spatial coordinates or time, resulting in their derivatives being zero.

In Eq. (2.23), the terms on the left-hand side are zero because $\vec{v} = \vec{0}$ in equilibrium. The first term under the gradient on the right-hand side is also zero since it does not depend on spatial coordinates due to its dependence on n_0, s_0. As for the second term under the gradient, we can use the fact that $n = n_0, n' = n_0$, so the integral is only over a function that depends on $\vec{x}, \vec{x}'$ through $\vec{x} - \vec{x}'$. This allows us to change variables under the integral to $\vec{r} = \vec{x} - \vec{x}'$, making it independent of $\vec{x}$.

Finally, let us consider the remaining nonlocal terms on the right-hand side. We can use the fact that n, s, n_- are all uniform in space, so the integrals become over a full derivative with respect to $\vec{x}$, which can be integrated by parts to become zero.

The expanded continuity equations up to the first order are as follows.

$$\frac{\partial n_1}{\partial t} + n_0(\vec{\nabla} \cdot \vec{v}_1) = 0, \quad \frac{\partial s_1}{\partial t} = 0. \tag{2.25}$$

To expand the equation of motion for $\vec{v}$, given by Eq. (2.23), up to the first order, we use the fact that the functions inside the integrals often depend on $\vec{x}, \vec{x}'$ solely through $\vec{x} - \vec{x}'$. This allows us to switch from derivatives with respect to $\vec{x}$ to derivatives with respect to $\vec{x}'$, enabling us to apply integration by parts. The resulting linearized equation for $\vec{v}_1$ shows that n_1, s_1 only appear in it through gradients.

To combine the linearized equations of motion, we take the gradient of Eq. (2.25) and an additional time derivative of the linearized equation of motion for $\vec{v}_1$. This yields the following equation, which depends solely on $\vec{v}_1$, with the subscript "0" indicating that a function is evaluated at equilibrium values. We also simplify using $g_0 = (g^T)_0$ and $(\partial g/\partial n)_0 =$

$(\partial g^T/\partial n')_0$.

$$
\begin{aligned}
m\frac{\partial^2\vec{v}_1}{\partial t^2} &= \vec{\nabla}(\vec{\nabla}\cdot\vec{v}_1)\left(\left[\frac{\partial}{\partial n}\left(\frac{3}{2}k_B n^2\frac{\partial T}{\partial n}\Big|_s\right)\Big|_s\right]_0\right. \\
&+\frac{q_+^2 n_0}{8\pi\varepsilon_0}\int\frac{1}{|\vec{x}-\vec{x}'|}\left[\frac{\partial}{\partial n}\left(n^2\frac{\partial g}{\partial n}\Big|_{s,|\vec{x}-\vec{x}'|}\right)\Big|_{s,|\vec{x}-\vec{x}'|}\right]_0 \mathrm{d}\vec{x}'\Bigg) \\
&+\frac{q_+^2 n_0}{4\pi\varepsilon_0}\int\frac{\vec{\nabla}'(\vec{\nabla}'\cdot\vec{v}_1')}{|\vec{x}-\vec{x}'|}\left(g_0+n_0\left[\frac{\partial g}{\partial n}\Big|_{s,|\vec{x}-\vec{x}'|}\right]_0\right)\mathrm{d}\vec{x}'
\end{aligned}
\tag{2.26}
$$

To solve this equation, we use the Fourier transform with respect to the spatial coordinates, $\vec{x}$, and use the following convention.

$$
\vec{V}(\vec{k},t)=\widehat{\vec{v}_1}(\vec{k},t)=\int\vec{v}_1(\vec{x},t)e^{-i\vec{k}\cdot\vec{x}}\mathrm{d}\vec{x} \tag{2.27}
$$

With this convention, we find that for any functions f, g that depend on $\vec{x}$, $\widehat{\partial f/\partial x_j}=ik_j\widehat{f}$ and $\widehat{f*g}=\widehat{f}\widehat{g}$, where $*$ denotes convolution. Using these results and changing variables under the first integral from $\vec{x}'$ to $\vec{r}=\vec{x}-\vec{x}'$, which has a unit Jacobian, one can take the Fourier transform of Eq. (2.26) to obtain a differential equation for each value of $\vec{k}$.

One must be careful with the convergence of integrals. From thermodynamics [23], it is known that for the equilibrium pair distribution function, $g(n_0,s_0,|\vec{r}|)\to 1$ as $|\vec{r}|\to\infty$. Therefore, it is convenient to rewrite everything in terms of $g-1$ instead of g. Additionally, we use that the Fourier transform of $1/|\vec{r}|$ is $4\pi/|\vec{k}|^2$ [50].

$$
\begin{aligned}
m\frac{\partial^2\vec{V}}{\partial t^2} &= -\vec{k}(\vec{k}\cdot\vec{V})\left(\left[\frac{\partial}{\partial n}\left(\frac{3}{2}k_B n^2\frac{\partial T}{\partial n}\Big|_s\right)\Big|_s\right]_0\right. \\
&+\frac{q_+^2 n_0}{8\pi\varepsilon_0}\int\frac{1}{|\vec{r}|}\left[\frac{\partial}{\partial n}\left(n^2\frac{\partial(g-1)}{\partial n}\Big|_{s,|\vec{r}|}\right)\Big|_{s,|\vec{r}|}\right]_0\mathrm{d}\vec{r} \\
&+\frac{q_+^2 n_0}{\varepsilon_0|\vec{k}|^2}+\frac{q_+^2 n_0}{4\pi\varepsilon_0}\int\frac{e^{-i\vec{k}\cdot\vec{r}}}{|\vec{r}|}\left((g-1)_0+n_0\left[\frac{\partial(g-1)}{\partial n}\Big|_{s,|\vec{r}|}\right]_0\right)\mathrm{d}\vec{r}\Bigg)
\end{aligned}
\tag{2.28}
$$

To simplify the analysis of the longitudinal and transverse dispersion modes, it is convenient to rotate the coordinate system so that, in the rotated coordinate system, $\vec{k}=(0,0,|\vec{k}|)$. In this case, the transverse modes correspond to the x, y directions, while the longitudinal mode corresponds to the z direction. To do this, we use the fact that the differential equation

is linear, consider the properties of the dot product under a rotation, and also rotate the integration variable. Moreover, we can simplify further by switching to spherical coordinates and performing the angular integrals.

We find that for the transverse directions, $\partial^2 V_x/\partial t^2 = \partial^2 V_y/\partial t^2 = 0$, indicating the absence of transverse modes. In other words, the transverse dispersion law is $\omega_T(|\vec{k}|) = 0$. For the longitudinal direction, we have the following dispersion law.

$$\begin{aligned}\omega_L^2(|\vec{k}|) = \frac{q_+^2 n_0}{m\varepsilon_0} + |\vec{k}|^2 \Bigg(\Bigg[\frac{\partial}{\partial n} \Big(\frac{3k_B}{2m} n^2 \frac{\partial T}{\partial n}\Big|_s \Big) \Big|_s \Bigg]_0 \\ + \frac{q_+^2 n_0}{2m\varepsilon_0} \int_0^\infty r \Bigg[\frac{\partial}{\partial n} \Big(n^2 \frac{\partial (g-1)}{\partial n}\Big|_{s,r} \Big) \Big|_{s,r} \Bigg]_0 \mathrm{d}r \Bigg) \\ + \frac{q_+^2 n_0 |\vec{k}|}{m\varepsilon_0} \int_0^\infty \sin(|\vec{k}|r) \Bigg((g-1)_0 + n_0 \Bigg[\frac{\partial (g-1)}{\partial n}\Big|_{s,r} \Bigg]_0 \Bigg) \mathrm{d}r\end{aligned} \tag{2.29}$$

One can see that the longitudinal dispersion relation does not only depend on the equilibrium pair distribution function but also on its adiabatic derivatives, in other words, derivatives with respect to the number density at constant entropy. In the usual case of Euler equations, the dispersion relation depends on the adiabatic derivatives of the local energy [1]. In our case, the nonlocal contribution to the energy of the OCP depends on the pair distribution function, as can be seen in Eq. (2.20). Therefore, the adiabatic derivatives of the pair distribution function in the dispersion relation are related to the adiabatic derivatives of the nonlocal energy. This means that our dispersion relation accounts for both local and nonlocal contributions to the total energy of the OCP in a way consistent with thermodynamics.

In thermal equilibrium, it is convenient to work with a parameter that describes the ratio between the average potential Coulomb energy of the moving particles and their average thermal kinetic energy, $\Gamma = q_+^2/4\pi\varepsilon_0 a k_B T$, where T is the temperature, and a is the average interparticle distance defined by $4\pi a^3/3 = 1/n$ [23, 24]. It is known that $g(n, s, |\vec{r}|) = g(\Gamma, |\vec{r}|/a)$, and the expressions for the equilibrium energy E_0 and equilibrium pressure p_0

are as follows, where u is the excess internal energy describing nonlocal contributions.

$$\frac{E_0}{Nk_BT} = \frac{3}{2} + u(\Gamma), \quad \frac{p_0}{nk_BT} = 1 + \frac{u(\Gamma)}{3}. \tag{2.30}$$

When analyzing the dispersion relation of the OCP, the newly introduced variables Γ and a will also oscillate around their respective equilibrium values, Γ_0, a_0, due to their dependence on n, s. Nevertheless, it is convenient to rewrite the longitudinal dispersion law in Eq. (2.29) in terms of normalized variables, so that the dispersion law is parametrized only in terms of Γ_0, similar to E_0, p_0. To do this, one introduces the plasma frequency of the moving particles, ω_p, as $\omega_p^2 = q_+^2 n_0/m\varepsilon_0$, and the normalized wavevector $\vec{q}_0 = \vec{k}a_0$ [29, 30, 31]. To compute the term in Eq. (2.29) that is related to the temperature derivatives, we use the following result from thermodynamics [51]. Note that to compute it, we need knowledge of both E_0 and p_0.

$$\frac{\partial T}{\partial V}\Big|_s = -\frac{(\partial E_0/\partial V|_T + p_0)}{\partial E_0/\partial T|_V} \tag{2.31}$$

As mentioned in the discussion of the energy law, we are interested in the thermodynamic limit, where the number of moving particles $N \to \infty$ and the volume of the system $V \to \infty$. Therefore, it is convenient to work with densities and E_0/N. One can use the chain rule to rewrite derivatives of V in terms of n in the previous equation. Combining this with Eq. (2.30) leads to the following.

$$\frac{n}{T}\frac{\partial T}{\partial n}\Big|_s = \frac{2}{3}\frac{\Big(1 - (\Gamma^2/3)\mathrm{d}(u/\Gamma)/\mathrm{d}\Gamma\Big)}{\Big(1 - (2\Gamma^2/3)\mathrm{d}(u/\Gamma)/\mathrm{d}\Gamma\Big)} = \frac{2}{3}f_1(\Gamma) \tag{2.32}$$

This result also allows us to take derivatives at constant s of functions of Γ. In particular, we have the following, derived from the definition of Γ.

$$n\frac{\partial \Gamma}{\partial n}\Big|_s = n\left(\frac{\partial \Gamma}{\partial n}\Big|_T + \frac{\partial \Gamma}{\partial T}\Big|_n \frac{\partial T}{\partial n}\Big|_s\right) = \frac{\Gamma}{3} - \frac{2\Gamma}{3}f_1(\Gamma) \tag{2.33}$$

To analyze the terms in Eq. (2.29) with integrals of $g - 1$, in addition to the previous identities, we use the fact that $g = g(\Gamma, |\vec{r}|/a)$. To do this, we move the number density derivatives outside of the integrals, change variables inside the integrals to $x = r/a$, and introduce the normalized wavevector $\vec{q} = \vec{k}a$. In this case, the integrals are rewritten in

terms of functions of Γ and $|\vec{q}|$, allowing us to use the following identity, which holds for an arbitrary function $f(\Gamma, |\vec{q}|)$, to perform number density derivatives at constant s. Here, we use Eq. (2.33) and $\partial|\vec{q}|/\partial n|_s = -|\vec{q}|/3n$.

$$n\frac{\partial f}{\partial n}\Big|_s(\Gamma, |\vec{q}|) = \frac{1}{3}\left(\frac{\partial f}{\partial \Gamma}\Big|_{|\vec{q}|}\Gamma\Big(1 - 2f_1(\Gamma)\Big) - \frac{\partial f}{\partial |\vec{q}|}\Big|_\Gamma |\vec{q}|\right) \tag{2.34}$$

Combining all of the computations, we obtain the following longitudinal dispersion relation in Eq. (2.35) in the normalized variables, which indeed depends solely on the equilibrium value Γ_0. The terms appearing in the dispersion relation are given by Eqs. (2.32), (2.36), (2.37), (2.38), and the derivative at a constant value of s is given by Eq. (2.34).

$$\begin{aligned}\left(\frac{\omega_L}{\omega_p}\right)^2(\Gamma_0, |\vec{q}_0|) = 1 + \frac{|\vec{q}_0|^2}{\Gamma_0}f_2(\Gamma_0) + \left(n\frac{\partial j}{\partial n}\Big|_s\right)(\Gamma_0, |\vec{q}_0|) \\ + \left(n\frac{\partial}{\partial n}\left(n\frac{\partial j}{\partial n}\Big|_s\right)\Big|_s\right)(\Gamma_0, |\vec{q}_0|) + h(\Gamma_0, |\vec{q}_0|) + \left(n\frac{\partial h}{\partial n}\Big|_s\right)(\Gamma_0, |\vec{q}_0|),\end{aligned} \tag{2.35}$$

$$f_2(\Gamma) = \frac{1}{3}\left(f_1(\Gamma) + \frac{2}{3}f_1^2(\Gamma) + \frac{\Gamma}{3}\frac{\mathrm{d}f_1}{\mathrm{d}\Gamma}(\Gamma)\Big(1 - 2f_1(\Gamma)\Big)\right), \tag{2.36}$$

$$j(\Gamma, |\vec{q}|) = \frac{|\vec{q}|^2}{2}\int_0^\infty x\Big(g - 1\Big)(\Gamma, x)\mathrm{d}x, \tag{2.37}$$

$$h(\Gamma, |\vec{q}|) = |\vec{q}|\int_0^\infty \Big(g - 1\Big)(\Gamma, x)\sin(|\vec{q}|x)\mathrm{d}x. \tag{2.38}$$

In principle, the longitudinal dispersion relation can now be computed for an arbitrary pair distribution function, $g(\Gamma, |\vec{r}|/a)$. However, it is important to notice that it depends not only on the integrals with respect to the variable $x = |\vec{r}|/a$ but also on the Γ derivatives of such integrals. This implies that, for a precise evaluation of the dispersion law, a pair distribution function should be known precisely as a function of Γ. Precise fits for the excess internal energy in Eq. (2.30), $u(\Gamma)$, are known [26, 27]. However, we are not aware of a precise numerical fit for $g(\Gamma, |\vec{r}|/a)$. For example, a multiparameter fit for the pair distribution function that is accurate for a wide range of Γ values as a function of $x = |\vec{r}|/a$ is known [25]. Nevertheless, the Γ derivative of such a fit is imprecise, as can be confirmed when using it to numerically compute the thermodynamic heat capacity because the obtained results contradict the direct results from Monte Carlo simulations [23, 24, 26]. For other theoretical

approaches, such as QLCA [34, 35], this is not an issue as their predictions do not include Γ derivatives.

To address this issue, we will use an approximation for the pair distribution function that has previously been employed in QLCA and has yielded good results when compared to using the pair distribution function without any approximations [36]. We assume that the pair distribution function, $g(\Gamma, |\vec{r}|/a)$, takes the form of a step function with a value of 0 when $|\vec{r}|/a < (R/a)(\Gamma)$ and 1 when $|\vec{r}|/a > (R/a)(\Gamma)$. Notice that these values have been chosen to be consistent with the behavior of the pair distribution function as $|\vec{r}| \to 0$ and $|\vec{r}| \to \infty$ [23, 24, 25]. More complicated approximations for the pair distribution function are also possible, such as the two-step approximation that has been used to analyze strongly coupled Yukawa fluids [52]. However, in that case, it was noticed that it does not provide a significant improvement over the single-step function approximation [36]. Because of that, in our calculations, we decided to use the single-step function approximation.

To establish the correct dependence on Γ, we compute the equilibrium energy in Eq. (2.20) using this approximation and use Eq. (2.30) to establish the relationship between $(R/a)(\Gamma)$ and $u(\Gamma)$. The latter is known with precision. In particular, in Eq. (2.20), we go to spherical coordinates, change variables to $x = |\vec{r}|/a$, and then apply the assumed form for $g(\Gamma, |\vec{r}|/a)$, along with the definitions of a and Γ. This yields the following result.

$$\frac{E_0}{N} = \frac{3}{2}k_BT - \frac{3}{4}k_BT\Gamma\left(\frac{R}{a}\right)^2(\Gamma) \tag{2.39}$$

When comparing this expression to Eq. (2.30), one can derive the following.

$$\left(\frac{R}{a}\right)(\Gamma) = \sqrt{-\frac{4}{3}\frac{u(\Gamma)}{\Gamma}} \tag{2.40}$$

This step function approximation also simplifies the calculation of the dispersion law. The integrals in Eqs. (2.37), (2.38) can now be evaluated exactly, leading to simpler and more practical expressions while avoiding additional numerical errors resulting from the computation of the integral.

$$j(\Gamma, |\vec{q}|) = -\frac{|\vec{q}|^2}{4}\left(\frac{R}{a}\right)^2(\Gamma), \quad h(\Gamma, |\vec{q}|) = \cos\left(|\vec{q}|\left(\frac{R}{a}\right)(\Gamma)\right) - 1. \tag{2.41}$$

First, let us consider a simple fit $u(\Gamma) = -0.9\Gamma$, which is accurate for very strong coupling where $\Gamma \gg 1$ [27]. For such a fit, where $u(\Gamma)$ is linear in Γ, we can observe from Eq. (2.40) that R/a is independent of Γ. In this case, $R/a = \sqrt{6/5}$. This means that, according to Eq. (2.41), the functions j, h are both independent of Γ. This greatly simplifies taking number density derivatives at constant s as described in Eq. (2.34). Additionally, it is worth noting that for such a fit, $f_1(\Gamma) = 1$ based on Eq. (2.32), as $u(\Gamma)/\Gamma$ is independent of Γ.

For this particular fit, the longitudinal dispersion law in Eq. (2.35), complemented with Eq. (2.36) and the simplified expressions in Eq. (2.41), takes the following form. The first term, proportional to the $|\vec{q}_0|^2$, represents the local and nonlocal parts of the pressure, which are the terms under the gradient in Eq. (2.23). The last two terms arise from the remaining force terms in Eq. (2.23).

$$\left(\frac{\omega_L}{\omega_p}\right)^2 (\Gamma_0, |\vec{q}_0|) = \left(\frac{5}{9\Gamma_0} + \frac{1}{15}\right) |\vec{q}_0|^2 + \cos\left(\sqrt{\frac{6}{5}}|\vec{q}_0|\right) + \sqrt{\frac{2}{15}}|\vec{q}_0| \sin\left(\sqrt{\frac{6}{5}}|\vec{q}_0|\right) \tag{2.42}$$

The results for different values of Γ_0 are presented in Fig. 2.3(a). Several key properties can be observed from the figure. For weak coupling, where $\Gamma_0 = 1$, the dispersion relation resembles the behavior of an ideal gas. However, as Γ_0 increases, the behavior undergoes a dramatic change. At a critical value of $\Gamma_0 = 4.2$, we observe the onset of negative dispersion. In other words, for small values of $|\vec{q}_0|$, it holds true that $\omega_L \leq \omega_p$ instead of $\omega_L \geq \omega_p$. Additionally, as Γ_0 increases, an unstable region emerges, where $\omega_L^2 < 0$.

The simpler fit for $u(\Gamma)$ does not incorporate thermal effects for the nonlocal interaction [27]. Due to this limitation, it is interesting to consider a more precise fit, $u(\Gamma) = -0.9\Gamma + 0.5944\Gamma^{1/3} - 0.2786$, which is accurate for $\Gamma \geq 1$ and includes thermal effects [27]. The results for different values of Γ_0 are presented in Fig. 2.3(b), and one can observe that the results are qualitatively similar to those obtained with the simpler fit, with small quantitative differences. For instance, the onset of negative dispersion is now observed at $\Gamma_0 = 4.9$.

The results for the more precise fit are also compared to the results obtained by QLCA [36] using the same pair distribution function approximation. Additionally, we compare them to the current fluctuation spectra obtained from molecular dynamics simulations, provided by

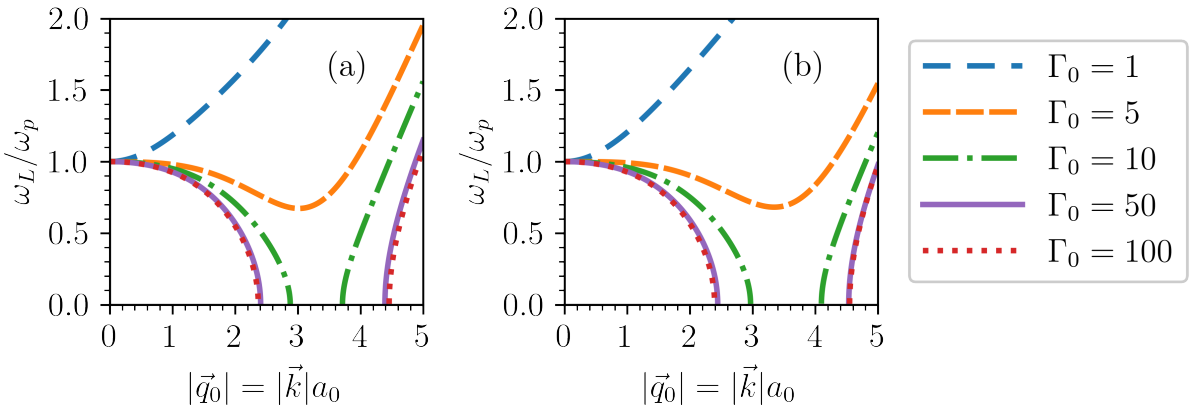

Figure 2.3: The longitudinal dispersion law in the Eulerian approach using normalized variables for different values of Γ_0, as given by Eq. (2.35). The step function approximation for the pair distribution function is assumed, and we use Eqs. (2.32), (2.36), (2.40), (2.41) for a given $u(\Gamma)$ defined in Eq. (2.30). In (a), we set $u(\Gamma) = -0.9\Gamma$, and the corresponding result is given by Eq. (2.42). In (b), we use $u(\Gamma) = -0.9\Gamma + 0.5944\Gamma^{1/3} - 0.2786$.

the authors of Ref. [30], where dispersion laws are identified by the peaks of the spectra. The comparison for the longitudinal dispersion law is presented in Fig. 2.1. It can be observed that for small values of Γ_0, where $\Gamma_0 = 1$ or $\Gamma_0 = 5$, the predicted longitudinal dispersion law reasonably agrees with the results of molecular dynamics simulations, unlike the QLCA result. However, as Γ_0 increases, the predicted dispersion law starts to diverge from the results of the molecular dynamics simulations.

In particular, the latter do not exhibit regions of instability where $\omega_L^2 < 0$. Additionally, the onset of negative dispersion for the predicted dispersion law occurs at $\Gamma_0 = 4.9$, in contrast to the range of values from $\Gamma_0 = 9.5$ to $\Gamma_0 = 10.0$ estimated by the molecular dynamics simulations [30, 31]. Furthermore, the predicted longitudinal dispersion law in the limit as $\Gamma_0 \to \infty$ does not converge to the QLCA result, which is considered accurate in such a limit [36].

The comparison for the transverse dispersion law is presented in Fig. 2.2. It correctly predicts that for small values of the wavevector, there are no transverse waves. However, it fails to predict a result that is known numerically, where at large values of the wavevector,

transverse waves appear and are well-described by QLCA [32].

The issues found for the predicted dispersion laws and their comparison with the results from QLCA and molecular dynamics simulations motivate us to consider an alternative variational approach, where we consider formulating it in the Lagrangian coordinates. It is discussed in the next Section 2.3.

2.3 Lagrangian approach

2.3.1 Equations of motion

Let us assume once again that we are dealing with the OCP, which consists of two species of charged particles. The particles in motion have a charge q_+, while the particles forming the stationary neutralizing background have a charge q_-. However, in this case, we consider a Lagrangian approach that employs Lagrangian coordinates. Similar to the case of Euler equations [45, 46], we assume that the complete set of variables for the hydrodynamic motion comprises solely the displacement field $\vec{x}$. This field represents the current location of a particle in the fluid at time t, given that its position in some conveniently chosen reference state was $\vec{a}$. The choice of a reference state usually depends on the specific problem. For example, one can select the reference positions as the initial positions at the start of the experiment. Alternatively, as is useful in the case of the dispersion law, one can choose them to be the corresponding positions of the particles in thermal equilibrium.

In the Lagrangian coordinates, the number density n and specific entropy s are not independent hydrodynamic functions that need to be solved. Instead, they can be expressed in terms of the displacement field $\vec{x}$ and time-independent number density n^{ref} and specific entropy s^{ref} that correspond to the reference state. The continuity equations, as given in Eq. (2.1), are rewritten in Lagrangian variables as follows [45, 46].

$$n(\vec{x},t) = \frac{n^{\mathrm{ref}}}{\det\left(\partial\vec{x}/\partial\vec{a}\right)}, \quad s(\vec{x},t) = s^{\mathrm{ref}}. \tag{2.43}$$

As discussed in the Eulerian approach, our objective is to formulate a variational principle

with a nonlocal Lagrangian density for the OCP that includes the effects of strong coupling. In the case of Lagrangian coordinates, this formulation should yield an equation of motion for $\vec{x}$.

As in the case of the Eulerian approach, we may consider the Lagrangian given in Eq. (2.2), which can be rewritten in Lagrangian coordinates by changing the variables under the integral from $\vec{x}, \vec{x}'$ to the reference state coordinates $\vec{a}, \vec{a}'$. For the stationary particles, we can choose an independent reference state. For convenience, we will choose it to be the one where $\vec{a}$ represents the initial position of the stationary particle, making $\vec{x} = \vec{a}$. Additionally, it is useful to introduce the number density of the stationary neutralizing background in the reference state, n_-^{ref}.

In the case of Lagrangian variables, the number density n and the specific entropy s are not independent variables, eliminating the need to introduce constraint fields α, β. So, the Lagrangian used in the Eulerian approach is as follows when rewritten in Lagrangian coordinates, where the notation $(n^{\mathrm{ref}})'$ now indicates that the function n^{ref} is evaluated at $\vec{a}'$ instead of $\vec{a}$.

$$\begin{aligned} L &= \int \mathcal{L}_1 \mathrm{d}\vec{a} + \iint \mathcal{L}_2 \mathrm{d}\vec{a}\mathrm{d}\vec{a}' \\ &= \int \left(\frac{1}{2} m n^{\mathrm{ref}} \left(\frac{\partial \vec{x}}{\partial t} \right)^2 - n^{\mathrm{ref}} f\left(\frac{n^{\mathrm{ref}}}{\det\left(\partial \vec{x}/\partial \vec{a}\right)}, s^{\mathrm{ref}} \right) \right) \mathrm{d}\vec{a} \\ &+ \iint \Big(- n^{\mathrm{ref}} (n^{\mathrm{ref}})' F\left(\frac{n^{\mathrm{ref}}}{\det\left(\partial \vec{x}/\partial \vec{a}\right)}, \frac{(n^{\mathrm{ref}})'}{\det\left(\partial \vec{x}'/\partial \vec{a}'\right)}, s^{\mathrm{ref}}, (s^{\mathrm{ref}})', |\vec{x} - \vec{x}'| \right) \\ &\quad - n^{\mathrm{ref}} (n_-^{\mathrm{ref}})' \phi_{+-}(|\vec{x} - \vec{a}'|) - \frac{1}{2} n_-^{\mathrm{ref}} (n_-^{\mathrm{ref}})' \phi_{--}(|\vec{a} - \vec{a}'|) \Big) \mathrm{d}\vec{a}\mathrm{d}\vec{a}' \end{aligned} \tag{2.44}$$

It is not surprising that when one performs the variations, the equation of motion for $\vec{x}$, which arises from the Lagrangian in Eq. (2.44) and is subsequently rewritten in Eulerian variables, is identical to Eq. (2.7). This is because the only difference in the calculations lies in using a different coordinate system, while the form of the Lagrangian remains the same. However, in Lagrangian variables, it becomes evident how one can generalize the Lagrangian shown in Eq. (2.44). In particular, each particle has two positions available: the position of the particle in the laboratory frame $\vec{x}$ and its reference position $\vec{a}$. Therefore, one can

assume that the function F also depends on $\vec{a}, \vec{a}'$. This extension does not contradict any of the conservation laws but allows for a different model for the OCP, as we will discuss next.

As an alternative to the Lagrangian given in Eq. (2.44), we propose the following Lagrangian.

$$\begin{aligned} L^{\mathrm{L}} &= \int \mathcal{L}_1^{\mathrm{L}} \mathrm{d}\vec{a} + \iint \mathcal{L}_2^{\mathrm{L}} \mathrm{d}\vec{a}\mathrm{d}\vec{a}' \\ &= \int \left(\frac{1}{2} m n^{\mathrm{ref}} \left(\frac{\partial \vec{x}}{\partial t} \right)^2 - n^{\mathrm{ref}} f \left(\frac{n^{\mathrm{ref}}}{\det\left(\partial \vec{x}/\partial \vec{a}\right)}, s^{\mathrm{ref}} \right) \right) \mathrm{d}\vec{a} \\ + \iint \Big(&- n^{\mathrm{ref}} (n^{\mathrm{ref}})' F \left(\frac{n^{\mathrm{ref}}}{\det\left(\partial \vec{x}/\partial \vec{a}\right)}, \frac{(n^{\mathrm{ref}})'}{\det\left(\partial \vec{x}'/\partial \vec{a}'\right)}, s^{\mathrm{ref}}, (s^{\mathrm{ref}})', |\vec{x} - \vec{x}'|, \vec{a}, \vec{a}' \right) \\ &- n^{\mathrm{ref}} (n_-^{\mathrm{ref}})' \phi_{+-}(|\vec{x} - \vec{a}'|) - \frac{1}{2} n_-^{\mathrm{ref}} (n_-^{\mathrm{ref}})' \phi_{--}(|\vec{a} - \vec{a}'|) \Big) \mathrm{d}\vec{a}\mathrm{d}\vec{a}' \end{aligned} \tag{2.45}$$

As in the case of Eulerian coordinates, one must be cautious when performing variations of the nonlocal terms, but the strategy is analogous. To carry out the variations, change variables under the integral from $(\vec{a}, \vec{a}')$ to $(\vec{a}', \vec{a})$, which has a unit Jacobian. It is once again useful to introduce the notation f^T for each function f that indicates taking f but now, as we are working in Lagrangian coordinates, replacing all occurrences of $\vec{a}$ with $\vec{a}'$ and all occurrences of $\vec{a}'$ with $\vec{a}$. For example, $f^T(\vec{x}, \vec{x}') = f(\vec{x}', \vec{x})$. In this case, for any argument Ψ of a nonlocal function and any functions f, g, we have that $(fg)^T = f^T g^T$, and $(\partial_{\Psi'} f)^T = \partial_{\Psi}(f^T)$. Additionally, we can use the following property of determinants [45] that holds for all directions i, j.

$$\sum_{j=1}^{3} \frac{\partial}{\partial a_j} \left(\frac{\partial(\det\left(\partial \vec{x}/\partial \vec{a}\right))}{\partial(\partial_j x_i)} \right) = 0 \tag{2.46}$$

Combining these results, we obtain the following equation of motion for each of the directions of $\vec{x}$ parametrized by $i = 1, 2, 3$. At this point, functions f and F are still arbitrary. Again, notice that, unlike in the Eulerian case, there are no constraint functions in the Lagrangian given in Eq. (2.45). Therefore, the resulting equations of motion are

already in their final form, and no additional manipulations are needed.

$$
\begin{aligned}
m n^{\mathrm{ref}} \frac{\partial^2 x_i}{\partial t^2} = &- \sum_{j=1}^{3} \frac{\partial(\det(\partial\vec{x}/\partial\vec{a}))}{\partial(\partial_j x_i)} \frac{\partial}{\partial a_j} \Bigg(n^2 \frac{\partial f}{\partial n}\Big|_s \\
&+ \int n^2 (n^{\mathrm{ref}})' \frac{\partial(F+F^T)}{\partial n}\Big|_{n',s,s',|\vec{x}-\vec{x}'|,\vec{a},\vec{a}'} \mathrm{d}\vec{a}' \Bigg) \\
- \int \Bigg(& n^{\mathrm{ref}} (n^{\mathrm{ref}})' \frac{\partial(F+F^T)}{\partial x_i}\Big|_{n,n',s,s',\vec{x}',\vec{a},\vec{a}'} + n^{\mathrm{ref}} (n_-^{\mathrm{ref}})' \frac{\partial \phi_{+-}}{\partial x_i}\Big|_{\vec{a}'} \Bigg) \mathrm{d}\vec{a}'
\end{aligned}
\tag{2.47}
$$

To check the consistency with the Eulerian approach, it can be demonstrated that if F does not depend on $\vec{a}, \vec{a}'$, then Eq. (2.47) can be rewritten in Eulerian variables by changing coordinates from $(\vec{a}, \vec{a}')$ to $(\vec{x}, \vec{x}')$. This transformation results in exactly Eq. (2.7). Here, Eq. (2.43) is used, along with the following identity for an arbitrary function f, which is obtained from the chain rule [45] and holds for all directions i, j.

$$
\sum_{j=1}^{3} \frac{\partial(\det(\partial\vec{x}/\partial\vec{a}))}{\partial(\partial_j x_i)} \frac{\partial f}{\partial a_j} = \det\left(\frac{\partial\vec{x}}{\partial\vec{a}}\right) \frac{\partial f}{\partial x_i} \tag{2.48}
$$

2.3.2 Conservation laws

Let us consider the momentum and energy conservation laws of our theory in the Lagrangian approach. As in the Eulerian case, the energy conservation law will be important because the expression for the conserved energy coming from the variational principle can be computed in equilibrium and compared to the expression found in thermodynamics. This ensures that the Lagrangian approach is also consistent with thermal equilibrium and allows to identify functions in the variational principle in terms of the thermodynamic quantities. Such comparison also shows how the Lagrangian approach is different from the previously described Eulerian approach.

We now examine the momentum conservation law in each of the directions, $i = 1, 2, 3$. As in the Eulerian case, the momentum conservation law now also relies on the observation that in Eq. (2.45), the local part of the Lagrangian density, $\mathcal{L}_1^{\mathrm{L}}$, does not depend on $\vec{x}$ explicitly but only on its derivatives. Furthermore, the term with F in the nonlocal part of this Lagrangian density, $\mathcal{L}_2^{\mathrm{L}}$, depends on $\vec{x}, \vec{x}'$ only in a translationally invariant combination,

$\vec{x}-\vec{x}'$, as well as on their derivatives. It is important to note that it is not true that $\mathcal{L}_2^{\mathrm{L}}$ depends explicitly on $\vec{x},\vec{x}'$ in a translationally invariant way, as ϕ_{+-} depends on $\vec{x}-\vec{a}'$.

In the Lagrangian variables, the variational principle is applied to the displacement field $\vec{x}$ to obtain the equations of motion. Therefore, the momentum conservation law is determined by the equations of motion obtained in Eq. (2.47). To show that it nearly takes the form of a conservation law, we rewrite it by considering that n^{ref} does not depend on time and applying the product rule along with Eq. (2.46).

$$\begin{aligned}
&\frac{\partial}{\partial t}\left(mn^{\mathrm{ref}}\frac{\partial x_i}{\partial t}\right)+\sum_{j=1}^{3}\frac{\partial}{\partial a_j}\left(\frac{\partial(\det\left(\partial\vec{x}/\partial\vec{a}\right))}{\partial(\partial_j x_i)}n^2\frac{\partial f}{\partial n}\Big|_s\right.\\
&\left.+\frac{\partial(\det\left(\partial\vec{x}/\partial\vec{a}\right))}{\partial(\partial_j x_i)}\int n^2(n^{\mathrm{ref}})'\frac{\partial(F+F^T)}{\partial n}\Big|_{n',s,s',|\vec{x}-\vec{x}'|,\vec{a},\vec{a}'}\mathrm{d}\vec{a}'\right)\\
&=-\int\left(n^{\mathrm{ref}}(n^{\mathrm{ref}})'\frac{\partial(F+F^T)}{\partial x_i}\Big|_{n,n',s,s',\vec{x}',\vec{a},\vec{a}'}+n^{\mathrm{ref}}(n_-^{\mathrm{ref}})'\frac{\partial\phi_{+-}}{\partial x_i}\Big|_{\vec{a}'}\right)\mathrm{d}\vec{a}'
\end{aligned}\tag{2.49}$$

The momentum conservation law, as given in Eq. (2.49), allows us to define the total momentum $\vec{P}$ of the particles moving in the OCP and examine how it changes over time. To accomplish this, integrate Eq. (2.49) with respect to $\vec{a}$ and use integration by parts. For further simplification of nonlocal terms, employ the properties that hold for all functions f,g, $(f^T)^T=f,(f+g)^T=f^T+g^T,(fg)^T=f^Tg^T$, and note that the integral of f over $\vec{a},\vec{a}'$ is the same as the integral of f^T. Additionally, use an analogous identity as in Eq. (2.10), where F now depends also on $\vec{a},\vec{a}'$ as well. By combining these results with the assumption that F depends explicitly on $\vec{x},\vec{x}'$ only through the combination $\vec{x}-\vec{x}'$, we get that the following integral is zero.

$$\iint n^{\mathrm{ref}}(n^{\mathrm{ref}})'\frac{\partial(F+F^T)}{\partial x_i}\Big|_{n,n',s,s',\vec{x}',\vec{a},\vec{a}'}\mathrm{d}\vec{a}\mathrm{d}\vec{a}'=0\tag{2.50}$$

The time evolution of the momentum $\vec{P}$ in each direction is provided below. Here, it is evident that the momentum of moving particles may not be conserved and can change due to the force exerted by the stationary neutralizing background.

$$\frac{\mathrm{d}P_i}{\mathrm{d}t}=\frac{\mathrm{d}}{\mathrm{d}t}\left(\int mn^{\mathrm{ref}}\frac{\partial x_i}{\partial t}\mathrm{d}\vec{a}\right)=-\iint n^{\mathrm{ref}}(n_-^{\mathrm{ref}})'\frac{\partial\phi_{+-}}{\partial x_i}\Big|_{\vec{a}'}\mathrm{d}\vec{a}\mathrm{d}\vec{a}'\tag{2.51}$$

One can demonstrate that the expression for momentum in the Lagrangian approach is the same as in the Eulerian approach, as given by Eq. (2.12), by changing the coordinates under the integral from $\vec{a}$ to $\vec{x}$ and using the definition of n provided by Eq. (2.43). Additionally, as in the Eulerian case, the momentum of moving particles is conserved when the neutralizing background is both uniform and infinite. This can be shown from Eq. (2.51) by noting that ϕ_{+-} depends on $\vec{x}, \vec{a}'$ only through the combination $\vec{x} - \vec{a}'$ and by applying integration by parts.

Now, let us explore the energy conservation law, which we will use to match functions in the variational principle to the thermodynamic quantities. The energy conservation law is based on the observation that in the proposed Lagrangian in Eq. (2.45), both the local part of the Lagrangian density, $\mathcal{L}_1^{\mathrm{L}}$, and the nonlocal part, $\mathcal{L}_2^{\mathrm{L}}$, do not explicitly depend on time t.

To derive the energy conservation law for our nonlocal variational principle, we follow a similar approach to that used in the case of local variational principles [12, 49] and in the Eulerian approach. We employ the chain rule to expand the full derivatives of $\mathcal{L}_1^{\mathrm{L}}$ and, guided by the equation of motion provided in Eq. (2.47), $(1/2)\int(\mathcal{L}_2^{\mathrm{L}}+(\mathcal{L}_2^{\mathrm{L}})^T)\mathrm{d}\vec{a}'$ with respect to t. These calculations are then combined and simplified using all the equations of motion obtained from the variational principle, along with the product rule. Similar to the case of equations of motion, computations in the Lagrangian coordinates offer the advantage over Eulerian coordinates as they require no additional manipulations for the resulting energy law, as there are no constraint fields.

$$\frac{\partial \mathcal{E}^{\mathrm{L}}}{\partial t} + \sum_{j=1}^{3} \frac{\partial J_j^{\mathrm{L}}}{\partial a_j} = \sigma^{\mathrm{L}}, \tag{2.52}$$

$$\begin{aligned} \mathcal{E}^{\mathrm{L}} = \frac{1}{2} m n^{\mathrm{ref}} \left(\frac{\partial \vec{x}}{\partial t}\right)^2 + n^{\mathrm{ref}} f + \frac{1}{2} \int \Bigg(& n^{\mathrm{ref}} (n^{\mathrm{ref}})'(F + F^T) \\ & + n^{\mathrm{ref}} (n_-^{\mathrm{ref}})' \phi_{+-}(|\vec{x} - \vec{a}'|) + (n^{\mathrm{ref}})' n_-^{\mathrm{ref}} \phi_{+-}(|\vec{x}' - \vec{a}|) \\ & + n_-^{\mathrm{ref}} (n_-^{\mathrm{ref}})' \phi_{--}(|\vec{a} - \vec{a}'|) \Bigg) \mathrm{d}\vec{a}', \end{aligned} \tag{2.53}$$

$$J_j^{\mathrm{L}} = \sum_{i=1}^{3} \frac{\partial x_i}{\partial t} \frac{\partial(\det(\partial\vec{x}/\partial\vec{a}))}{\partial(\partial_j x_i)} \left(n^2 \frac{\partial f}{\partial n}\Big|_s + \int n^2 (n^{\mathrm{ref}})' \frac{\partial(F+F^T)}{\partial n}\Big|_{n',s,s',|\vec{x}-\vec{x}'|,\vec{a},\vec{a}'} \mathrm{d}\vec{a}' \right), \tag{2.54}$$

$$\begin{aligned}
\sigma^{\mathrm{L}} = \frac{1}{2} \sum_{i=1}^{3} \sum_{j=1}^{3} \int \Bigg(& n^2 (n^{\mathrm{ref}})' \frac{\partial(F+F^T)}{\partial n}\Big|_{n',s,s',|\vec{x}-\vec{x}'|,\vec{a},\vec{a}'} \frac{\partial(\det(\partial\vec{x}/\partial\vec{a}))}{\partial(\partial_j x_i)} \frac{\partial^2 x_i}{\partial a_j \partial t} \\
& - n^{\mathrm{ref}} (n')^2 \frac{\partial(F+F^T)}{\partial n'}\Big|_{n,s,s',|\vec{x}-\vec{x}'|,\vec{a},\vec{a}'} \frac{\partial(\det(\partial\vec{x}'/\partial\vec{a}'))}{\partial(\partial'_j x'_i)} \frac{\partial^2 x'_i}{\partial a'_j \partial t} \Bigg) \mathrm{d}\vec{a}' \\
& + \frac{1}{2} \sum_{i=1}^{3} \int n^{\mathrm{ref}} (n^{\mathrm{ref}})' \Bigg(\frac{\partial(F+F^T)}{\partial x'_i}\Big|_{n,n',s,s',\vec{x},\vec{a},\vec{a}'} \frac{\partial x'_i}{\partial t} \\
& - \frac{\partial(F+F^T)}{\partial x_i}\Big|_{n,n',s,s',\vec{x}',\vec{a},\vec{a}'} \frac{\partial x_i}{\partial t} \Bigg) \mathrm{d}\vec{a}' + \frac{1}{2} \sum_{i=1}^{3} \int \Bigg((n^{\mathrm{ref}})' n_-^{\mathrm{ref}} \frac{\partial \phi_{+-}}{\partial x'_i}\Big|_{\vec{a}} \frac{\partial x'_i}{\partial t} \\
& - n^{\mathrm{ref}} (n_-^{\mathrm{ref}})' \frac{\partial \phi_{+-}}{\partial x_i}\Big|_{\vec{a}'} \frac{\partial x_i}{\partial t} \Bigg) \mathrm{d}\vec{a}'.
\end{aligned} \tag{2.55}$$

Note that the energy conservation law in Eq. (2.52) can also be derived by directly computing the time derivative of the correct energy density given in Eq. (2.53) using the equations of motion, as shown in Eq. (2.47). To simplify, we apply the chain rule, use the definition of n as given in Eq. (2.43), and consider that in the reference state $n^{\mathrm{ref}}, s^{\mathrm{ref}}, n_-^{\mathrm{ref}}$ are all independent of time. Afterward, we can combine terms using the product rule and apply the identity regarding determinants, as shown in Eq. (2.46). Similar to the Eulerian case, the drawback of this approach is the requirement to know the correct expression for the energy density.

In the case where the function F does not depend on $\vec{a}, \vec{a}'$, one can demonstrate that the energy law in the Lagrangian approach can be rewritten in Eulerian variables by changing coordinates from $(\vec{a}, \vec{a}')$ to $(\vec{x}, \vec{x}')$. This results in precisely the same energy law as in the Eulerian approach, as given by Eqs. (2.14), (2.15), (2.16), and (2.17). One has to be careful as $\vec{a}$ might represent the reference state position of either moving particles or the neutralizing stationary background.

For the term in Eq. (2.53) with ϕ_{--}, it is worth noting that due to n_-^{ref} being independent of time, its time derivative is zero, just like for the analogous term in the Eulerian energy density in Eq. (2.15). That means that terms with ϕ_{--} can be added or removed as needed. For the term in Eq. (2.53) with $(n^{\mathrm{ref}})' n_-^{\mathrm{ref}}$, one can compute the time derivative using the chain

rule. This computation results in the following, which corresponds to a term in Eq. (2.55).

$$\frac{\partial}{\partial t}\left(\frac{1}{2}\int\left((n^{\mathrm{ref}})'n_-^{\mathrm{ref}}\phi_{+-}(|\vec{x}'-\vec{a}|)\right)\mathrm{d}\vec{a}'\right)=\frac{1}{2}\sum_{i=1}^{3}\int\left((n^{\mathrm{ref}})'n_-^{\mathrm{ref}}\frac{\partial\phi_{+-}}{\partial x_i'}\Big|_{\vec{a}}\frac{\partial x_i'}{\partial t}\right)\mathrm{d}\vec{a}' \tag{2.56}$$

Due to this identity, change of variables can be carried out independently for these two terms, separate from the others. To achieve this, switch from $\vec{a}$ to $\vec{x}$ by using the assumed displacement field for the neutralizing stationary background, where $\vec{x}=\vec{a}$. Consequently, we also have $n_-=n_-^{\mathrm{ref}}$. As for the integrals, perform variable transformations from $\vec{a}'$ to $\vec{x}'$ using the displacement field of the moving particles and make use of Eq. (2.43).

For all the other terms, replace n^{ref} in terms of n using Eq. (2.43). Change from $\vec{a}$ to $\vec{x}$ by using the displacement field of the moving particles, and switch from $\vec{a}'$ to $\vec{x}'$ using either the displacement field of the moving particles or that of the neutralizing stationary background, where $\vec{x}'=\vec{a}'$ and $n_-^{\mathrm{ref}}=n_-$. To simplify these terms, apply the chain and product rules, along with the properties of determinants given in Eqs. (2.46), (2.48), and the following property [53], where $\vec{v}$ represents Eulerian velocity, and $\vec{\nabla}$ denotes the gradient with respect to $\vec{x}$.

$$\frac{\partial}{\partial t}\left(\det\left(\frac{\partial\vec{x}}{\partial\vec{a}}\right)\right)=\det\left(\frac{\partial\vec{x}}{\partial\vec{a}}\right)(\vec{\nabla}\cdot\vec{v}) \tag{2.57}$$

The energy conservation law, as given in Eq. (2.52), allows us to define the energy E^{L} in the Lagrangian approach for the OCP and examine how it changes over time. To achieve this, we integrate this equation with respect to $\vec{a}$ and employ integration by parts. To further simplify nonlocal terms, we use the following properties: for all functions f,g, we have $(f^T)^T=f,(f+g)^T=f^T+g^T,(fg)^T=f^Tg^T$. Additionally, the integral of f over $\vec{a},\vec{a}'$ is the same as the integral of f^T. Moreover, for any argument Ψ of a nonlocal function, $(\partial_{\Psi'}f)^T=\partial_{\Psi}(f^T)$. To simplify nonlocal terms with ϕ_{+-}, we use the definition of transpose. In the following, the energy density $\mathcal{E}^{\mathrm{L}}$ is as defined in Eq. (2.53).

$$\frac{\mathrm{d}E^{\mathrm{L}}}{\mathrm{d}t}=\frac{\mathrm{d}}{\mathrm{d}t}\left(\int\mathcal{E}^{\mathrm{L}}\mathrm{d}\vec{a}\right)=0 \tag{2.58}$$

It can be shown that if the nonlocal function F does not depend on $\vec{a},\vec{a}'$, the expression for the conserved energy in the Lagrangian approach is identical to the one in the Eulerian

approach, as given by Eq. (2.18). To demonstrate this, change the variables inside the integrals from $(\vec{a}, \vec{a}')$ to $(\vec{x}, \vec{x}')$, apply the continuity equation given in Eq. (2.43), and note that for the neutralizing stationary background, the reference state was selected so that $\vec{x} = \vec{a}$ and, consequently, $n_- = n_-^{\text{ref}}$.

Let us now consider equilibrium solutions and calculate the value of the energy, E^{L}, in a thermodynamic equilibrium. In the Lagrangian case, the only time-dependent hydrodynamic function is the displacement of the moving particles, $\vec{x}$. We choose a reference state for the moving particles where $\vec{a}$ represents the equilibrium position of a given particle, or equivalently, its initial position, as in thermal equilibrium there is no macroscopic motion. Therefore, $\vec{x} = \vec{a}$ for all particles at all times. This also implies that the number density and specific entropy of the moving particles in the reference state are their equilibrium number density and equilibrium specific entropy, which are assumed to be uniform and time-independent with values $n^{\text{ref}} = n_0, s^{\text{ref}} = s_0$.

Similar to the Eulerian case, to fully specify the value of the energy in equilibrium, we assume that the number density of the stationary neutralizing background is uniform, with a value $n_-^{\text{ref}} = n_{-,0}$. We also apply the charge neutrality condition $q_+ n_0 + q_- n_{-,0} = 0$, which, as discussed before, is consistent with the experiments. In the thermodynamic limit, where the number of moving particles $N \to \infty$ and the volume of the system $V \to \infty$ while the number density is fixed, the equilibrium energy of the OCP diverges. Therefore, we consider the equilibrium energy per particle, E_0/N.

From Eqs. (2.53), (2.58), we obtain the following result. Simplification occurs when one uses the assumed form of the potential $\phi_{ij}(r) = q_i q_j / 4\pi\varepsilon_0 r$, where i, j are the corresponding species of the particles, and r is the distance between the particles. For integrals involving ϕ_{+-}, ϕ_{--}, one can change variables to $\vec{R} = (\vec{a} + \vec{a}')/2, \vec{r} = \vec{a} - \vec{a}'$, which has a unit Jacobian.

$$\begin{aligned} \frac{E_0}{N} = f(n_0, s_0) + \frac{N}{2V^2} \iint (F + F^T)(n_0, n_0, s_0, s_0, |\vec{a} - \vec{a}'|, \vec{a}, \vec{a}') \mathrm{d}\vec{a} \mathrm{d}\vec{a}' \\ - \frac{n_0}{2} \int \frac{q_+^2}{4\pi\varepsilon_0 |\vec{r}|} \mathrm{d}\vec{r} \end{aligned} \tag{2.59}$$

This expression can be compared to the expression for the thermodynamic equilibrium

energy of the OCP per moving particle, E_{th}/N, as given in Eq. (2.20). It is important to note that in thermodynamics, the nonlocal integral term depends solely on $\vec{r} = |\vec{a} - \vec{a}'|$. Therefore, to maintain consistency with this result, we modify our assumption from F depending on $\vec{a}, \vec{a}'$ to instead depend on the combination $|\vec{a} - \vec{a}'|$. Consequently, the integral involving $F + F^T$ in Eq. (2.59) can also be simplified by changing variables to $\vec{R} = (\vec{a} + \vec{a}')/2, \vec{r} = \vec{a} - \vec{a}'$.

When comparing the result to Eq. (2.20), we derive the following constraints on the functions f, F. Here, we can use the fact that $F^T(n_0, n_0, s_0, s_0, |\vec{r}|, |\vec{r}|) = F(n_0, n_0, s_0, s_0, |\vec{r}|, |\vec{r}|)$, directly from the definition.

$$f(n_0, s_0) = \frac{3}{2} k_B T(n_0, s_0), \quad F(n_0, n_0, s_0, s_0, |\vec{r}|, |\vec{r}|) = \frac{q_+^2}{8\pi\varepsilon_0 |\vec{r}|} g(n_0, s_0, |\vec{r}|). \tag{2.60}$$

In the Lagrangian approach, we encounter the same issue as we did in the Eulerian approach, namely that the constraint in Eq. (2.60) uniquely determines the function f but not F. This occurs because F is specified by this constraint only for values when n is equal to n' and when s is equal to s'. As discussed previously, we address this by modifying our choice of F to a more restrictive one that depends solely on $n, s, |\vec{x} - \vec{x}'|, |\vec{a} - \vec{a}'|$.

However, in the Lagrangian approach, this still does not uniquely determine F due to its dependence on $\vec{a}, \vec{a}'$ because the constraint is specified only for the case when $|\vec{x} - \vec{x}'|$ is equal to $|\vec{a} - \vec{a}'|$. Now, let us consider four simple possible options for F that are consistent with the equilibrium constraint, but they differ in their dependence on $|\vec{x} - \vec{x}'|$ and $|\vec{a} - \vec{a}'|$.

$$F(n, s, |\vec{x} - \vec{x}'|, |\vec{a} - \vec{a}'|) = \frac{q_+^2}{8\pi\varepsilon_0 |\vec{x} - \vec{x}'|} g(n, s, |\vec{x} - \vec{x}'|), \tag{2.61}$$

$$F(n, s, |\vec{x} - \vec{x}'|, |\vec{a} - \vec{a}'|) = \frac{q_+^2}{8\pi\varepsilon_0 |\vec{x} - \vec{x}'|} g(n, s, |\vec{a} - \vec{a}'|), \tag{2.62}$$

$$F(n, s, |\vec{x} - \vec{x}'|, |\vec{a} - \vec{a}'|) = \frac{q_+^2}{8\pi\varepsilon_0 |\vec{a} - \vec{a}'|} g(n, s, |\vec{x} - \vec{x}'|), \tag{2.63}$$

$$F(n, s, |\vec{x} - \vec{x}'|, |\vec{a} - \vec{a}'|) = \frac{q_+^2}{8\pi\varepsilon_0 |\vec{a} - \vec{a}'|} g(n, s, |\vec{a} - \vec{a}'|). \tag{2.64}$$

The first option, as provided in Eq. (2.61), exactly corresponds to the function F that we considered in the Eulerian approach and will result in the same equations of motion. In

contrast, the third and fourth options, given in Eqs. (2.63), (2.64), under the assumption of weak coupling, where $g(n, s, |\vec{r}|) = 1$, will yield $\partial(F + F^T)/\partial x_i = 0$. Consequently, these options will not generate the nonlocal electrostatic force between the moving particles, as described in Eq. (2.47). Therefore, we now turn our attention to the second option provided in Eq. (2.62). In this case, we can rewrite the equations of motion, as given in Eq. (2.47), by using the fact that $\phi_{ij}(r) = q_i q_j / 4\pi\varepsilon_0 r$, where i, j represent the corresponding species of the particles, and r represents the distance between the particles.

$$\begin{aligned} mn^{\text{ref}} \frac{\partial^2 x_i}{\partial t^2} = -\sum_{j=1}^{3} \frac{\partial(\det(\partial\vec{x}/\partial\vec{a}))}{\partial(\partial_j x_i)} \frac{\partial}{\partial a_j} \Bigg(& \frac{3}{2} k_B n^2 \frac{\partial T}{\partial n}\Big|_s \\ & + \frac{q_+^2}{8\pi\varepsilon_0} \int \frac{n^2 (n^{\text{ref}})'}{|\vec{x} - \vec{x}'|} \frac{\partial g}{\partial n}\Big|_{s, |\vec{a} - \vec{a}'|} \mathrm{d}\vec{a}' \Bigg) \\ - \frac{q_+ n^{\text{ref}}}{4\pi\varepsilon_0} \int \Bigg(& q_+ (n^{\text{ref}})' \frac{(g + g^T)}{2} \frac{\partial}{\partial x_i} \left(\frac{1}{|\vec{x} - \vec{x}'|} \right) \Big|_{\vec{x}'} \\ & + q_- (n_-^{\text{ref}})' \frac{\partial}{\partial x_i} \left(\frac{1}{|\vec{x} - \vec{a}'|} \right) \Big|_{\vec{a}'} \Bigg) \mathrm{d}\vec{a}' \end{aligned} \tag{2.65}$$

As one can observe from this equation, the equations of motion in the Lagrangian approach differ from those in the Eulerian approach, as given by Eq. (2.23), due to the nonlocal force term. In this term, now $(g + g^T)/2$ is no longer inside the derivative with respect to $\vec{x}$. Therefore, it is possible to generate the vorticity required for transverse waves.

2.3.3 Dispersion laws

While discussing the energy conservation law, we explored equilibrium solutions, where the reference state for the moving particles is chosen such that $\vec{a}$ represents the position of a particle in thermal equilibrium, and as a result, $\vec{x} = \vec{a}$ at all times. Additionally, the number density and specific entropy of the moving particles in this reference state correspond to thermal equilibrium, where they are assumed to be uniform and time-independent, with values $n^{\text{ref}} = n_0$, $s^{\text{ref}} = s_0$. The stationary neutralizing background also has a uniform number density in the reference state corresponding to thermal equilibrium, with a value $n_-^{\text{ref}} = n_{-,0}$. This value is related to n_0 through the charge neutrality assumption $q_+ n_0 + q_- n_{-,0} = 0$.

Now, we would like to examine the linearized equations of motion that correspond to the OCP being close to thermodynamic equilibrium. In that scenario, we assume the following form for the displacement field $\vec{x}$, where $\vec{\xi}$ denotes the first-order correction.

$$\vec{x} = \vec{a} + \vec{\xi}(\vec{a}, t) \tag{2.66}$$

With this assumption about $\vec{x}$, we will expand the equations of motion given in Eq. (2.65) up to the first order. However, let us first consider these equations of motion and determine whether they are satisfied for the proposed equilibrium solution.

The left-hand side of Eq. (2.65) is zero because $\vec{x} = \vec{a}$ does not depend on time. On the right-hand side, the sum over derivatives with respect to a_j is zero because the function for which this derivative is taken does not depend on $\vec{a}$. To see this, we can use the continuity equations provided in Eq. (2.43), along with the result that for $\vec{x} = \vec{a}$, we have $\det(\partial\vec{x}/\partial\vec{a}) = 1$. This leads to the conclusion that $n = n_0, s = s_0$.

For the integral, we notice that the functions inside it only depend on $\vec{r} = \vec{a} - \vec{a}'$, so we can eliminate the dependence on $\vec{a}$ by changing the integration variable to $\vec{r}$. To demonstrate that the nonlocal force is zero, we directly perform derivatives with respect to x_i and use the equilibrium results along with $n = n_0, s = s_0$ to show that the functions inside the integral depend on $\vec{a}, \vec{a}'$ only through the combination $\vec{r} = \vec{a} - \vec{a}'$. After changing the integration variable to $\vec{r}$, we can use the fact that the function inside the integral is odd with respect to r_i.

Let us now consider the linearized equations. Since the equations of motion given in Eq. (2.65) depend on n, s, it is useful to expand the continuity equations, as given in Eq. (2.43), up to the first order.

$$n(\vec{x}, t) = n_0(1 - \vec{\nabla} \cdot \vec{\xi}) + ..., \quad s(\vec{x}, t) = s_0. \tag{2.67}$$

Now, let us expand the equations of motion provided in Eq. (2.65) up to the first order. The derivatives of $\det(\partial\vec{x}/\partial\vec{a})$ can be expanded through direct computation. Other terms can be simplified using Eq. (2.67), $q_+ n_0 + q_- n_{-,0} = 0$, as well as the fact that for any function

f depending solely on $\vec{x}, \vec{x}'$ through the combination $\vec{x} - \vec{x}'$, we have $\partial f/\partial x_i = -\partial f/\partial x_i'$. For some integrals, it is useful to change the integration variable to $\vec{r} = \vec{a} - \vec{a}'$. Additionally, we reintroduce the notation where the subscript "0" signifies that a function is evaluated at equilibrium values. Using this notation, we can further simplify the result by using $g_0 = (g^T)_0$ and $(\partial g/\partial n)_0 = (\partial g^T/\partial n')_0$.

$$\begin{aligned} m\frac{\partial^2 \xi_i}{\partial t^2} = \frac{\partial(\vec{\nabla}\cdot\vec{\xi})}{\partial a_i}\Bigg(&\left[\frac{\partial}{\partial n}\left(\frac{3}{2}k_B n^2 \frac{\partial T}{\partial n}\Big|_s\right)\Big|_s\right]_0 \\ &+\frac{q_+^2 n_0}{8\pi\varepsilon_0}\int \frac{1}{|\vec{r}|}\left[\frac{\partial}{\partial n}\left(n^2\frac{\partial g}{\partial n}\Big|_{s,|\vec{r}|}\right)\Big|_{s,|\vec{r}|}\right]_0 \mathrm{d}\vec{r}\Bigg) \\ -\frac{q_+^2 n_0^2}{8\pi\varepsilon_0}\sum_{j=1}^{3}\frac{\partial}{\partial a_i}&\left(\int\left[\frac{\partial g}{\partial n}\Big|_{s,|\vec{a}-\vec{a}'|}\right]_0 \frac{\partial}{\partial a_j}\left(\frac{1}{|\vec{a}-\vec{a}'|}\right)\Big|_{\vec{a}'}(\xi_j - \xi_j')\mathrm{d}\vec{a}'\right) \\ +\frac{q_+^2 n_0^2}{8\pi\varepsilon_0}&\int\left[\frac{\partial g}{\partial n}\Big|_{s,|\vec{a}-\vec{a}'|}\right]_0 \frac{\partial}{\partial a_i}\left(\frac{1}{|\vec{a}-\vec{a}'|}\right)\Big|_{\vec{a}'}\left((\vec{\nabla}\cdot\vec{\xi}) + (\vec{\nabla}'\cdot\vec{\xi}')\right)\mathrm{d}\vec{a}' \\ -\frac{q_+^2 n_0}{4\pi\varepsilon_0}&\sum_{j=1}^{3}\int\frac{\partial^2}{\partial a_i \partial a_j}\left(\frac{1}{|\vec{a}-\vec{a}'|}\right)\Big|_{\vec{a}'}\Big((g-1)_0\xi_j - g_0\xi_j'\Big)\mathrm{d}\vec{a}' \end{aligned} \tag{2.68}$$

To solve this equation, we employ the Fourier transform with respect to the spatial coordinates $\vec{a}$ and use the same convention as we did in the Eulerian approach, as given in Eq. (2.27).

$$\vec{\Psi}(\vec{k},t) = \widehat{\vec{\xi}}(\vec{k},t) = \int \vec{\xi}(\vec{a},t)e^{-i\vec{k}\cdot\vec{a}}\mathrm{d}\vec{a} \tag{2.69}$$

With this convention, we once again obtain the results that, for any functions f, g that depend on $\vec{a}$, $\widehat{\partial f/\partial a_j} = ik_j\widehat{f}$ and $\widehat{f * g} = \widehat{f}\widehat{g}$, where $*$ denotes convolution. Using these results, we take the Fourier transform of Eq. (2.68) to obtain a differential equation for each value of $\vec{k}$. As in the Eulerian approach, we simplify by changing the integration variable to $\vec{r} = \vec{a} - \vec{a}'$ when it is convenient.

Once again, it is important to be careful regarding the convergence of integrals. As before, we rely on the result from thermodynamics [23] that $g(n_0, s_0, |\vec{r}|) \to 1$ as $|\vec{r}| \to \infty$. Therefore, it is convenient to express everything in terms of $g - 1$ instead of g. In addition to using the Fourier transform of $1/|\vec{r}|$ being $4\pi/|\vec{k}|^2$ [50], we use the following results [54] for the derivatives of $1/|\vec{r}|$, where $\delta(\vec{r})$ represents the Dirac delta distribution centered at the

origin.

$$\frac{\partial}{\partial r_j}\left(\frac{1}{|\vec{r}|}\right) = -\frac{r_j}{|\vec{r}|^3}, \quad \frac{\partial^2}{\partial r_i \partial r_j}\left(\frac{1}{|\vec{r}|}\right) = \frac{3r_i r_j - \delta_{ij}|\vec{r}|^2}{|\vec{r}|^5} - \frac{4\pi}{3}\delta_{ij}\delta(\vec{r}). \tag{2.70}$$

Combining these results, we can express the Fourier transform of Eq. (2.68) as follows.

$$\begin{aligned} m\frac{\partial^2 \vec{\Psi}}{\partial t^2} = -\vec{k}(\vec{k}\cdot\vec{\Psi})\Bigg(&\frac{q_+^2 n_0}{\varepsilon_0|\vec{k}|^2} + \left[\frac{\partial}{\partial n}\left(\frac{3}{2}k_B n^2 \frac{\partial T}{\partial n}\Big|_s\right)\Big|_s\right]_0 \\ &+\frac{q_+^2 n_0}{8\pi\varepsilon_0}\int \frac{1}{|\vec{r}|}\left[\frac{\partial}{\partial n}\left(n^2\frac{\partial(g-1)}{\partial n}\Big|_{s,|\vec{r}|}\right)\Big|_{s,|\vec{r}|}\right]_0 \mathrm{d}\vec{r}\Bigg) \\ &+\frac{iq_+^2 n_0^2 \vec{k}}{8\pi\varepsilon_0}\int\left[\frac{\partial(g-1)}{\partial n}\Big|_{s,|\vec{r}|}\right]_0 \frac{(\vec{r}\cdot\vec{\Psi})}{|\vec{r}|^3}\left(1-e^{-i\vec{k}\cdot\vec{r}}\right)\mathrm{d}\vec{r} \\ &-i(\vec{k}\cdot\vec{\Psi})\frac{q_+^2 n_0^2}{8\pi\varepsilon_0}\int\left[\frac{\partial(g-1)}{\partial n}\Big|_{s,|\vec{r}|}\right]_0 \frac{\vec{r}}{|\vec{r}|^3}\left(1+e^{-i\vec{k}\cdot\vec{r}}\right)\mathrm{d}\vec{r} \\ &-\frac{q_+^2 n_0}{4\pi\varepsilon_0}\int (g-1)_0\left(\frac{3\vec{r}(\vec{r}\cdot\vec{\Psi})}{|\vec{r}|^5} - \frac{\vec{\Psi}}{|\vec{r}|^3}\right)\left(1-e^{-i\vec{k}\cdot\vec{r}}\right)\mathrm{d}\vec{r} \end{aligned} \tag{2.71}$$

To simplify the analysis of the longitudinal and transverse dispersion modes, we employ the same strategy used in the Eulerian approach, where the coordinate system is rotated in such a way that, in the rotated coordinate system, $\vec{k} = (0, 0, |\vec{k}|)$. In this case, the transverse modes correspond to the x, y directions, while the longitudinal mode corresponds to the z direction. To achieve this, we use the fact that the differential equation is linear, properties of the dot product under a rotation, and rotate the integration variable. It is worth noting that due to some of the functions under the integrals being odd with respect to the integration variables, certain integrals become zero. Further simplification for the remaining integrals can be achieved by going to spherical coordinates and performing the angular integrals.

We find that for the transverse directions, $\partial^2\Psi_x/\partial t^2 = -\omega_T^2(|\vec{k}|)\Psi_x$ and $\partial^2\Psi_y/\partial t^2 = -\omega_T^2(|\vec{k}|)\Psi_y$. It is in contrast to the Eulerian approach, as now there are transverse modes, as given by the following transverse dispersion law. It is worth noting that this expression exactly matches the QLCA result [34, 35, 36].

$$\omega_T^2(|\vec{k}|) = \frac{q_+^2 n_0}{m\varepsilon_0}\int_0^\infty \frac{(g-1)_0}{|\vec{k}|r^2}\left(\sin(|\vec{k}|r) + 3\frac{\cos(|\vec{k}|r)}{|\vec{k}|r} - 3\frac{\sin(|\vec{k}|r)}{|\vec{k}|^2 r^2}\right)\mathrm{d}r \tag{2.72}$$

For the longitudinal direction, we find $\partial^2\Psi_z/\partial t^2 = -\omega_L^2(|\vec{k}|)\Psi_z$, along with the following longitudinal dispersion law. When comparing this to the longitudinal dispersion law obtained

in the Eulerian approach, as given in Eq. (2.29), we observe that the terms independent of $|\vec{k}|$ and the terms purely proportional to $|\vec{k}|^2$ are the same. Furthermore, the terms that do not contain derivatives with respect to the number density n are identical to those given by the QLCA [34, 35, 36].

$$\begin{aligned}\omega_L^2(|\vec{k}|) = \frac{q_+^2 n_0}{m\varepsilon_0} + |\vec{k}|^2 \Bigg(& \left[\frac{\partial}{\partial n} \left(\frac{3k_B}{2m} n^2 \frac{\partial T}{\partial n}\Big|_s \right) \Big|_s \right]_0 \\ & + \frac{q_+^2 n_0}{2m\varepsilon_0} \int_0^\infty r \left[\frac{\partial}{\partial n} \left(n^2 \frac{\partial (g-1)}{\partial n}\Big|_{s,r} \right) \Big|_{s,r} \right]_0 \mathrm{d}r \Bigg) \\ & + \frac{q_+^2 n_0^2}{m\varepsilon_0} \int_0^\infty \frac{1}{r} \left[\frac{\partial (g-1)}{\partial n}\Big|_{s,r} \right]_0 \left(\frac{\sin(|\vec{k}|r)}{|\vec{k}|r} - \cos(|\vec{k}|r) \right) \mathrm{d}r \\ & + \frac{2q_+^2 n_0}{m\varepsilon_0} \int_0^\infty \frac{(g-1)_0}{|\vec{k}|r^2} \left(3\frac{\sin(|\vec{k}|r)}{|\vec{k}|^2 r^2} - 3\frac{\cos(|\vec{k}|r)}{|\vec{k}|r} - \sin(|\vec{k}|r) \right) \mathrm{d}r \end{aligned} \tag{2.73}$$

From the obtained dispersion laws given in Eqs. (2.72), (2.73), we see that the transverse dispersion relation depends solely on the equilibrium pair distribution function, whereas the longitudinal dispersion relation also depends on its adiabatic derivatives, similar to the Eulerian approach. This is expected, as the nonlocal contribution to the energy of the OCP depends on the pair distribution function, as shown in Eq. (2.20). Therefore, the adiabatic derivatives of the pair distribution function in the dispersion relation are related to the adiabatic derivatives of the nonlocal energy. This parallels the usual Euler equations [1] and shows that the dispersion relation accounts for both local and nonlocal contributions to the total energy of the OCP, consistent with results in thermodynamics.

As discussed in the Eulerian approach, it is convenient to express the obtained dispersion laws in the normalized variables. We can again use the results from thermodynamics, which state that $g(n, s, |\vec{r}|) = g(\Gamma, |\vec{r}|/a)$ and that the expressions for equilibrium energy E_0 and equilibrium pressure p_0 are given by Eq. (2.30), which also define the excess internal energy u. As before, the variables Γ and a will oscillate around their respective equilibrium values Γ_0, a_0 due to their dependence on n, s.

To compute the term with the temperature derivatives at constant entropy in the longitudinal dispersion law given in Eq. (2.73), one uses previously discussed results on the

temperature derivative as in Eq. (2.32) and on the derivative at constant entropy of a function of Γ as in Eq. (2.34).

To analyze terms with integrals of $g-1$ in both of the dispersion laws, in addition to the previous identities, use the strategy already discussed in the Eulerian approach. Using $g = g(\Gamma, |\vec{r}|/a)$, take number density derivatives outside of the integrals, change variables inside the integrals to $x = r/a$, and introduce normalized wavevector $\vec{q} = \vec{k}a$. In that case, integrals are rewritten in terms of functions of Γ and $|\vec{q}|$, and we can use the identity given in Eq. (2.34).

Combining all of these results, one gets the following transverse dispersion relation in the normalized variables that is parametrized only by the equilibrium value Γ_0. Again, we emphasize that this result exactly corresponds to the QLCA result [34, 35, 36].

$$\left(\frac{\omega_T}{\omega_p}\right)^2(\Gamma_0,|\vec{q}_0|) = \int_0^\infty \frac{(g-1)(\Gamma_0,x)}{|\vec{q}_0|x^2}\left(\sin(|\vec{q}_0|x) + 3\frac{\cos(|\vec{q}_0|x)}{|\vec{q}_0|x} - 3\frac{\sin(|\vec{q}_0|x)}{|\vec{q}_0|^2x^2}\right)\mathrm{d}x \tag{2.74}$$

The result for the longitudinal dispersion relation in the normalized variables that is parametrized only by the equilibrium value Γ_0 is given next in Eq. (2.75). Here, the terms appearing in the dispersion relation are given by Eqs. (2.32), (2.36), (2.37), (2.76), (2.77), and the derivative at constant s is given by Eq. (2.34).

$$\begin{aligned}\left(\frac{\omega_L}{\omega_p}\right)^2(\Gamma_0,|\vec{q}_0|) &= 1 + \frac{|\vec{q}_0|^2}{\Gamma_0}f_2(\Gamma_0) + \left(n\frac{\partial j}{\partial n}\Big|_s\right)(\Gamma_0,|\vec{q}_0|)\\ &+ \left(n\frac{\partial}{\partial n}\left(n\frac{\partial j}{\partial n}\Big|_s\right)\Big|_s\right)(\Gamma_0,|\vec{q}_0|) + b(\Gamma_0,|\vec{q}_0|) + \left(n\frac{\partial \ell}{\partial n}\Big|_s\right)(\Gamma_0,|\vec{q}_0|),\end{aligned} \tag{2.75}$$

$$b(\Gamma,|\vec{q}|) = 2\int_0^\infty \frac{\big(g-1\big)(\Gamma,x)}{|\vec{q}|x^2}\left(3\frac{\sin(|\vec{q}|x)}{|\vec{q}|^2x^2} - 3\frac{\cos(|\vec{q}|x)}{|\vec{q}|x} - \sin(|\vec{q}|x)\right)\mathrm{d}x, \tag{2.76}$$

$$\ell(\Gamma,|\vec{q}|) = \int_0^\infty \frac{\big(g-1\big)(\Gamma,x)}{x}\left(\frac{\sin(|\vec{q}|x)}{|\vec{q}|x} - \cos(|\vec{q}|x)\right)\mathrm{d}x. \tag{2.77}$$

As in the Eulerian approach, in principle, the obtained dispersion laws in the normalized variables can now be computed for an arbitrary pair distribution function, $g(\Gamma, |\vec{r}|/a)$. However, as before, the longitudinal dispersion relation depends on derivatives with respect to Γ of integrals that include the pair distribution function. This means that for a precise

evaluation of the longitudinal dispersion law, a pair distribution function should be known precisely as a function of Γ. However, as discussed in detail while analyzing the Eulerian approach, such precise fits are not known in the literature. Only the precise dependence of the excess internal energy, $u(\Gamma)$, is known as a function of Γ.

To resolve this issue, we will use the same approximation as discussed in the Eulerian approach, where the pair distribution function, $g(\Gamma, |\vec{r}|/a)$, takes the form of a step function with a value of 0 when $|\vec{r}|/a < (R/a)(\Gamma)$, and 1 when $|\vec{r}|/a > (R/a)(\Gamma)$. The dependence of R/a on Γ is obtained by computing the equilibrium energy given in Eq. (2.20) for the assumed approximation. We use Eq. (2.30) to relate it to $u(\Gamma)$, the result of which is given in Eq. (2.40). This approximation simplifies the integrals appearing in the dispersion law, leading to simpler and more practical expressions and allowing us to avoid additional numerical errors due to the computation of the integral. The transverse dispersion relation is now given in Eq. (2.78). In this equation, R/a is taken to be the correct value for a given Γ_0 and agrees with the QLCA result for the same pair distribution function approximation [36].

$$\left(\frac{\omega_T}{\omega_p}\right)^2 (\Gamma_0, |\vec{q}_0|) = \frac{1}{3} + \frac{\cos(|\vec{q}_0|R/a)}{(|\vec{q}_0|R/a)^2} - \frac{\sin(|\vec{q}_0|R/a)}{(|\vec{q}_0|R/a)^3} \tag{2.78}$$

The integrals in the longitudinal dispersion relation, as given by Eqs. (2.37), (2.76), (2.77), can be rewritten as shown in Eqs. (2.41), (2.79), with R/a taken to be the correct value for a given Γ.

$$b(\Gamma, |\vec{q}|) = -\frac{2}{3} - 2\frac{\cos(|\vec{q}|R/a)}{(|\vec{q}|R/a)^2} + 2\frac{\sin(|\vec{q}|R/a)}{(|\vec{q}|R/a)^3}, \quad \ell(\Gamma, |\vec{q}|) = \frac{\sin(|\vec{q}|R/a)}{(|\vec{q}|R/a)} - 1. \tag{2.79}$$

Now, let us consider different fits for the excess internal energy $u(\Gamma)$ as defined in Eq. (2.30). First, let us consider a simple fit $u(\Gamma) = -0.9\Gamma$ that is accurate for a very strong coupling where $\Gamma \gg 1$ [27]. As discussed before, for such a fit, $R/a = \sqrt{6/5}$, independent of the value of Γ. From Eq. (2.78) it can be observed that in this approximation the transverse dispersion relation is independent of Γ. The results for various values of Γ_0 are shown in Fig. 2.4(a).

Moreover, from Eqs. (2.41), (2.79), this implies that the functions j, b, ℓ appearing in

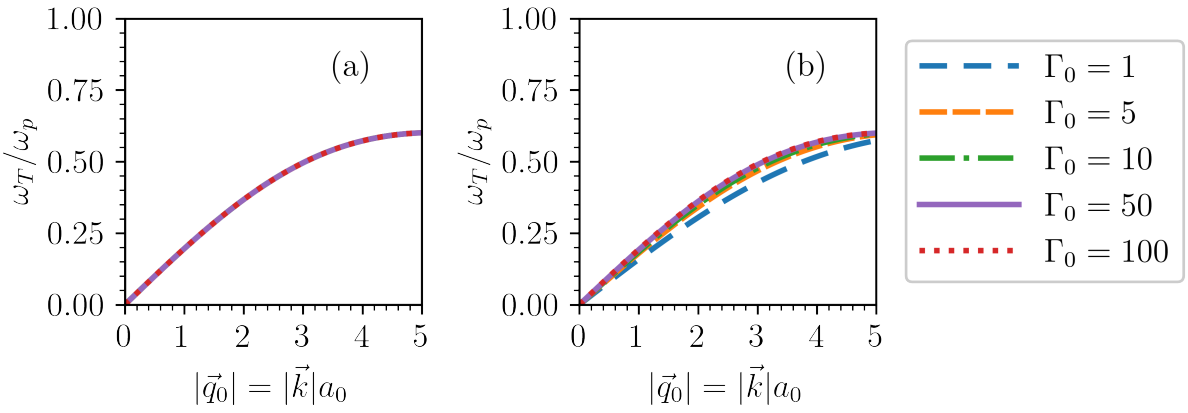

Figure 2.4: The transverse dispersion law in the Lagrangian approach, expressed in normalized variables, is shown for different values of Γ_0 as given by Eq. (2.78). We assume the step function approximation for the pair distribution function for a given $u(\Gamma)$ defined in Eq. (2.30). In (a), $u(\Gamma) = -0.9\Gamma$. In (b), $u(\Gamma) = -0.9\Gamma + 0.5944\Gamma^{1/3} - 0.2786$.

the longitudinal dispersion relation given in Eq. (2.75) are also independent of Γ. These results greatly simplify the calculations of taking number density derivatives at constant s, as shown in Eq. (2.34). Furthermore, as before, for such a fit, we have $f_1(\Gamma) = 1$ by Eq. (2.32). With these results, the longitudinal dispersion law given in Eq. (2.75), supplemented with Eq. (2.36) and the simplified expressions in Eqs. (2.41), (2.79), becomes as follows.

$$\begin{aligned}\left(\frac{\omega_L}{\omega_p}\right)^2(\Gamma_0, |\vec{q}_0|) &= \frac{1}{3} + \left(\frac{5}{9\Gamma_0} + \frac{1}{15}\right)|\vec{q}_0|^2 \\ &+ \left(\frac{1}{3} + \frac{2}{\left(\sqrt{\frac{6}{5}}|\vec{q}_0|\right)^2}\right)\left(\frac{\sin\left(\sqrt{\frac{6}{5}}|\vec{q}_0|\right)}{\sqrt{\frac{6}{5}}|\vec{q}_0|} - \cos\left(\sqrt{\frac{6}{5}}|\vec{q}_0|\right)\right)\end{aligned} \tag{2.80}$$

The results for different values of Γ_0 are presented in Fig. 2.5(a). Several key properties can be observed from the figure. Similar to the Eulerian approach, for weak coupling where $\Gamma_0 = 1$, the dispersion relation resembles the behavior of an ideal gas. However, as Γ_0 is increased, the behavior changes dramatically. Nonetheless, at no value of Γ_0 do we observe the onset of negative dispersion because for small values of $|\vec{q}_0|$, $\omega_L \geq \omega_p$. Furthermore, this remains true for all values of $|\vec{q}_0|$.

The simpler fit for $u(\Gamma)$ does not account for thermal effects in the nonlocal interaction.

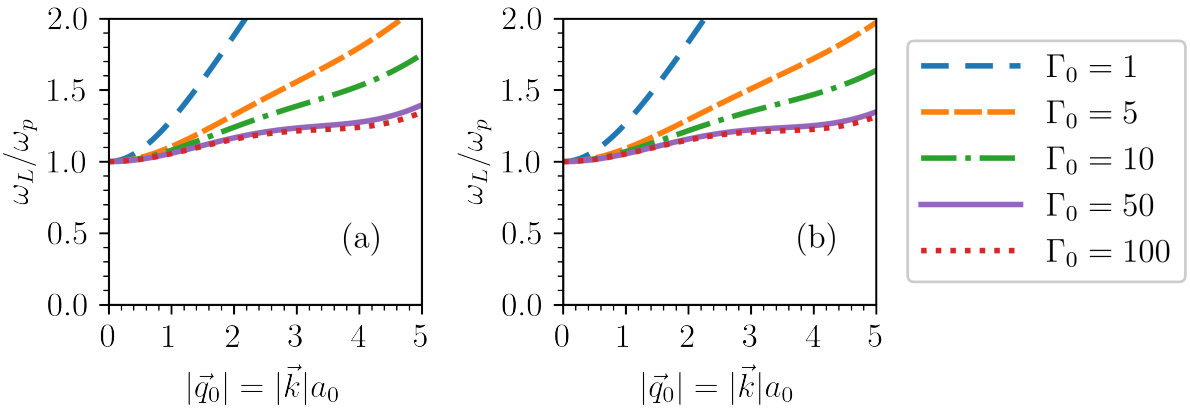

Figure 2.5: The longitudinal dispersion law in the Lagrangian approach, expressed in normalized variables, is shown for different values of Γ_0 as given by Eq. (2.75). We assume the step function approximation for the pair distribution function, and therefore, we use Eqs. (2.32), (2.36), (2.40), (2.41), (2.79) for a given $u(\Gamma)$ defined in Eq. (2.30). In (a), $u(\Gamma) = -0.9\Gamma$, and the result is provided by Eq. (2.80). In (b), $u(\Gamma) = -0.9\Gamma + 0.5944\Gamma^{1/3} - 0.2786$.

Therefore, we also consider a more precise fit, $u(\Gamma) = -0.9\Gamma + 0.5944\Gamma^{1/3} - 0.2786$, which is accurate for $\Gamma \geq 1$ and includes thermal effects [27]. The results for different values of Γ_0 for the transverse dispersion law are shown in Fig. 2.4(b), and for the longitudinal dispersion law, they are presented in Fig. 2.5(b). Similar to the Eulerian approach, it is evident that the more complex fit for $u(\Gamma)$ yields results that are qualitatively the same as in the case of the simpler fit, with minor quantitative differences.

The results for the more precise fit are also compared to the results obtained by QLCA [36] using the same approximation of the pair distribution function. The results are also compared to the current fluctuation spectra obtained from molecular dynamics simulations provided by the authors of Ref. [30], where dispersion laws are identified by the peaks of the spectra.

Results for QLCA and molecular dynamics for the longitudinal dispersion law can be seen in Fig. 2.1. It can be observed that as Γ_0 increases, the predicted dispersion law starts to differ from the results of the molecular dynamics simulations. In particular, the latter shows the onset of negative dispersion in the range of values from $\Gamma_0 = 9.5$ to $\Gamma_0 = 10.0$

[30, 31], contrary to the predicted dispersion law that has no such onset. Moreover, the predicted longitudinal dispersion law, in the limit as $\Gamma_0 \to \infty$, does not tend to the QLCA result, which is considered accurate in such a limit [36].

Results for QLCA and molecular dynamics for the transverse dispersion law can be seen in Fig. 2.2. The predicted transverse dispersion law, at all values of Γ_0, agrees with the QLCA result for the same pair distribution function approximation. It also agrees with the results of molecular dynamics simulations at large values of wavevector and correctly predicts that the transverse dispersion law tends to the value $\omega_p/\sqrt{3}$ in the limit as $|\vec{q}_0| = |\vec{k}|a_0 \to \infty$. However, it fails to predict the numerically observed disappearance of the transverse waves at small values of wavevector [32]. Nonetheless, as in the case of QLCA, this issue can be remedied by considering relaxation in the context of generalized hydrodynamics [32].

Compared to the Eulerian approach, the discussed Lagrangian approach now accurately predicts the transverse dispersion law for large values of wavevector. However, there are still issues with the longitudinal dispersion law. In the Lagrangian approach, there is no longer an onset of negative dispersion, and the results still do not agree with the results from QLCA and molecular dynamics simulations at high values of Γ_0. This motivates us to consider the final alternative variational approach, discussed in the next Section 2.3.4.

2.3.4 Modified Lagrangian approach

The difference in the previously described Eulerian and Lagrangian variational principles lies in how the pair distribution function is assumed to behave out of equilibrium. Specifically, in the Eulerian approach, the pair distribution function is a function of number density n, specific entropy s, and the difference in positions in the laboratory frame $|\vec{x}-\vec{x}'|$. In contrast, in the Lagrangian approach, it is assumed to depend on n, s, and the difference in positions in the reference state $|\vec{a} - \vec{a}'|$. Such a difference results in distinct dispersion laws. For example, it determines whether there are transverse dispersion modes and whether there are regions where longitudinal dispersion modes become unstable with $\omega_L^2 < 0$.

Notice that there are other possible changes to how the pair distribution function behaves

out of equilibrium. For example, instead of depending on n, it might depend on the number density n^{ref} in a reference state. Similarly, instead of depending on s, it might depend on the specific entropy s^{ref} in a reference state. Due to the continuity equations given by Eq. (2.43), changing the dependence from s to s^{ref} would not change the results, but changing it from n to n^{ref} might lead to significant differences. This possibility may be of particular interest, given that the transverse dispersion law in the Lagrangian approach reasonably agrees with the molecular dynamics simulations, unlike the longitudinal dispersion law. Notice that, as shown by Eqs. (2.72), (2.73), only the longitudinal dispersion law depends on derivatives of the pair distribution function with respect to number density. Therefore, only the longitudinal dispersion law would be sensitive to the discussed change. This might allow us to improve the longitudinal dispersion law without affecting the transverse modes.

In the case of the local energy term f, both of the previously considered variational approaches had it such that, out of all thermodynamic functions, it depends only on temperature T. To be consistent with the Euler equations [45, 46, 47], it is necessary to have it depend on n, s instead of $n^{\text{ref}}, s^{\text{ref}}$. This motivates the consideration of the pair distribution function out of equilibrium as a function of temperature T rather than specific entropy s, and to assume that T depends on n, s, and not on $n^{\text{ref}}, s^{\text{ref}}$.

However, there is a dependence on number density in the pair distribution function that does not come from the temperature, and there is no reason to believe it must depend on n rather than n^{ref}. In particular, both of our previously considered approaches assumed dependence on n, so we would like to explore what happens if one assumes dependence on n^{ref} instead. In other words, we assume that the pair distribution function out of equilibrium is a function of the form $g(n, s, |\vec{a} - \vec{a}'|) = g(n^{\text{ref}}, T(n, s), |\vec{a} - \vec{a}'|)$.

With such an assumption regarding the pair distribution function, the equations of motion remain as given by Eq. (2.65). The momentum law is still described by Eq. (2.49), and the energy law is still governed by Eqs. (2.52), (2.53), (2.54), (2.55), with the same identification of functions f, F as provided in Eqs. (2.60), (2.62). The transverse and longitudinal dispersion laws are also retained and described by Eqs. (2.72), (2.73). However, one must

be careful with computing derivatives at constant s.

As previously mentioned, it is convenient to rewrite the obtained dispersion laws in normalized variables. We again make use of results from thermodynamics, stating that in equilibrium, $g(n_0, s_0, |\vec{r}|) = g(\Gamma_0, |\vec{r}|/a_0)$, and the expressions for equilibrium energy E_0 and equilibrium pressure p_0 are provided in Eq. (2.30), which also define the excess internal energy u. With our new assumption regarding how g behaves out of equilibrium, we have $g(n, s, |\vec{r}|) = g(\Gamma(n_0, T(n, s)), |\vec{r}|/a_0)$. Consequently, the variable Γ will oscillate around its respective equilibrium value Γ_0 due to its dependence on n, s. However, the value of a remains fixed during the motion of the system at its equilibrium value a_0.

The computation of the term in the longitudinal dispersion law involving the temperature derivatives at constant entropy is the same as in both previous approaches. One uses results on the temperature derivative, as shown in Eq. (2.32), and on the derivative at constant entropy of a function of Γ, as demonstrated in Eq. (2.34).

To analyze terms with integrals of $g - 1$ in both of the dispersion laws, in addition to the previous identities, use the following strategy, which is slightly different from the strategy used in the two previous approaches. First, take number density derivatives outside of the integrals. Then, change variables inside the integrals to $x = r/a_0$ and introduce the normalized wavevector $\vec{q}_0 = \vec{k}a_0$. In this case, integrals are rewritten in terms of functions of $\Gamma(n_0, T(n, s))$ and $|\vec{q}_0|$. Next, one can use the following identity for an arbitrary function $f(\Gamma(n_0, T(n, s)), |\vec{q}_0|)$ on the derivative of number density at constant entropy, where we use the chain rule, Eq. (2.32), and the definition of Γ.

$$n\frac{\partial f}{\partial n}\Big|_s\big(\Gamma(n_0, T(n, s)), |\vec{q}_0|\big) = -\frac{2}{3}\Gamma(n_0, T(n, s))\frac{\partial f}{\partial \Gamma}\Big|_{|\vec{q}_0|} f_1\big(\Gamma(n, T)\big) \tag{2.81}$$

The transverse dispersion relation in the normalized variables is the same as in the Lagrangian approach, as given by Eq. (2.74), as it does not depend on number density derivatives at constant entropy.

However, the longitudinal dispersion relation in the normalized variables is now different. For each equilibrium value Γ_0, it is provided in Eq. (2.82). The terms appearing in the

dispersion relation are given by Eqs. (2.32), (2.36), (2.37), (2.76), (2.77), (2.83), (2.84), (2.85).

$$\left(\frac{\omega_L}{\omega_p}\right)^2(\Gamma_0,|\vec{q}_0|)=1+\frac{|\vec{q}_0|^2}{\Gamma_0}f_2(\Gamma_0)+j_1(\Gamma_0,|\vec{q}_0|)+j_2(\Gamma_0,|\vec{q}_0|) \\ +b(\Gamma_0,|\vec{q}_0|)+\ell_1(\Gamma_0,|\vec{q}_0|), \tag{2.82}$$

$$j_1(\Gamma,|\vec{q}|)=-\frac{2\Gamma}{3}\frac{\partial j}{\partial\Gamma}\Big|_{|\vec{q}|}(\Gamma,|\vec{q}|)\left(f_1(\Gamma)-\frac{2}{3}f_1^2(\Gamma)+\frac{\Gamma}{3}\frac{\mathrm{d}f_1}{\mathrm{d}\Gamma}(\Gamma)\Big(1-2f_1(\Gamma)\Big)\right), \tag{2.83}$$

$$j_2(\Gamma,|\vec{q}|)=\frac{4\Gamma^2}{9}f_1^2(\Gamma)\frac{\partial^2 j}{\partial\Gamma^2}\Big|_{|\vec{q}|}(\Gamma,|\vec{q}|), \tag{2.84}$$

$$\ell_1(\Gamma,|\vec{q}|)=-\frac{2\Gamma}{3}f_1(\Gamma)\frac{\partial \ell}{\partial\Gamma}\Big|_{|\vec{q}|}(\Gamma,|\vec{q}|). \tag{2.85}$$

As discussed in both previous variational approaches in detail, due to insufficient numerical data regarding how the pair distribution function $g(\Gamma,|\vec{r}|/a)$ depends on Γ, we use a step function approximation to simplify integrals and make calculations more practical. The step function approximation for the pair distribution function is such that it has a value of 0 when $|\vec{r}|/a<(R/a)(\Gamma)$, and 1 when $|\vec{r}|/a>(R/a)(\Gamma)$.

The dependence of R/a on Γ is determined by computing the equilibrium energy, as given in Eq. (2.20), for the given approximation. We then use Eq. (2.30) to relate it to $u(\Gamma)$. The result of this computation is provided in Eq. (2.40).

In this case, the transverse dispersion relation is provided in Eq. (2.78), where R/a is the correct value for a given Γ_0. This result agrees with the QLCA result for the same pair distribution function approximation [36]. The integrals found in the longitudinal dispersion relation, as given by Eqs. (2.37), (2.76), (2.77), can be simplified as before, as described by Eqs. (2.41), (2.79), where R/a is the correct value for a given Γ.

Now, let us consider different fits for the excess internal energy, $u(\Gamma)$, as defined in Eq. (2.30). First, let us examine a simple fit $u(\Gamma)=-0.9\Gamma$, which is accurate for very strong coupling where $\Gamma\gg 1$ [27]. As discussed previously, for such a fit, $R/a=\sqrt{6/5}$, independent of the value of Γ. The results for the transverse dispersion relation for different values of Γ_0 are presented as before in Fig. 2.4(a).

As before, from Eqs. (2.41), (2.79), it follows that the functions j, b, ℓ appearing in the longitudinal dispersion relation, as given in Eq. (2.82), are also independent of Γ. This significantly simplifies the dispresion relation, and from Eqs. (2.83), (2.84), (2.85), we deduce that j_1, j_2, ℓ_1 are all zero. Additionally, as previously discussed, for such a fit, we have $f_1(\Gamma) = 1$ according to Eq. (2.32). With these results, the longitudinal dispersion law, as given in Eq. (2.82) and supplemented with Eq. (2.36) and the simplified expression for b in Eq. (2.79), becomes as follows. It is worth noting that this result is exactly the ideal gas speed of sound term combined with the QLCA expression for the same pair distribution function approximation [36]. The idea of phenomenologically combining the ideal gas speed of sound term with the QLCA expression has appeared in the literature [37, 38]. However, here we have provided a more rigorous justification for such a result, as it was derived from a general theoretical framework. Additionally, notice that this result only holds when $u(\Gamma) = -0.9\Gamma$, and our theory allows for a consistent generalization to the case when the functional form of $u(\Gamma)$ is more complicated.

$$\left(\frac{\omega_L}{\omega_p}\right)^2 (\Gamma_0, |\vec{q}_0|) = \frac{1}{3} + \frac{5}{9}\frac{|\vec{q}_0|^2}{\Gamma_0} - 2\frac{\cos\left(\sqrt{\frac{6}{5}}|\vec{q}_0|\right)}{\left(\sqrt{\frac{6}{5}}|\vec{q}_0|\right)^2} + 2\frac{\sin\left(\sqrt{\frac{6}{5}}|\vec{q}_0|\right)}{\left(\sqrt{\frac{6}{5}}|\vec{q}_0|\right)^3} \tag{2.86}$$

The results for different values of Γ_0 are presented in Fig. 2.6(a), and the following properties can be observed from the figure. As in both previous approaches, for weak coupling where $\Gamma_0 = 1$, the dispersion relation resembles the behavior of an ideal gas. However, as Γ_0 increases, the behavior undergoes a dramatic change. Similar to the Eulerian approach, but unlike the original Lagrangian approach, there is a critical value of $\Gamma_0 = 7.0$ at which we observe the onset of negative dispersion. In other words, for small values of $|\vec{q}_0|$, $\omega_L \leq \omega_p$ instead of $\omega_L \geq \omega_p$. However, unlike the Eulerian approach but similar to the original Lagrangian approach, there are no unstable regions. This means that for all Γ_0, we find that $\omega_L^2 > 0$ for all $|\vec{q}_0|$.

The simpler fit for $u(\Gamma)$ does not account for thermal effects in the nonlocal interaction. Therefore, we also consider a more precise fit, $u(\Gamma) = -0.9\Gamma + 0.5944\Gamma^{1/3} - 0.2786$, which is accurate for $\Gamma \geq 1$ and includes thermal effects [27].

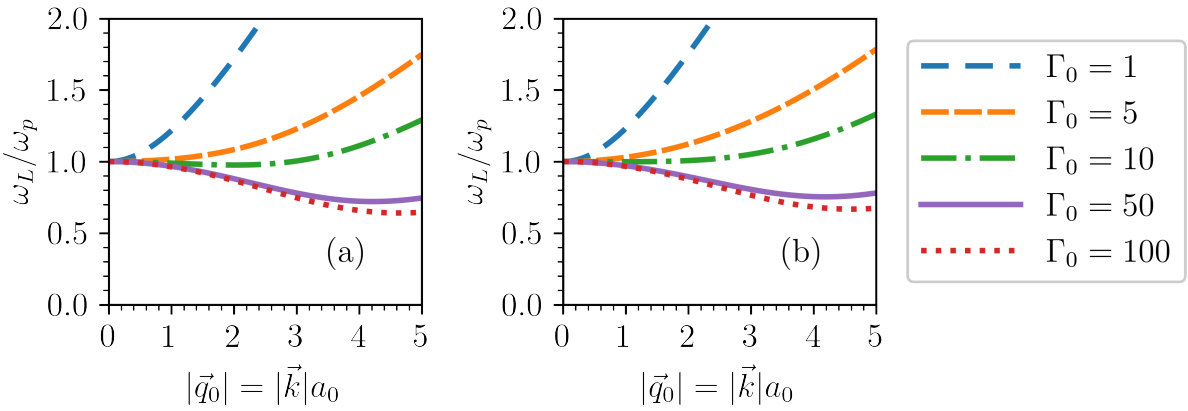

Figure 2.6: The longitudinal dispersion law in the modified Lagrangian approach, expressed in normalized variables, is shown for different values of Γ_0 as given by Eq. (2.82). We assume the step function approximation for the pair distribution function, and therefore, we use Eqs. (2.32), (2.36), (2.40), (2.41), (2.79) for a given $u(\Gamma)$ defined in Eq. (2.30). In (a), $u(\Gamma) = -0.9\Gamma$, and the result is provided by Eq. (2.86). In (b), $u(\Gamma) = -0.9\Gamma + 0.5944\Gamma^{1/3} - 0.2786$.

The results for different values of Γ_0 for the transverse dispersion law are presented in Fig. 2.4(b), and for the longitudinal dispersion law, they are shown in Fig. 2.6(b). As in both previous approaches, one can observe that the more complicated fit for $u(\Gamma)$ yields results that are qualitatively the same as in the case of the simpler fit, with small quantitative differences. For instance, the onset of negative dispersion is now observed at $\Gamma_0 = 9.5$.

The results for the more precise fit are also compared to the results obtained by QLCA [36] for the same approximation of the pair distribution function, as well as to current fluctuation spectra obtained from molecular dynamics simulations provided by the authors of Ref. [30], where dispersion laws are identified by the peaks in the spectra.

The comparison for the longitudinal dispersion law is presented in Fig. 2.1. The predicted dispersion law agrees with the molecular dynamics simulations. For $\Gamma_0 = 1, 5, 10$, the agreement extends through the range of $0 < |\vec{q}_0| < 5$. For the large value $\Gamma_0 = 80$, the agreement is observed for the range of $0 < |\vec{q}_0| < 2$. Additionally, the predicted onset of negative dispersion at $\Gamma_0 = 9.5$ aligns excellently with the range of values from $\Gamma_0 = 9.5$ to

$\Gamma_0 = 10.0$, estimated by the molecular dynamics simulations [30, 31]. Moreover, the predicted longitudinal dispersion law in the limit as $\Gamma_0 \to \infty$ tends to the QLCA result, which is considered accurate in such a limit [36]. This can be observed for a simpler fit for $u(\Gamma)$ by taking the limit $\Gamma_0 \to \infty$ directly in Eq. (2.86), while for the more complicated fit for $u(\Gamma)$, it was confirmed numerically. Consequently, in such a strong coupling limit, the predicted longitudinal dispersion law, following the QLCA result, tends towards the value $\omega_p/\sqrt{3}$ in the limit as $|\vec{q}_0| = |\vec{k}|a_0 \to \infty$.

The comparison for the transverse dispersion law is presented in Fig. 2.2. Similar to the previous case of the Lagrangian approach, the predicted dispersion law at all Γ_0 exactly agrees with the QLCA result and aligns with the results of molecular dynamics simulations at large values of wavevector. It correctly predicts that the transverse dispersion law tends to the value $\omega_p/\sqrt{3}$ in the limit as $|\vec{q}_0| = |\vec{k}|a_0 \to \infty$. However, it fails to predict the numerically observed disappearance of transverse waves at small values of the wavevector [32]. Nonetheless, similar to the case of QLCA, this can be remedied by considering relaxation in the context of generalized hydrodynamics [32].

2.4 Discussion and conclusion

We have explored variational principles for the hydrodynamics of the classical OCP in both the Eulerian approach to hydrodynamics, where the hydrodynamic functions depend on the position in the laboratory frame, and the Lagrangian approach, where the hydrodynamic functions depend on some reference position, such as the initial or equilibrium position of a fluid particle. We motivated Lagrangian densities that are used in the variational principles and showed how to obtain equations of motion and conservation laws for momentum and energy when the variational principle is nonlocal. In the Eulerian approach, one has to introduce constraint fields in the variational principle to obtain continuity equations for number density and specific entropy. Because of that, one has to be careful when eliminating the introduced constraint fields from the resulting equations, as we have shown. In the Lagrangian approach, such issues with constraint fields do not occur.

Consistency with equilibrium results from thermodynamics was ensured by employing the energy conservation law and calculating the energy expression from a given variational principle. This expression was evaluated in equilibrium and matched with the known thermodynamic expression. Consequently, all the considered variational principles yield the same result for equilibrium energy, even though their out-of-equilibrium behavior differs due to various assumptions regarding the pair distribution function. To fully specify each of the considered variational approaches, we also assumed that the out-of-equilibrium pair distribution function depends solely on number densities and specific entropies in terms of n, s, rather than using more complex models such as $(n + n')/2, (s + s')/2$ or $\sqrt{nn'}, \sqrt{ss'}$.

To analyze different proposed variational principles, we obtained linearized equations of motion and calculated longitudinal and transverse dispersion laws. In all of these approaches, the dispersion laws depend not only on the pair distribution function but also on its adiabatic derivatives. This is similar to the case of Euler equations, where dispersion laws depend on the adiabatic derivatives of energy. However, in our case, we have included a nonlocal contribution to the energy of the OCP that depends on the pair distribution function. Nevertheless, we are not aware of precise numerical data regarding the adiabatic derivatives of the pair distribution function.

Due to this lack of data, we used a simple step function approximation to the pair distribution function. We chose the radius for the transition of the step function to be consistent with the equilibrium energy expression. This approach allows us to significantly simplify integrals that appear in the dispersion laws. We hope that our accurate results will serve as motivation to perform a more careful numerical analysis of the pair distribution function in equilibrium in the future. With precise knowledge of its adiabatic derivatives, we can avoid the simple step function approximation we used and obtain even more accurate results.

In each of the considered variational approaches, dispersion laws were computed using two fits for the nonlocal contribution to the energy of the OCP. First, a simpler fit was considered, which is valid for large values of the plasma parameter, $\Gamma \gg 1$, and for which

simple analytical expressions for the dispersion laws can be obtained, see Eqs. (2.42), (2.78), (2.80), (2.86). Then, a more complicated fit that is valid for $\Gamma > 1$ was considered, for which dispersion laws were computed numerically. We found that compared to the simpler fit with its simple analytical expressions, the results are qualitatively the same, with some small quantitative differences. This can be seen in Figs. 2.3, 2.4, 2.5, 2.6.

Finally, we compared the obtained dispersion laws for different variational approaches across a wide range of equilibrium values of the plasma parameter, Γ_0, to the results of theoretical calculations using QLCA and the numerical results of molecular dynamics simulations. The results can be observed in Figs. 2.1, 2.2. Indeed, we can see that different variational approaches yield significantly different results for the dispersion laws, emphasizing the importance of understanding how the pair distribution function behaves out of equilibrium within the variational principles.

From the comparison of the transverse dispersion laws in Fig. 2.2, we can observe that for small values of the wavevector, $|\vec{q}_0|$, the Eulerian variational approach correctly predicts the absence of transverse waves in the system. Meanwhile, for large values of the wavevector, the modified Lagrangian approach agrees with the QLCA result and correctly predicts the presence of transverse waves. As with QLCA, one can improve our models by introducing relaxation, as done in generalized hydrodynamics, which allows for the accurate prediction of the disappearance of transverse waves for small wavevector values. The transverse dispersion law does not differentiate all of the variational principles from the QLCA result. To understand the differences between theoretical models, it is, therefore, better to examine the longitudinal dispersion law, as shown in Fig. 2.1.

From the comparison of the longitudinal dispersion laws, we conclude that the modified Lagrangian variational principle provides very accurate results for all values of the wavevector, $|\vec{q}_0|$, and for all considered values of Γ_0 when compared to the results of molecular dynamics calculations. It is also more accurate than the other variational approaches considered and QLCA. In the regime of large wavelengths, so, small wavevectors, the modified Lagrangian variational approach correctly predicts the onset of negative dispersion to occur

at $\Gamma_0 = 9.5$, in agreement with the range of values $9.5 \leq \Gamma_0 \leq 10.0$ predicted by the molecular dynamics simulations. In the limit of strong coupling, where $\Gamma_0 \to \infty$, the modified Lagrangian variational approach tends towards the QLCA result. Thus, in the regime of small wavelengths, so, large wavevectors, it predicts that both longitudinal and transverse dispersion laws tend towards the finite value $\omega_p/\sqrt{3}$ as $|\vec{q_0}| = |\vec{k}|a_0 \to \infty$.

The excellent agreement of the dispersion laws predicted by the modified Lagrangian variational principle, as compared to the molecular dynamics simulations, shows that our variational hydrodynamic approach can be used to describe motion on small length scales where the wavelength is comparable to the average distance between the particles. This suggests that one can apply this general variational approach with reasonable confidence in the future to nonlinear problems of the OCP, such as the motion of vortices and adiabatic expansion, where molecular dynamics data might not be available. It also suggests that one can apply it to other long-range systems, for example, Yukawa fluids, two-component plasma, two-dimensional OCP, and fluids consisting of electric or magnetic dipoles.

Determining the correct action indeed requires experimental input, and we have shown how the procedure of developing theory using the variational principle works. But once the correct input has been achieved, and the complete set of variables has been assumed, one gets the payoff that a self-consistent theory that can be applied to nonlinear processes has been obtained.

In our analysis, we have ignored the effects of viscosity, relaxation, and heat transfer. In the future, one can consider adding them by including additional terms in the equations of motion produced by the variational principle. Viscosity can be included by adding a term related to the velocity gradient, as seen in the case of the Navier-Stokes equations. Relaxation can be included by adding a linear in velocity friction force between moving particles and the stationary neutralizing background, as in the two-fluid plasma equations. Alternatively, relaxation can be introduced for the hydrodynamic variables for their approach to local thermodynamic equilibrium values, as in generalized hydrodynamics. Heat transfer can be accounted for by adding a term related to the temperature gradient to the energy

conservation law obtained from the variational principle, similar to the case of the Navier-Stokes equations.

CHAPTER 3

Rapid bubble collapse in a compressible Euler fluid

Section 3.2 is reproduced from D. Krimans and S. Putterman, "Power law singularity for cavity collapse in a compressible Euler fluid with Tait–Murnaghan equation of state," Phys. Fluids **35**, 086114 (2023), with the permission of AIP Publishing.

3.1 Introduction

Cavitation is the phenomenon wherein bubbles spontaneously form in a moving fluid. Their subsequent motion can be so strong as to damage nearby boundaries [55, 56] and their implosion can even form a light emitting plasma, a phenomenon called sonoluminescence [6, 57]. The singularity underlying this multi-scale process was derived by Rayleigh [58] for an empty cavity surrounded by an incompressible fluid. He showed that for spherical symmetry, at the late stages of the collapse, the radius collapses to zero at a finite time t_c according to the following power-law solution.

$$R(t) = A(t_c - t)^n, \tag{3.1}$$

where $n = 2/5$, $A = (5/2)^{2/5}(E/2\pi\rho_\infty)^{1/5}$, with ρ_∞ being the ambient mass density of the surrounding fluid at an external pressure p_∞, and $E = (4\pi/3)p_\infty R_m^3$, which is the initial energy of the fluid needed to form the initial cavity of radius R_m in an otherwise stationary fluid. If the cavity contains gas, this implosion can lead to a strong concentration of energy density, turning the gas into plasma that emits a picosecond-long flash of light [59]. Even when the cavity is empty, so that the pressure at the cavity wall is zero, a large pressure gradient appears inside the fluid near the wall [58]. The following expression applies at the

late stages of the collapse, and $\dot{R}(t)$ is the velocity of the cavity wall, which can be computed using Eq. (3.1).

$$p(r,t) = \frac{\rho_\infty \dot{R}^2(t)}{2}\left(\frac{R(t)}{r} - \left(\frac{R(t)}{r}\right)^4\right) \tag{3.2}$$

From this expression, the maximum pressure value in the fluid occurs at the location $r = 1.6R$ with the value $p_{\max} = 0.16p_\infty(R_m/R)^3$, where R is the instantaneous radius of the cavity. For an external pressure $p_\infty = 1$ atm, when the bubble's radius collapses to a value of $R_m/R = 27$, the pressure within the fluid exceeds 3000 atm, which is the yield stress of water. We refer here to the Tait-Murnaghan equation of state, which will be assumed for all compressible fluids under consideration, where γ is a constant, but both B and ρ_0 are slowly varying functions of specific entropy [2, 60, 61].

$$p(\rho) = B\left(\left(\frac{\rho}{\rho_0}\right)^\gamma - 1\right), \tag{3.3}$$

where for water, $B = 3000$ atm, $\gamma = 7$ [2, 60, 61], and ρ_0 is the density at zero pressure. As B is usually much greater than 1 atm, ρ_0 can be estimated using the known value of density at $p = 1$ atm. For example, taking the density of water at $p = 1$ atm and temperature $T = 20$ °C leads to $\rho_0 = 1000$ kg/m^3 [62].

The adiabatic speed of sound, c, for such an equation of state is given by the following equation:

$$c = \sqrt{\frac{\gamma(p+B)}{\rho}}, \tag{3.4}$$

which also allows to define the ambient speed of sound, c_∞, by evaluating the expression at pressure p_∞ and mass density ρ_∞. This is used to define the Mach number for a collapse in a compressible fluid as $\mathrm{M} = \dot{R}/c_\infty$.

So, if cavitation takes place in water, compressibility needs to be taken into account when the implosions are so strong that $R_m/R > 27$ is reached. In addition to its maximum radius R_m, a sonoluminescing bubble is characterized by its ambient radius R_0, achieved when the pressure in the gas inside the cavity is p_∞, and its minimum radius a, which is largely determined by the van der Waals hard core size of the gas atoms. This phenomenon

enjoys a broad parameter space: typically, $7 < R_0/a < 10$ and $8 < R_m/R_0 < 24$ have been achieved for light-emitting bubbles [7, 63]. Taken together, typical sonoluminescing bubbles in water reach $R_m/R > 100$, so, as emphasized by Ramsey [64], compressibility needs to be taken into account if one is interested in probing the extent to which cavitation focuses energy.

The speed at which a cavity collapses in an incompressible fluid after the initial stages of collapse can be determined from Eq. (3.1).

$$\dot{R}(t) = -\sqrt{\frac{2p_\infty}{3\rho_\infty}}\left(\frac{R_m}{R(t)}\right)^{3/2} \tag{3.5}$$

Comparing this velocity to the ambient adiabatic speed of sound in water, $c_\infty = 1400$ m/s, obtained using the values $p_\infty = 1$ atm and $\rho_\infty = 1000$ kg/m^3, yields a Mach number of $\mathrm{M} = 0.77$ when $R_m/R = 27$. Therefore, describing cavitation collapse in a real fluid requires analysis of high Mach number motion.

This point was made by Hunter [61], whose asymptotic calculation for the final stage of collapse of an empty cavity, including effects of compressibility of the outside fluid, yielded a power-law solution of the form given in Eq. (3.1) with $n = 0.56$ for water, different from the incompressible result $n = 0.40$. However, water is not the only fluid in which cavitation is possible and has been studied, and we will discuss the theory for fluids that have different compressibility than water. One such example is liquid lithium [65, 66], where $\gamma = 4.5$, $B = 22000$ atm [67], and $\rho_0 = 520$ kg/m^3, which is estimated using the density at $p = 1$ atm and the melting temperature $T = 450$ K [68]. Motivated by this perspective, in Section 3.2 we use Hunter's method and present an asymptotic calculation for the power-law exponents n for a wide range of materials described by the equation of state in Eq. (3.3). It can be shown that the power-law solution depends only on the parameter γ, and so we compute $n(\gamma)$ for a wide range of materials described by different values of γ, extending the results of Hunter for water and of Rayleigh for incompressible fluid. Key results are displayed in Fig. 3.1. For example, our results show that for liquid lithium, $n = 0.62$. These calculations provide an asymptotic limit that can be used to evaluate the accuracy of more general numerical solutions that we perform next and discuss in detail in Section 3.3.

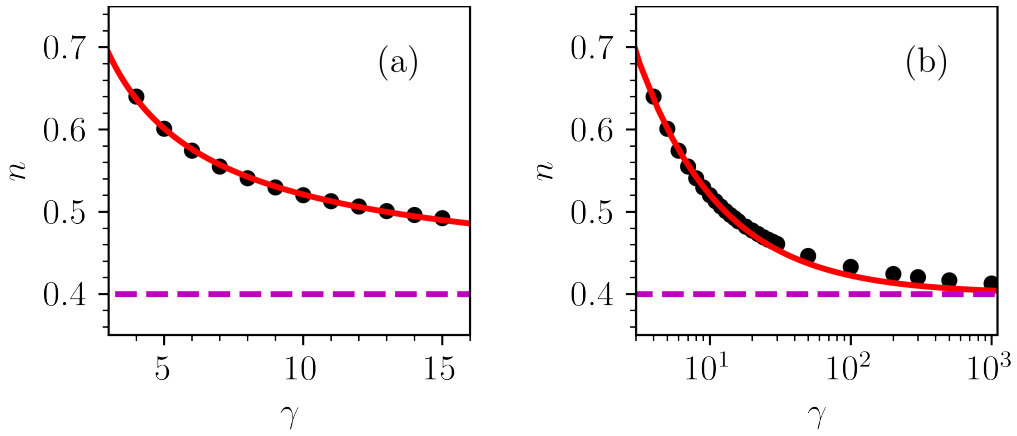

Figure 3.1: Predicted values of n as a function of γ (black dots), the proposed fit for the range of γ close to the value of water that has $\gamma = 7$ of the form $n = 0.4 + a\gamma^{-b}$, where $a = 0.657424$, $b = 0.735226$ (solid red line), and the value for the incompressible fluid $n = 0.4$ (dashed magenta line). In (a), values of γ are those close to the water that has $\gamma = 7$. In (b), a larger range of γ is considered.

The initial stages of bubble collapse can be well described by the incompressible Euler equations. As R decreases, there is a transition to the asymptotic domain determined by $n(\gamma)$. An understanding of the evolution of the energy density requires a connection between the initial state and the final stages of implosion, which in turn necessitates a description of the transition region and a solution to the Euler equations for all Mach numbers. The goal of the next calculation that we have performed is to demonstrate such a transition for the case of spherical symmetry. To achieve this goal, we follow Hunter [61] and assume homentropic flow, so the specific entropy is uniform and constant in time. This simplifies the calculations as a simple equation of state given by Eq. (3.3) can then be used, for which analytic asymptotic results are known. This allows us to confirm the accuracy of the obtained numerical solution in the final stages of the collapse. Moreover, we believe that for rapid collapses of interest, ignoring heat transfer can be a reasonable approximation. For additional simplicity, we ignore the effects of viscosity, surface tension and mass transfer.

Numerical solutions of compressible equations for describing cavitation have a long history. Hunter [61] solved the homentropic compressible Euler equations for the fluid outside

the cavity, but the cavity was assumed to be empty. Later, Wu and Roberts [69] solved Euler equations for the motion of the gas within the bubble, while the effects of compressibility of the outside fluid were introduced through an effective differential equation for the motion of the cavity wall instead of solving full Euler equations. Fuster, Dopazo and Hauke [70] computed spherical bubble collapse by solving the full hydrodynamic equations for both the gas in the cavity and the compressible fluid outside of it and considered sufficiently strong collapses where $R_m/R = 13$ was reached. The same problem, although without the assumption of spherical symmetry, was recently approached by an all-Mach solver implemented in the Basilisk solver [71] using the volume-of-fluid method. In that case, $R_m/R = 5$ was reached. This solver was then modified for the case of spherical symmetry, and adiabatic collapses reaching $R_m/R = 13$ were analyzed [72]. In none of these simulations, except Hunter, was the asymptotic limit of Fig. 3.1 clearly demonstrated.

To simulate a homentropic, spherically collapsing cavity with gas inside it, but for $R_m/R > 100$ relevant for experiments, we first considered the aforementioned all-Mach solvers [71, 72]. Due to the extreme physical parameters found in such strong collapses, a numerical instability appears near the cavity wall even in the initial stages of the collapse, where it is incompressible. The instability would not disappear even after refining the calculation to the limits of the available computational resources.

To resolve this issue, we modified the solver by introducing the uniform bubble approximation. Instead of directly solving the Euler equations for the gas in the cavity, we assume that the pressure and the mass density of the gas are always uniform and consistent with the equation of state. For simplicity, we adopt the form of an ideal adiabatic monatomic gas equation of state. This approximation is accurate for early times when the motion is nearly incompressible, as we will discuss later. Such an approach allows us to avoid the mentioned numerical instability, but at later times, it neglects the behavior of the gas that might be important, such as shock waves forming in the gas. Nevertheless, it provides a way to explore the effects of compressibility for large collapses and allows for quick and accurate computations. In future work, one can include corrections to the solution for the motion of the gas

by including higher-order terms in the Mach number of the gas that would correspond to nonuniformities.

Fig. 3.2 shows plots of the transition to the asymptotic domain of a compressible implosion in water. For $R_m/R_0 = 20$ and $R_0 = 2.2$ μm, motivated by experiments discussed in [6], for a cavity with ambient pressure $p_\infty = 1$ atm, ambient temperature $T_\infty = 293$ K, and containing an ideal xenon gas, the result based on our implementation of the all-Mach solver is shown as the black solid line. The maximum Mach number, $\mathrm{M} = \dot{R}/c_\infty$, in this calculation is 2.8, and the maximum ratio of radii is $R_m/R = 320$. This shows the necessity of an all-Mach solver to include compressibility effects for strong collapses found in experiments. The red dot-dashed lines in Fig. 3.2 are the solutions that describe the incompressible limit [2]. If the water remained incompressible, the Mach number would reach 140, and the maximum ratio of radii would be $R_m/R = 1460$. This figure also illustrates the goal of our work, which is a demonstration of the transition to the compressibility asymptote that controls the moment of collapse. The green dashed curve corresponds to the power-law solution of the form given in Eq. (3.1) with Hunter's value $n = 0.56$, which is a good fit to the asymptotic motion that precedes the moment of collapse.

Cavitation in liquid lithium has been studied with regard to erosion [65] and nuclear processes [66]. Using an ambient temperature $T_\infty = 450$ K relevant for the experiments, the motion of a bubble with putative parameters $R_m/R_0 = 20$ and $R_0 = 2.2$ μm is shown in Fig. 3.3. We again assume that the cavity contains ideal xenon gas and the ambient pressure is $p_\infty = 1$ atm. At small radii, the motion agrees with the power-law solution of the form given in Eq. (3.1) with $n = 0.62$, consistent with the asymptotic result obtained in Section 3.2. The maximum Mach number reached with respect to liquid lithium, $\mathrm{M} = \dot{R}/c_\infty$, for the incompressible case is 62, while for our compressible calculation, it is 1.6. Additionally, the maximum ratio of radii reached in the incompressible case is $R_m/R = 1460$, but it is $R_m/R = 340$ for the compressible scenario.

Figs. 3.2 and 3.3 are tests of the validity of our extension of the all-Mach solver to the compressibility asymptote. The obtained solutions will facilitate coupling the fluid to the

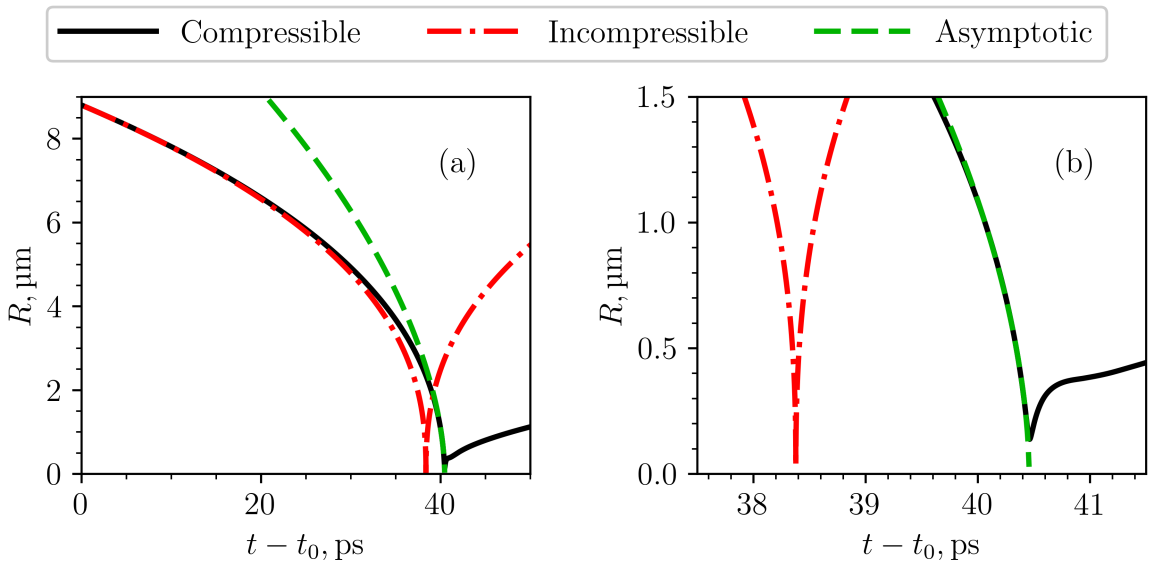

Figure 3.2: Implosion of an ideal gas xenon bubble in water for ambient pressure $p_\infty = 1$ atm and ambient temperature $T_\infty = 293$ K, with $R_m/R_0 = 20$ and $R_0 = 2.2$ μm. The red dot-dashed line represents the incompressible solution for the ambient density of water $\rho_\infty = 1000$ kg/m^3. The black solid line is obtained by our modified all-Mach solver with the uniform bubble approximation. The compressibility of water is given by Eq. (3.3) with $B = 3000$ atm, $\gamma = 7$, and $\rho_0 = 1000$ kg/m^3. The dashed green line is a power-law fit of the form as in Eq. (3.1) with $n = 0.56$, as predicted in [61]. The comparison is shown here from a time t_0, where $R(t_0) = R_m/5$, as before this time, the compressible and incompressible results agree. In (b), the solutions shown in (a) are zoomed in near the minimum radii of the curves.

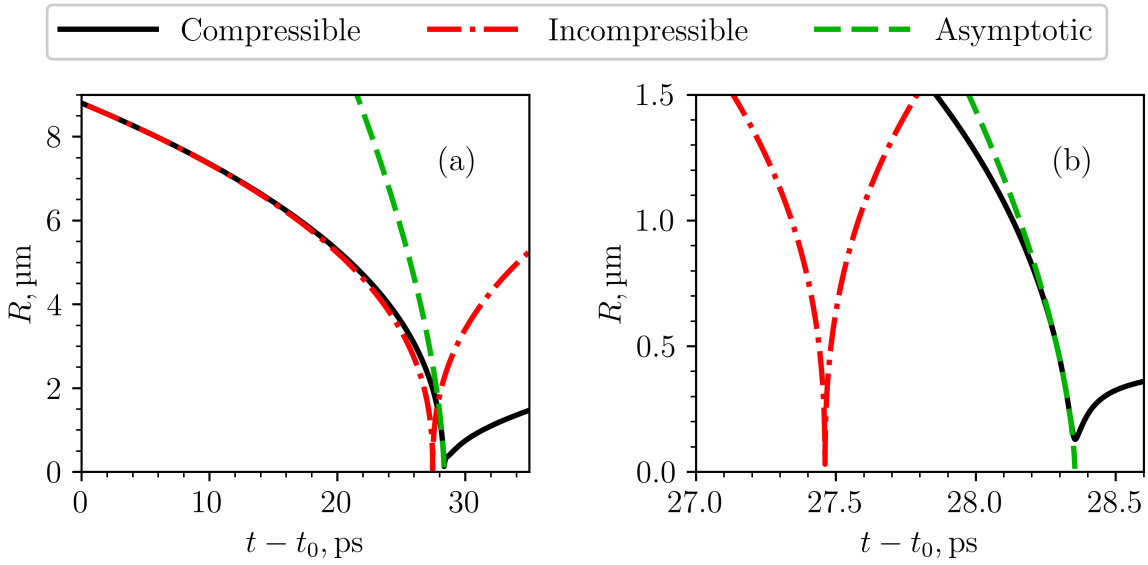

Figure 3.3: Implosion of an ideal gas xenon bubble in liquid lithium for ambient pressure $p_\infty = 1$ atm and ambient temperature $T_\infty = 450$ K, with $R_m/R_0 = 20$ and $R_0 = 2.2$ µm. The red dot-dashed line represents the incompressible solution for the ambient density of liquid lithium $\rho_\infty = 520$ kg/m^3. The black solid line is obtained by our modified all-Mach solver with the uniform bubble approximation. The compressibility of liquid lithium is given by Eq. (3.3) with $B = 22000$ atm, $\gamma = 4.5$, and $\rho_0 = 520$ kg/m^3. The dashed green line is a power-law fit of the form as in Eq. (3.1) with $n = 0.62$, as predicted in Section 3.2 and shown in Fig. 3.1. The comparison is shown here from a time t_0, where $R(t_0) = R_m/5$, as before this time, the compressible and incompressible results agree. In (b), the solutions shown in (a) are zoomed in near the minimum radii of the curves.

molecular dynamics of the internal gas [7, 8, 9, 10], which is a future effort. Such molecular dynamics simulations, when coupled to our results, would allow us to understand whether a shock wave is launched internally to the gas contained in the collapsing cavity [69]. This would set up a possibility for a second stage of energy focusing and would raise prospects for the use of acoustics to achieve thermal fusion. The compressibility of the fluid slows down the collapse and might inhibit the formation of a spherically focusing shock wave. However, fluids with different equation of state parameters B, γ, ρ_0 might allow for such higher levels of concentration of energy density. Therefore, our calculations might motivate a search for candidate liquids to achieve greater levels of energy focusing.

3.2 Asymptotic calculations for an empty cavity

3.2.1 Theory

In this section, we extend the results of Hunter [61] on the asymptotic calculation for the final stage of collapse of an empty cavity, where the effects of compressibility of the outside fluid are included. To do so, we use Hunter's method and, unlike Hunter, apply it not only to water but also to a wide range of materials described by the equation of state in Eq. (3.3). This subsection provides a summary of the methods used to perform the computations.

We assume a spherically symmetric scenario in which a spherical empty cavity has its center placed in the origin of the coordinate system and whose radius is described by a time dependent function $R(t)$. Outside of this radius, we assume an infinite ideal fluid which is described by mass conservation law and the Euler equation, where due to spherical symmetry fluid's only nonzero component of velocity is radial component u, and both radial velocity component and mass density ρ are only functions of radial coordinate r and time t. We do not consider an equation for entropy as we assume that the flow is homentropic. The following equations are considered for $r > R(t)$.

$$\rho\left(\frac{\partial u}{\partial t} + u\frac{\partial u}{\partial r}\right) = -\frac{\partial p}{\partial r}, \tag{3.6}$$

$$\frac{\partial \rho}{\partial t} + u\frac{\partial \rho}{\partial r} + \rho\left(\frac{2u}{r} + \frac{\partial u}{\partial r}\right) = 0. \tag{3.7}$$

To describe pressure p, we assume the Tait-Murnaghan equation of state given by Eq. (3.3). As the flow is assumed to be homentropic, both functions B and ρ_0 can be treated as constants.

We would like to enforce two boundary conditions for both radial velocity u and pressure p, where one is at the interface between the empty cavity and fluid at $r = R(t)$, and the other one is far from the cavity as $r \to \infty$. For radial velocity, we assume that the empty cavity is a free surface and that far away from the cavity the fluid is at rest. For pressure, we assume that at the surface of the cavity, pressure is zero as the cavity is empty, and far away it approaches some finite value p_∞. Boundary conditions are summarized next, where the dot represents the derivative with respect to the time.

$$u(R(t), t) = \dot{R}(t), \qquad \lim_{r\to\infty} u(r, t) = 0. \tag{3.8}$$

$$p(R(t), t) = 0, \qquad \lim_{r\to\infty} p(r, t) = p_\infty. \tag{3.9}$$

Using the assumed equation of state, it is possible to compute the speed of sound squared c^2 as a function of ρ, and change variables describing fluid from u, ρ to u, c^2. This is convenient in order to apply similarity theory for the later parts of the collapse when $R(t) \to 0$, as both variables u and c^2 can be directly compared to the velocity of cavity's wall $\dot{R}(t)$.

$$c^2 = \frac{\partial p}{\partial \rho} = \frac{B\gamma\rho^{\gamma-1}}{\rho_0^\gamma}, \qquad \rho = \left(\frac{\rho_0^\gamma c^2}{B\gamma}\right)^{1/(\gamma-1)}. \tag{3.10}$$

Using the expression for c^2 in terms of density ρ as in Eq. (3.10), spherical Euler equation, Eq. (3.6), and mass conservation law, Eq. (3.7), are rewritten in terms of variables u, c^2 as follows.

$$\frac{\partial u}{\partial t} + u\frac{\partial u}{\partial r} + \frac{1}{(\gamma-1)}\frac{\partial c^2}{\partial r} = 0, \tag{3.11}$$

$$\frac{\partial c^2}{\partial t} + u\frac{\partial c^2}{\partial r} + c^2(\gamma-1)\left(\frac{2u}{r} + \frac{\partial u}{\partial r}\right) = 0. \tag{3.12}$$

Using Eqs. (3.3), (3.10), it is possible to compute boundary conditions for c^2 given by constants c_0^2, c_∞^2, from the corresponding boundary conditions for pressure as in Eq. (3.9).

$$c^2(R(t),t) = \frac{B\gamma}{\rho_0} = c_0^2, \qquad \lim_{r\to\infty} c^2(r,t) = c_\infty^2. \tag{3.13}$$

Instead of solving the system of partial differential equations given by Eqs. (3.11), (3.12) which would mean that we have to supply initial conditions, we consider similarity theory that is motivated by numerical results [61]. As we approach the last phase of the collapse where $R(t) \to 0$, we assume that the length scale of the problem is given by $R(t)$ and the scale for velocities is given by $\dot{R}(t)$. So, we seek solutions of the following form, where we are interested in finding functions f and g. The goal is to reduce the problem to a system of ordinary differential equations for f and g.

$$\frac{u(r,t)}{\dot{R}(t)} = f\left(\frac{r}{R(t)}\right), \qquad \frac{c^2(r,t)}{\dot{R}^2(t)} = g\left(\frac{r}{R(t)}\right). \tag{3.14}$$

Motivated by the numerical results of the full hydrodynamic equations given in Eqs. (3.11), (3.12) in the case of water [61], we additionally assume the power-law form $R(t) = A_n(t_c - t)^n$, where t_c is a time at which collapse happens and n is a power-law exponent that we would like to compute. Using such power-law assumption and similarity approach for u, c^2 as in Eq. (3.14), we can rewrite Eqs. (3.11), (3.12) as two coupled ordinary differential equations for functions f and g, where we introduce variable $x = r/R(t)$. Then, differential equations have to be solved in the range $x > 1$.

$$f'(x)\left(f(x) - x\right) + \left(1 - \frac{1}{n}\right) f(x) + \frac{g'(x)}{(\gamma - 1)} = 0, \tag{3.15}$$

$$g'(x)\left(f(x) - x\right) + 2\left(1 - \frac{1}{n}\right) g(x) + g(x)(\gamma - 1)\left(\frac{2f(x)}{x} + f'(x)\right) = 0. \tag{3.16}$$

As these equations are ordinary differential equations, we do not have to worry about what kind of initial conditions to choose for u, c^2, as functions f and g can be solved only by the boundary conditions. To compute boundary conditions from those of u, c^2 given in Eqs. (3.8), (3.13), we use definitions of f, g in terms of u, c^2 as in Eq. (3.14). However, for the assumed form of c^2 in Eq. (3.14), boundary conditions cannot be satisfied. Instead, because

$\dot{R}(t) \to -\infty$ as $R(t) \to 0$, to get finite speeds of sounds at boundaries, we assume that g is zero at the boundaries if all we are interested in is the late stage of the collapse.

$$f(1) = 1, \qquad \lim_{x\to\infty} f(x) = 0. \tag{3.17}$$

$$g(1) = 0, \qquad \lim_{x\to\infty} g(x) = 0. \tag{3.18}$$

The goal now is for each value of γ describing the equation of state of the fluid to find the value of n so that differential equations given by Eqs. (3.15), (3.16) are satisfied with the appropriate boundary conditions given by Eqs. (3.17), (3.18).

3.2.2 Numerical analysis

It is convenient to rewrite differential equations given by Eqs. (3.15), (3.16) in the following way so that each equation contains a derivative of only one of the functions. To do this, insert the expression for $g'(x)$ from Eq. (3.16) to Eq. (3.15), or insert the expression for $f'(x)$ from Eq. (3.15) to Eq. (3.16).

$$\begin{aligned} f'(x)\left((f(x)-x)^2 - g(x)\right) = &-\left(1-\frac{1}{n}\right) f(x)(f(x)-x) \\ &+2\left(1-\frac{1}{n}\right)\frac{g(x)}{(\gamma-1)} + \frac{2f(x)g(x)}{x}, \end{aligned} \tag{3.19}$$

$$\begin{aligned} g'(x)\left((f(x)-x)^2 - g(x)\right) = &\left(1-\frac{1}{n}\right)(\gamma-1)f(x)g(x) \\ &-2\left(1-\frac{1}{n}\right) g(x)(f(x)-x) + 2(\gamma-1)f(x)g(x)\frac{(x-f(x))}{x}. \end{aligned} \tag{3.20}$$

Notice that the Eqs. (3.19), (3.20) are singular at $x = 1$ with the boundary conditions chosen as Eqs. (3.17), (3.18) as at $x = 1$ it is not possible to solve for $f'(1)$ and $g'(1)$ which then would be used to numerically approximate values of f, g for some $x > 1$. So, instead of solving equations numerically from $x = 1$, we start from $x = 1 + \varepsilon$, where $0 < \varepsilon \ll 1$. To do that, we have to understand what are the new boundary conditions at such a point. To compute them, we expand both functions in ε around $x = 1$ as given next, where we use

boundary conditions at $x = 1$ as in Eqs. (3.17), (3.18).

$$\begin{aligned} f(1+\varepsilon) &= f(1) + f'(1)\varepsilon + O(\varepsilon^2) = 1 + f'(1)\varepsilon + O(\varepsilon^2), \\ f'(1+\varepsilon) &= f'(1) + f''(1)\varepsilon + O(\varepsilon^2). \end{aligned} \tag{3.21}$$

$$\begin{aligned} g(1+\varepsilon) &= g(1) + g'(1)\varepsilon + O(\varepsilon^2) = g'(1)\varepsilon + O(\varepsilon^2), \\ g'(1+\varepsilon) &= g'(1) + g''(1)\varepsilon + O(\varepsilon^2). \end{aligned} \tag{3.22}$$

Consider differential equations given by Eqs. (3.19), (3.20) up to first order in ε. As equations are singular at $x = 1$, no information is obtained from the zeroth order in ε. However, from the first order in ε, it is possible to compute values of $f'(1), g'(1)$ and to approximate boundary conditions as follows.

$$f(1+\varepsilon) \approx 1 + \frac{1}{\gamma}\left(3 - 2\left(1 - \frac{1}{n}\right) - 2\gamma\right)\varepsilon, \tag{3.23}$$

$$g(1+\varepsilon) \approx \left(1 - \frac{1}{n}\right)(1-\gamma)\varepsilon. \tag{3.24}$$

For a given choice of γ, we search through values of n and for each guess of n we numerically integrate Eqs. (3.19), (3.20) starting from $x = 1 + \varepsilon$, where boundary conditions given by Eqs. (3.23), (3.24) are used, until $x = 5$. The maximum value of x is chosen from practical considerations as then it is clear whether boundary conditions as $x \to \infty$ given by Eqs. (3.17), (3.18) are satisfied or not. If they are, we report this value of n as the predicted value for the power law exponent of the cavity wall's collapse. Value of ε used in numerical calculations is $\varepsilon = 10^{-3}$. It was checked that if this value is taken to be smaller then the results do not change significantly. For example, if $\gamma = 8$, then predicted values for $\varepsilon = 10^{-3}, 10^{-4}, 10^{-5}$ are $n = 0.540799, 0.540801, 0.540801$, respectively. As an example of a search of n for $\gamma = 8$, consider results in Fig. 3.4 which show how solutions of the function g look like if n is smaller, equal, or greater than the predicted value.

First, we consider obtained results for n as a function of γ, where a range of γ is chosen to be close to the value for water, $\gamma = 7$. We predict that the majority of materials have γ values close to the one of water, so for this range, we propose the following fit that might be useful for practical applications, $n = 0.4 + a\gamma^{-b}$, where $a = 0.657424$, $b = 0.735226$. For

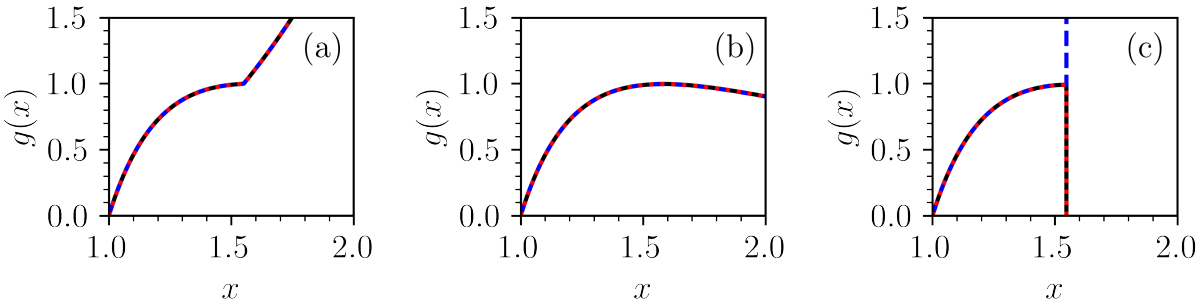

Figure 3.4: Numerically obtained solutions for $g(x)$ shown here from $x = 1 + \varepsilon$ until $x = 2$, where $\varepsilon = 10^{-3}$ (solid black line), $\varepsilon = 10^{-4}$ (dashed blue line), $\varepsilon = 10^{-5}$ (dotted red line). In (a), the guessed value of n is smaller than the predicted one by 10^{-4}. In (b), it is equal to the predicted value $n = 0.540799, 0.540801, 0.540801$ for $\varepsilon = 10^{-3}, 10^{-4}, 10^{-5}$, respectively. In (c), the guessed value of n is larger than the predicted value by 10^{-4}. The guessed solutions in (a) and (c) are not satisfactory because they are not smooth at around $x = 1.55$ and do not satisfy the boundary condition given in Eq. (3.18) as $x \to \infty$.

this range of γ, the results are shown in Fig. 3.1(a). We have checked that our calculation for the case where $\gamma = 7$, that corresponds to the water, agrees with the obtained value of n of Hunter [61]. However, the described method can also be used to compute n for large values of γ, results for which are given in Fig. 3.1(b). We see that as $\gamma \to \infty$, values indeed approach the incompressible limit $n = 0.4$ [58].

3.3 Full calculations using the Euler equation

3.3.1 Theory

Just as during the analysis of asymptotic calculations, we assume a spherically symmetric and homentropic scenario, where the center of the cavity filled with gas is placed at the origin of the coordinate system. For both the gas inside the cavity and the fluid outside of it, motion is described by the mass conservation law and the Euler equation, as given in Eqs. (3.6) and (3.7). Due to our assumption of homentropic flow, we do not consider the differential equation for specific entropy.

These equations apply to the compressible fluid in the region outside the cavity, $r > R(t)$, corresponding to the subscript "f" in the future formulas, and to the gas which occupies the space within the cavity, $r < R(t)$, corresponding to the subscript "g". To close the equations of motion, an expression for pressure is required. For the compressible fluid in the region $r > R(t)$, the Tait-Murnaghan equation of state is assumed as given in Eq. (3.3). Because the flow is homentropic, functions B and ρ_0 can be treated as constants. For the gas inside the cavity, the assumed equation of state is that of an ideal adiabatic monatomic gas, where the function C, which generally depends on specific entropy, in a homentropic flow can be treated as a constant [2]. Such a choice is consistent with our goal of isolating the effects of compressibility and taking the simplest case where such effects could be observed.

$$p(\rho) = C\rho^{5/3} \tag{3.25}$$

Even though the general goal is to solve the full hydrodynamic Eqs. (3.6) and (3.7) for the gas in the cavity, when discussing numerical results, we will motivate and explain an approximation that was used to avoid numerical instabilities and decrease the computational time. In this approximation, the hydrodynamic equations for the gas inside the cavity are solved under the assumption that both mass density and pressure are uniform within the entire cavity at all times, and consistent with the equation of state given by Eq. (3.25).

The boundary conditions must be given at the boundaries of the domain, so, as $r \to 0$ and $r \to \infty$, but also at the interface between two fluids at $r = R(t)$. As $r \to 0$, the boundary conditions are motivated by requiring that functions describing the mass density of the gas, $\rho_g(r,t)$, and radial velocity, $u_g(r,t)$, are smooth at the origin [70].

$$\frac{\partial \rho_g}{\partial r}(0,t) = 0, \qquad u_g(0,t) = 0. \tag{3.26}$$

As $r \to \infty$, a set of intuitive boundary conditions are that the outside fluid is at rest at an ambient pressure, as given in Eqs. (3.8) and (3.9). However, the boundary conditions assumed in our calculations differ. By assuming smoothness of solutions, alternative boundary conditions can be derived from the more natural boundary conditions, but they offer the

advantage of faster numerical convergence.

$$\lim_{r\to\infty}\frac{\partial\rho_f}{\partial r}(r,t)=0, \qquad \lim_{r\to\infty}\frac{\partial u_f}{\partial r}(r,t)=0. \tag{3.27}$$

Finally, at the interface, viscosity, mass transfer, and surface tension effects are ignored, so the boundary conditions are as follows [2].

$$u_g(R(t),t)=u_f(R(t),t), \qquad p_g(R(t),t)=p_f(R(t),t). \tag{3.28}$$

Due to the continuity of the radial velocity across the interface, the evolution of the cavity's wall is described in the following way.

$$\dot{R}(t)=u_g(R(t),t)=u_f(R(t),t) \tag{3.29}$$

The initial conditions must also be provided for the hydrodynamic functions for both fluids and for the initial state of the cavity's wall. Instead of specifying them for the radial velocity and mass density of the fluids, we specify the radial velocity and pressure. From this information, the initial mass density can be computed using the corresponding equation of state. We take the initial state to be at time $t=0$, where the cavity is at its maximum radius R_m, and the collapse starts from rest.

$$\begin{aligned} R(0)&=R_m, \qquad \dot{R}(0)=0,\\ u_g(r,0)&=0, \qquad \text{for all } r<R_m,\\ u_f(r,0)&=0, \qquad \text{for all } r>R_m. \end{aligned} \tag{3.30}$$

The initial conditions for the pressure are estimated, assuming that the motion near the beginning of the collapse is incompressible, as everything starts from rest. For the outside fluid in the region $r>R(t)$, the incompressible solution is given as follows [2, 58].

$$u_f(r,t)=\dot{R}(t)\left(\frac{R(t)}{r}\right)^2, \tag{3.31}$$

$$p_f(r,t)=\frac{\rho_\infty\dot{R}^2(t)}{2}\left(\frac{R(t)}{r}-\left(\frac{R(t)}{r}\right)^4\right)+p_\infty\left(1-\frac{R(t)}{r}\right)+p_g\left(R(t)\right)\frac{R(t)}{r}, \tag{3.32}$$

$$\ddot{R}(t)R(t) + \frac{3}{2}\dot{R}^2(t) = -\frac{(p_\infty - p_g(R(t)))}{\rho_\infty}. \tag{3.33}$$

In Eqs. (3.32) and (3.33), $p_g(R(t))$ represents the uniform pressure for the gas in the bubble at any given radius $R(t)$. If the mass density for the gas is assumed to be uniform, then by the mass conservation law and assuming ambient conditions with a radius of R_0 and a mass density of $\rho_{g,0}$,

$$\rho_g(R) = \rho_{g,0}\left(\frac{R_0}{R}\right)^3. \tag{3.34}$$

The ambient uniform mass density of the gas can be computed from the ideal gas law if the ambient temperature T_∞ and the mass of a single gas atom m are known. Here, k_B represents the Boltzmann constant.

$$p_\infty = \frac{\rho_{g,0}k_BT_\infty}{m} \tag{3.35}$$

Together with the assumed equation of state in Eq. (3.25), this provides the uniform pressure for the ideal gas under consideration, which can then be used in Eqs. (3.32) and (3.33).

$$p_g(R) = p_\infty\left(\frac{R_0}{R}\right)^5 \tag{3.36}$$

Using these results, we adopt the following uniform initial pressure and mass density profiles that are valid for all $r < R_m$, and $\rho_{g,0}$ is estimated from Eq. (3.35).

$$p_g(r,0) = p_\infty\left(\frac{R_0}{R_m}\right)^5, \qquad \rho_g(r,0) = \rho_{g,0}\left(\frac{R_0}{R_m}\right)^3. \tag{3.37}$$

The initial pressure profile for the outside fluid for all $r > R_m$ is then derived from Eq. (3.32) combined with Eq. (3.36), and evaluated at the initial conditions of the cavity's wall.

$$p_f(r,0) = p_\infty + \left(\left(\frac{R_0}{R_m}\right)^5 - 1\right)\frac{p_\infty R_m}{r} \tag{3.38}$$

From here, the initial mass density profile for the outside fluid, $\rho_f(r,0)$, can be obtained by inverting Eq. (3.38) using the equation of state provided by Eq. (3.3).

Our interest in cavity collapse is driven by our desire to understand the limits of energy focusing achievable with sonoluminescence. As mentioned, this requires a parameter space

where $R_m/R_0 > 8$, where, at least for water, Eqs. (3.31), (3.32), and (3.33) are inaccurate at long timescales. Nonetheless, comparing our calculations to such incompressible solutions allows us to understand when the effects of compressibility become significant. Additionally, later, we will discuss an improvement to the initialization of our computation by starting it from a lower radius, as during the initial stage of the collapse, the compressibility effects are negligible. In such a case, the initial conditions will be modified and estimated from the incompressible solution, enabling faster numerical calculations.

3.3.2 Numerical analysis

To numerically solve the proposed problem, we use an all-Mach semi-implicit numerical solver that employs the volume-of-fluid method [71], implemented in the Basilisk solver [73]. We modify it for the case of spherical symmetry, as previously done in [72]. Here, we summarize the key properties of this formulation.

To solve the Euler equations for two immiscible fluids, the interface at $r = R(t)$ is described by introducing a characteristic function $f(r,t)$ that is 0 in the region $r < R(t)$ and 1 in the region $r > R(t)$. The interface is located by the point of discontinuity of this function. As the boundary moves with radial velocity $\dot{R}(t)$, the characteristic function satisfies the following advection equation, which must be understood in the weak sense.

$$\frac{\partial f}{\partial t} + \dot{R}(t)\frac{\partial f}{\partial r} = 0 \tag{3.39}$$

The volume-of-fluid method numerically solves this differential equation by introducing the volume of a reference phase with respect to the total volume of the grid interval. In practice, the function f is smoothened within each computational grid interval, creating regions where $0 < f(r,t) < 1$. These regions are then interpreted as parts of the interface between two fluids. For example, the radius of the cavity, $R(t)$, can be numerically evaluated as follows. Here, i represents a grid interval in the numerical domain, each of them having the same width Δr, and f_i is the smoothed value of f in a grid interval.

$$R(t) = \Delta r \sum_i (1 - f_i) \tag{3.40}$$

For example, the Euler equation in Eq. (3.6) can be combined with the mass continuity law in Eq. (3.7) to obtain the equation for the momentum density ρu for each of the fluids.

$$\frac{\partial(\rho u)}{\partial t} + \frac{\partial(\rho u^2)}{\partial r} + \frac{2\rho u^2}{r} = -\frac{\partial p}{\partial r} \tag{3.41}$$

This equation is then averaged using the characteristic function f to obtain a single differential equation over the whole domain $r > 0$ for the averaged quantities [72]. For example, the averaged radial velocity is defined by $\overline{u} = (1-f)u_g + f u_f$, which, due to velocities at the interface being continuous, is also continuous. From this definition, indeed, if $r < R(t)$, $f(r,t) = 0$, and $\overline{u} = u_g$, while for $r > R(t)$, $f(r,t) = 1$, and $\overline{u} = u_f$, consistent with the previous definitions.

$$\frac{\partial(\overline{\rho u})}{\partial t} + \frac{\partial(\overline{\rho u}\ \overline{u})}{\partial r} + \frac{2\overline{\rho u}\ \overline{u}}{r} = -\frac{\partial \overline{p}}{\partial r} \tag{3.42}$$

To summarize, the boundary condition at $r = R(t)$ is replaced by the differential equation for f, and two sets of Euler equations for $r < R(t)$ and $r > R(t)$ are replaced by a single evolution equation for the various averaged quantities. In addition to Eqs. (3.39) and (3.42), the averaged equations for the individual components of densities and energies are solved.

All-Mach semi-implicit solvers are known to produce accurate results for compressible problems even if shock waves are formed, while numerical schemes based on the volume-of-fluid method have the advantage of sharply representing the interface between two fluids and behaving well in the incompressible regime. The described numerical approach also employs a consistent advection scheme of conservative quantities, avoiding any numerical diffusion of mass, momentum, and energy across the interface during the advection step, thus greatly reducing errors that appear during the advection of discontinuities. This is crucial in cases of large density differences between the two fluids, which occur in our problem.

To solve the problem numerically, a uniform spatial grid with grid intervals of width Δr is used. In the future, the results could be improved by implementing adaptive gridding. The full numerical region is taken to be $0 < r < \lambda R(t=0)$, where λ is a numerical parameter specifying the high-radius cutoff, typically $\lambda = 4$ or 8, and $R(t=0)$ is the initial radius,

which in our simulations is either $R(t=0) = R_m$ or $R_m/5$. The boundary conditions given in Eq. (3.27), which theoretically apply in the limit of $r \to \infty$, are applied at the cutoff $r = \lambda R(t=0)$. For the sake of quick calculations, it is useful to take λ as small as possible, but this influences the accuracy of the obtained results due to the lower accuracy of the boundary condition. The optimal value is determined by performing convergence studies, which will be discussed later.

The time step size Δt during the computation is not fixed and is chosen by a combination of a fixed time step size parameter with adaptive time step size schemes. The time step size parameter $\Delta t_{\max}$ remains fixed throughout the calculation and determines the largest used time step size. Two adaptive time step size schemes, $\Delta t_{\overline{u}}$ and $\Delta t_{\overline{c}}$, are used, both inspired by the CFL condition. Here, $|\overline{u}|_{\max}$ is the largest magnitude of the average radial velocity across all grid intervals, and $|\overline{c}|_{\max}$ is the largest magnitude of the average speed of sound across all grid intervals.

$$\Delta t_{\overline{u}} = \frac{\Delta r}{2|\overline{u}|_{\max}}, \qquad \Delta t_{\overline{c}} = \frac{\Delta r}{2|\overline{c}|_{\max}}. \tag{3.43}$$

Finally, at each instant, the time step size Δt is determined as the smallest value among $\Delta t_{\max}$, $\Delta t_{\overline{u}}$, and $\Delta t_{\overline{c}}$. The adaptive methods allow for simple estimates of what the time step size should be for the complicated nonlinear problem at hand, while $\Delta t_{\max}$ allows for further refinement until the desired level of accuracy. Additionally, a small value of $\Delta t_{\max}$ leads to fewer iterations and better convergence of the underlying multigrid Poisson solver.

For each specific problem, we start by fixing the value of $\lambda = 4$. Then, runs are performed for various Δr without using $\Delta t_{\max}$ in the computation of Δt, and we find the smallest value of Δr that allows us to solve the problem quickly. For this Δr, we check numerical convergence in λ by increasing it in factors of two and finding the value that will be used for the remaining runs. Then, numerical convergence in Δr and $\Delta t_{\max}$ is analyzed. The first value of $\Delta t_{\max}$ is taken to be the typical value of Δt in previous runs, where only adaptive time step size methods were used. Then, both Δr and $\Delta t_{\max}$ are decreased in factors of two until the desired accuracy is achieved or the limits of computational resources are reached. Simultaneous refinement of Δr and $\Delta t_{\max}$ saves time spent studying the convergence of

numerical solutions and was observed to enhance convergence for the obtained $\dot{R}(t)$ curves.

As the first numerical example before considering more rapid collapse, where $R_m/R_0 = 20$, we solved for a smaller but still strong collapse with $R_m/R_0 = 10$. The full hydrodynamic equations are numerically solved for both the gas and the fluid outside the cavity with the previously described boundary conditions. The gas inside the cavity is assumed to be xenon, while the outside fluid is taken to be water. The initial conditions correspond to both the gas and the fluid starting from rest, with the cavity at the maximum radius R_m. The ambient physical parameters, $R_0 = 2.2$ μm, $p_\infty = 1$ atm, and $T_\infty = 293$ K, are motivated by the values found in the experiments [6].

During the initial stage of the collapse, when $R(t)$ is still close to R_m, it is observed that the mass density profile of the gas quickly transitions from being uniform to having a region of low density near the cavity wall, while in the same region the speed of sound becomes extremely high. As a result, the adaptive time step size based on the speed of sound becomes very small, making the computation unfeasible. This effect does not completely disappear with further refinement within the limits of the available computational resources. An example with numerical parameters $\lambda = 4$, $\Delta r = R_m/512$, and $\Delta t_{\max} = (1/4) \times 10^{-5} R_0 \sqrt{\rho_\infty/p_\infty}$, is shown in Fig. 3.5. Indeed, after $t = R_0\sqrt{\rho_\infty/p_\infty}$, where $R(t) = 0.995R_m$, Fig. 3.5(c) shows a region in the gas near the cavity's wall where the mass density is not uniform. A region with a size of about $R_m/20 = R_0/2$ is observed, where the mass density of the gas is much smaller than everywhere else in the gas. On the other hand, the speed of sound, shown in Fig. 3.5(d), at this time does not show unusual behavior. However, after $t = 2R_0\sqrt{\rho_\infty/p_\infty}$, with $R(t) = 0.980R_m$, Fig. 3.5(e) shows the mass density in the gas with nonuniformity on a length scale of $R_m/2 = 5R_0$, and near the cavity's wall there is a region with a size of around $R_m/5 = 2R_0$, where the mass density is extremely small. Moreover, an extremely high value of the speed of sound in the gas is observed in such a region. As can be seen from Fig. 3.5(f), the speed of sound near the cavity's wall reaches an extreme value of $\bar{c} = 7 \times 10^6 \sqrt{p_\infty/\rho_\infty}$. If instead the pressure and mass density in the gas were uniform, the speed of sound, from Eq. (3.25), combined with mass density from Eq. (3.34) and pressure from Eq. (3.36), would

be $\bar{c} = 1.8\sqrt{p_\infty/\rho_\infty}$ at $R(t) = 0.980R_m$.

To argue that the observed effect is a numerical artifact and not a physical process, we use the observation that the effect happens at times sufficiently close to the initial state, where $R(t) \approx R_m$. As the cavity starts from rest, the motion of the gas can be analyzed using a low Mach number expansion [74, 75], which is valid when the following dimensionless parameter is small.

$$\varepsilon = \frac{u_{\text{ref}}}{\sqrt{p_{\text{ref}}/\rho_{\text{ref}}}} \tag{3.44}$$

In this definition, u_{ref}, p_{ref}, and ρ_{ref} correspond to the typical (or reference) values of radial velocity, pressure, and mass density, respectively, for the flow under consideration. In this case, the leading term for the solution of both mass density and pressure is spatially uniform but possibly time-dependent. The next-order correction describing nonuniformity is of order ε^2.

We now estimate ε for the initial motion of the gas. To estimate the typical values of mass density and pressure, we use Eqs. (3.34) and (3.36), with $R(t) = 0.980R_m$, that leads to $p_{\text{ref}} = 1.1 \times 10^{-5} p_\infty$ and $\rho_{\text{ref}} = 5.7 \times 10^{-6} \rho_\infty$. The typical velocity can be estimated from the velocity of the bubble using Eq. (3.33), by rewriting it in the energy form [58] and using that $p_{\text{ref}} \ll p_\infty$.

$$\dot{R}(t) = -\sqrt{\frac{2p_\infty}{3\rho_\infty}\left(\left(\frac{R_m}{R(t)}\right)^3 - 1\right)} \tag{3.45}$$

Evaluating this expression at $R(t) = 0.980R_m$ leads to $u_{\text{ref}} = -0.20\sqrt{p_\infty/\rho_\infty}$. Combining these results, we obtain $\varepsilon = -0.144$ and $\varepsilon^2 = 0.021 \ll 1$. This indeed shows that the low Mach number expansion for the motion of the gas should be reasonable and that the effects of nonuniformity should be small, contradicting the observed numerical behavior.

We were not able to use the original all-Mach solver to obtain numerical results without the issue of a region with small density appearing in the gas near the wall, and this led us to consider an alternative approach. Motivated by the low Mach number expansion, which should be accurate near the maximum radius, we assume that at all times the mass density and the pressure inside the gas is uniform but time-dependent. Although at later times

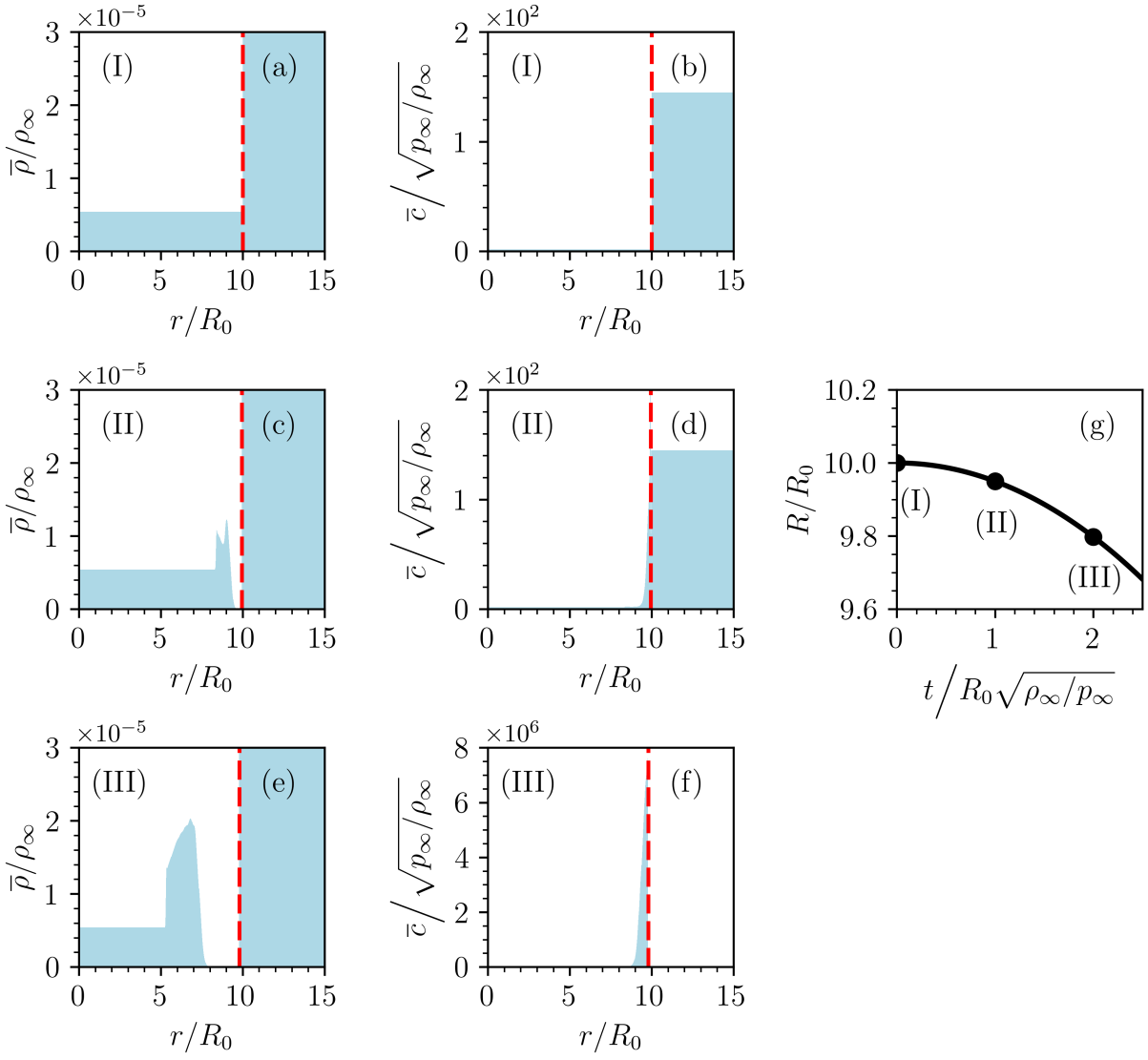

Figure 3.5: Implosion of an ideal gas xenon bubble in compressible water with ambient pressure $p_\infty = 1$ atm and ambient temperature $T_\infty = 293$ K, with $R_m/R_0 = 10$ and $R_0 = 2.2$ µm. The full hydrodynamic equations are solved for both the gas and the outside fluid starting from the maximum radius R_m, where cavity is at rest. The numerical parameters are $\lambda = 4$, $\Delta r = R_m/512$, and $\Delta t_{\max} = (1/4)\times 10^{-5} R_0\sqrt{\rho_\infty/p_\infty}$. The figure shows the solution at three times $t = 0.0, 1.0, 2.0$, in units of $R_0\sqrt{\rho_\infty/p_\infty}$, corresponding to (I), (II), (III), respectively. Figures (a), (c), (e) show profiles of the average mass density, $\overline{\rho}$, while (b), (d), (f) show the average speed of sound, $\overline{c}$. In (a)-(f), the red dashed line denotes the location of the cavity's wall at a given time. In (g), $R(t)$ is shown.

the cavity's velocity increases by many orders of magnitude and such approximation would start to fail, it allows us to consider the effects of compressibility of the outside fluid on the collapse and bypass the mentioned numerical instability. Indeed, this is similar to the incompressible solution given in Eqs. (3.32) and (3.33), where the pressure in the gas is assumed to be uniform. However, such an approach does not allow us to directly capture effects of nonuniformities in the gas, such as the formation of shock waves, but these could be captured in the future by adding more terms in the low Mach number expansion solution for the gas.

To numerically realize the uniform bubble approximation, during each time step we first let the original all-Mach solver to perform all its procedures, such as solving Eq. (3.42) for all $r > 0$, which includes the region with the gas. These procedures then also update the location of the bubble, $R(t)$, and its velocity, $\dot{R}(t)$. The value $R(t)$ is found numerically by Eq. (3.40), while $\dot{R}(t)$ is found by identifying the grid interval i with radial coordinates $r_i < r < r_{i+1} = r_i + \Delta r$ where $R(t)$ is located, and estimating $\dot{R}(t)$ using the grid-centered average radial velocity $\overline{u}_i$ for this interval. Finally, before the time step is completed, we additionally find all grid intervals i where $f_i = 0$, which correspond to the interval being occupied only by the gas. In all such grid intervals, according to our uniform bubble approximation, we overwrite the values of mass density to be given by Eq. (3.34) and pressure to be given by Eq. (3.36), both evaluated at the current radius $R(t)$. Additionally, the velocity field in the gas is rewritten according to the low Mach number result [74, 75].

$$u_g(r,t) = \dot{R}(t)\frac{r}{R(t)} \tag{3.46}$$

To see how such an approximation influences numerical solutions, we consider the same problem with the same physical and numerical parameters as the one we considered before for a $R_m/R_0 = 10$ collapse, which was previously solved using the original all-Mach solver formulation. The results can be seen in Fig. 3.6, where we have enforced the region with low mass density and high speed of sound to disappear. Additionally, the result at late times is shown in Fig. 3.7, where one can observe that the numerical solution behaves well even close to and after the minimum radius, where the collapse is the most rapid. For example,

we can resolve the outgoing shock wave in the outside fluid that appears after reaching the minimum radius at around $t = 9.435R_0\sqrt{\rho_\infty/p_\infty}$.

In our simulations with the uniform bubble approximation, we also noticed that the initial stage of the collapse is indistinguishable from the incompressible collapse. Because of this, we introduce an additional approximation, where we start the bubble from a smaller radius, in our calculations $R = R_m/5$. Then, the previously discussed initial conditions, corresponding to the cavity starting at the maximum radius and from rest, are modified.

For the cavity's wall, we take $R(t = 0) = R_m/5$ and $\dot{R}(t = 0)$ from Eq. (3.45), evaluated at $R(t = 0)$, where the approximation that the pressure in the gas is negligible compared to p_∞ is justified for strong collapses under consideration by Eq. (3.36). Using the uniform bubble approximation, the initial values for the uniform mass density and pressure profiles are given by Eqs. (3.34) and (3.36), while the velocity profile is given by the low Mach solution in Eq. (3.46). As the motion of the outside fluid is still incompressible, the velocity and pressure profiles are given by the incompressible solutions in Eqs. (3.31) and (3.32), while the mass density profile is obtained by inverting the initial profile of pressure using the equation of state given in Eq. (3.3).

Using the two introduced approximations: uniform gas in the bubble and starting the calculation from $R = R_m/5$, we could obtain results for strong collapses, where $R_m/R_0 = 20$, as shown in Figs. 3.2 and 3.3. For the case of water shown in Fig. 3.2, the numerical parameters are $\lambda = 4$, $\Delta r = R_0/2^{14} = R_0/16384$, and $\Delta t_{\max} = (1/64) \times 10^{-6} R_0\sqrt{\rho_\infty/p_\infty}$. For the case of liquid lithium shown in Fig. 3.3, the numerical parameters are $\lambda = 8$, $\Delta r = R_0/2^{13} = R_0/8192$, and $\Delta t_{\max} = (1/64)\times 10^{-6} R_0\sqrt{\rho_\infty/p_\infty}$. To produce the asymptotic power-law solutions shown in Figs. 3.2 and 3.3, we used the form given in Eq. (3.1). For a given $n(\gamma)$ value, the constants A and t_c were computed using two points $R(t_1) = 2R_{\min}$ and $R(t_2) = 4R_{\min}$ from the obtained numerical result, where $R_{\min}$ is the smallest radius value in $R(t)$.

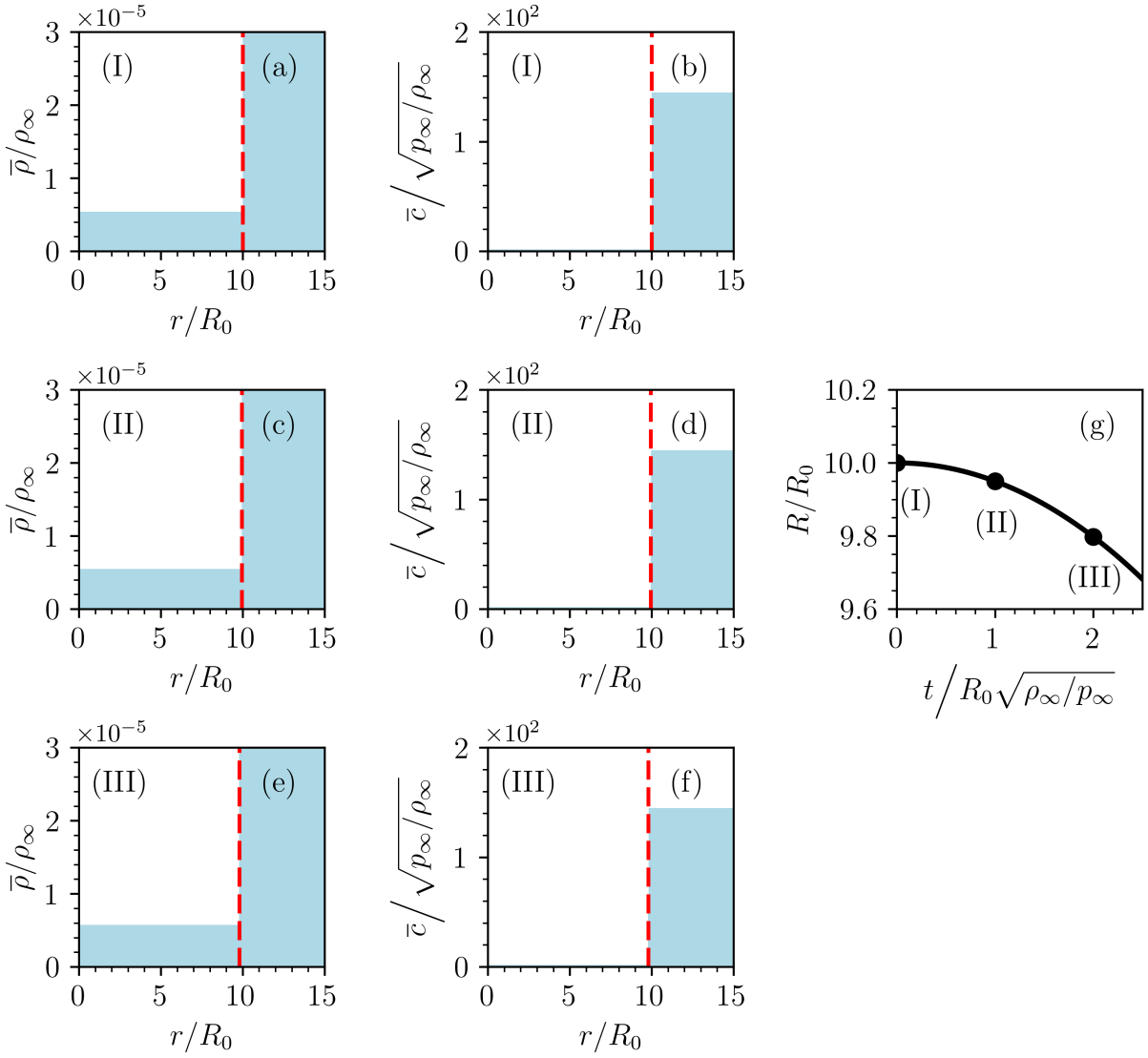

Figure 3.6: Implosion of an ideal gas xenon bubble in compressible water with ambient pressure $p_\infty = 1$ atm and ambient temperature $T_\infty = 293$ K, with $R_m/R_0 = 10$ and $R_0 = 2.2$ µm. The solution is obtained using the uniform bubble approximation and starts from the maximum radius R_m, where the cavity is at rest. The numerical parameters are $\lambda = 4$, $\Delta r = R_m/512$, and $\Delta t_{\max} = (1/4) \times 10^{-5} R_0 \sqrt{\rho_\infty/p_\infty}$. The figure shows the solution at three times $t = 0.0, 1.0, 2.0$, in units of $R_0\sqrt{\rho_\infty/p_\infty}$, corresponding to (I), (II), (III), respectively. Figures (a), (c), (e) show profiles of the average mass density, $\overline{\rho}$, while (b), (d), (f) show the average speed of sound, $\overline{c}$. In (a)-(f), the red dashed line denotes the location of the cavity's wall at a given time. In (g), $R(t)$ is shown.

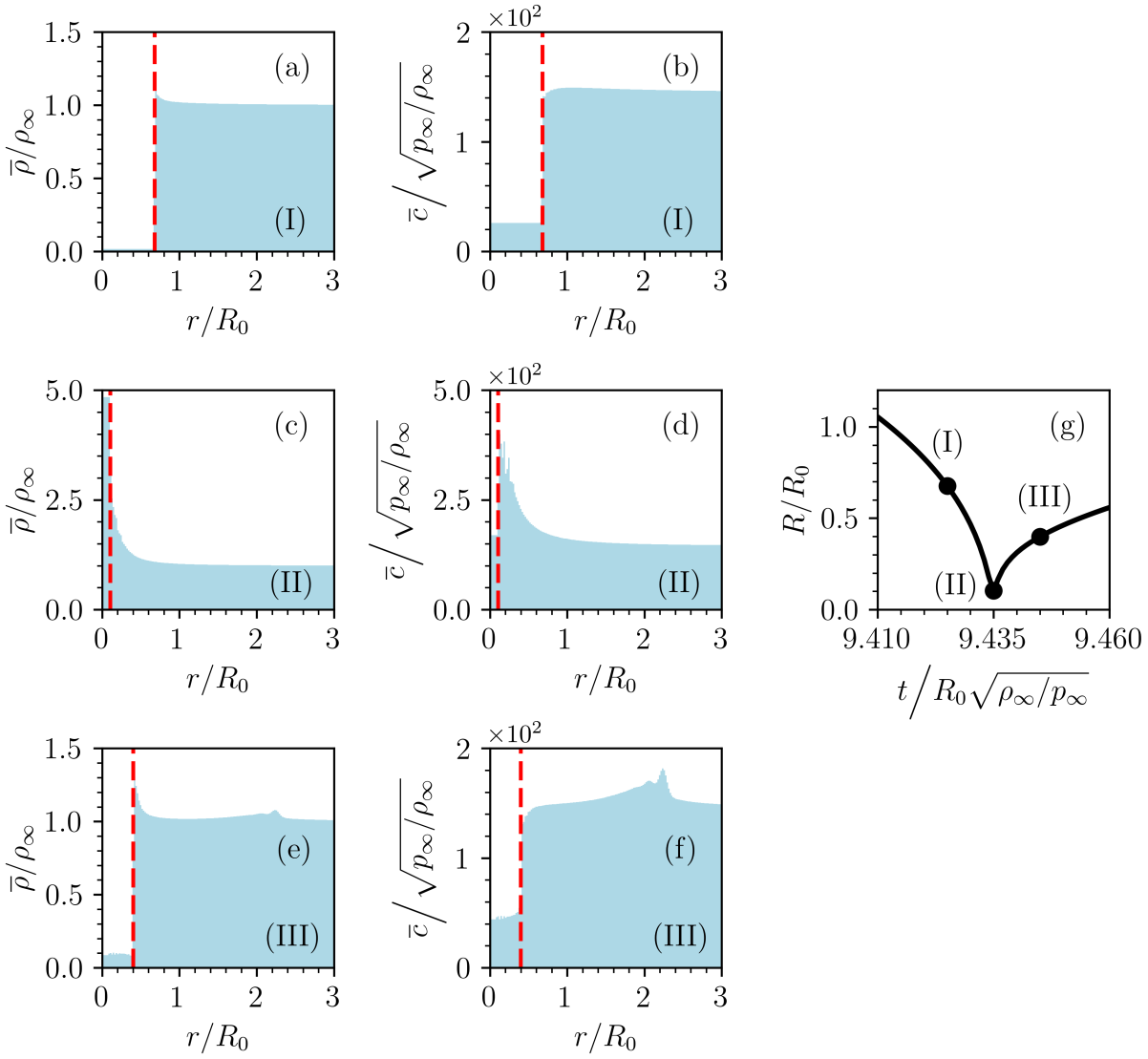

Figure 3.7: Implosion of an ideal gas xenon bubble in compressible water with ambient pressure $p_\infty = 1$ atm and ambient temperature $T_\infty = 293$ K, with $R_m/R_0 = 10$ and $R_0 = 2.2$ µm. The solution is obtained using the uniform bubble approximation and starts from the maximum radius R_m, where the cavity is at rest. The numerical parameters are $\lambda = 4$, $\Delta r = R_m/512$, and $\Delta t_{\max} = (1/4) \times 10^{-5} R_0 \sqrt{\rho_\infty/p_\infty}$. The figure shows the solution at three times $t = 9.425, 9.435, 9.445$, in units of $R_0\sqrt{\rho_\infty/p_\infty}$, corresponding to (I), (II), (III), respectively. Figures (a), (c), (e) show profiles of the average mass density, $\overline{\rho}$, while (b), (d), (f) show the average speed of sound, $\overline{c}$. In (a)-(f), the red dashed line denotes the location of the cavity's wall at a given time. In (g), $R(t)$ is shown.

3.4 Conclusion

Our key interest in cavity collapse is driven by the singular manner in which it leads to a spontaneous concentration of the energy density. The limitation of the extent to which energy can be focused and especially the role of the compressibility of the fluid in controlling this phenomenon is of particular interest. To isolate the issue of compressibility, we ignore the effects of viscosity, surface tension, and mass transfer, which can be added later. A standout feature of fluid compressibility is that for adiabatic equations of state, the collapse approaches a finite-time singularity with an exponent that depends on the parameters in this equation of state. Capturing this exponent using a computer simulation of fluid motion is a key measure of whether one has a physically relevant theory of a strong collapse. This problem has been specifically formulated and developed here.

First, we use the self-similar solution developed by Hunter to analyze water, and extend the analytic results for the asymptotic behavior of an empty cavity collapse to a wide range of compressible fluids described by the Tait-Murnaghan equation of state. Using the proposed fit of our numerical data, one can readily apply our results for practical applications. From the obtained quantitative results, we see that in the late stages of collapse, collapse is faster if γ is larger. Therefore, selecting materials with high γ will facilitate achieving higher levels of energy density focusing in a bubble. However, this result is true only in the asymptotic regime, so the next goal was to understand whether such a regime can be reached for the parameters found in experiments. Regardless of whether such a regime can be reached experimentally, these results can also be used to check two-fluid numerical solvers that use compressible Euler hydrodynamic equations by comparing the full solutions to the asymptotic empty cavity result.

The approach to simulate the transition to the compressible asymptote is based on an extension of the all-Mach solver available in the literature. Resolving the asymptotic exponent requires a strong collapse, which we have found is beyond the resolution of various papers on cavity collapse. Indeed, inserting initial conditions that are sufficiently violent to reach the asymptotic regime leads to strong anomalies in the simulation. For instance, a

bubble starting out at the maximum radius after a very short time experiences an extremely large speed of sound in the gas within the cavity, and an unphysical vacuum appears near the boundary of the bubble wall - even though the wall is moving inward. To overcome this issue, we have imposed the uniform bubble approximation, where at each step in the calculation the gas in the interior of the cavity has spatially uniform pressure and mass density profiles, consistent with the ideal gas equation of state. In the future, one can alternatively improve the solver by moving from a fixed grid to a grid with adaptive grid size, which might allow for faster calculations and obtain a resolution that would avoid the mentioned issue and accurately solve the full Euler equations for the gas in the cavity. Additionally, one can consider higher-order terms for the low Mach number expansion of the motion of the gas, which would allow for the inclusion of effects of nonuniformities that should be important near the minimum radius.

Within our uniform bubble approximation, we have been able to compare the collapse of a bubble surrounded by an incompressible fluid, a bubble in compressible water, and a bubble in compressible liquid lithium. In each case, a strong collapse reaches the asymptotic regime. The results for the radius and velocity of the cavity's wall, as approaching the most singular regions of motion, have been simulated at increasing levels of resolution and found to converge to the analytically predicted asymptotes. These simulations also enabled the calculation of the strong outgoing pulses that are launched by the implosion. The results give us confidence that the effects of fluid compressibility have been captured and that the method can be used to search for an optimal fluid in which bubble collapse would be the most rapid. Our results can now also be coupled with a molecular dynamics simulation where the peak internal temperature of the gas can be predicted.

Bibliography

[1] L. D. Landau and E. M. Lifshitz, *Fluid Mechanics: Volume 6 (Course of Theoretical Physics)*, 2nd ed. (Butterworth-Heinemann, 1987).

[2] G. K. Batchelor, *An Introduction to Fluid Dynamics* (Cambridge Univ. Press, Cambridge, 2000).

[3] L. D. Landau and E. M. Lifshitz, *Theory of Elasticity: Volume 7 (Course of Theoretical Physics)*, 3rd ed. (Butterworth-Heinemann, 1986).

[4] F. F. Chen, *Introduction to Plasma Physics and Controlled Fusion*, 3rd ed. (Springer, 2015).

[5] J. P. Mithen, J. Daligault, and G. Gregori, "Extent of validity of the hydrodynamic description of ions in dense plasmas," Phys. Rev. E **83**, 015401 (2011).

[6] B. P. Barber, R. A. Hiller, R. Löfstedt, S. J. Putterman, and K. R. Weninger, "Defining the unknowns of sonoluminescence," Phys. Rep. **281**, 65–143 (1997).

[7] A. Bass, S. J. Ruuth, C. Camara, B. Merriman, and S. Putterman, "Molecular Dynamics of Extreme Mass Segregation in a Rapidly Collapsing Bubble," Phys. Rev. Lett. **101**, 234301 (2008a).

[8] S. J. Ruuth, S. Putterman, and B. Merriman, "Molecular dynamics simulation of the response of a gas to a spherical piston: Implications for sonoluminescence," Phys. Rev. E **66**, 036310 (2002).

[9] A. Bass, S. Putterman, B. Merriman, and S. J. Ruuth, "Symmetry reduction for molecular dynamics simulation of an imploding gas bubble," J. Comput. Phys. **227**, 2118–2129 (2008b).

[10] D. Schanz, B. Metten, T. Kurz, and W. Lauterborn, "Molecular dynamics simulations of cavitation bubble collapse and sonoluminescence," New J. Phys. **14**, 113019 (2012).

[11] L. D. Landau and E. M. Lifshitz, *Mechanics: Volume 1 (Course of Theoretical Physics)*, 3rd ed. (Butterworth-Heinemann, 1976).

[12] L. D. Landau and E. M. Lifshitz, *The Classical Theory of Fields: Volume 2 (Course of Theoretical Physics)*, 4th ed. (Butterworth-Heinemann, 1980).

[13] H. DeWitt and Y. Rosenfeld, "Derivation of the one component plasma fluid equation of state in strong coupling," Phys. Lett. A **75**, 79–80 (1979).

[14] H. M. van Horn, "Crystallization of White Dwarfs," Astrophys. J. **151**, 227 (1968).

[15] H. M. van Horn, "The crystallization of white dwarf stars," Nat. Astron. **3**, 129–130 (2019).

[16] F. Demmel, S. Hosokawa, W.-C. Pilgrim, and S. Tsutsui, "Evidences for optic modes in molten NaI," Nucl. Instrum. Methods Phys. Res. B **238**, 98–101 (2005).

[17] F. Demmel, S. Hosokawa, and W.-C. Pilgrim, "Collective particle dynamics of molten NaCl by inelastic x-ray scattering," J. Phys. Condens. Matter **33**, 375103 (2021).

[18] J. P. Hansen and I. R. McDonald, "Statistical mechanics of dense ionized matter. IV. Density and charge fluctuations in a simple molten salt," Phys. Rev. A **11**, 2111–2123 (1975).

[19] A. Bataller, A. Latshaw, J. P. Koulakis, and S. Putterman, "Dynamics of strongly coupled two-component plasma via ultrafast spectroscopy," Opt. Lett. **44**, 5832–5835 (2019).

[20] T. Killian, T. Pattard, T. Pohl, and J. Rost, "Ultracold neutral plasmas," Phys. Rep. **449**, 77–130 (2007).

[21] J. M. Maxson, I. V. Bazarov, W. Wan, H. A. Padmore, and C. E. Coleman-Smith, "Fundamental photoemission brightness limit from disorder induced heating," New J. Phys. **15**, 103024 (2013).

[22] G. E. Morfill and A. V. Ivlev, "Complex plasmas: An interdisciplinary research field," Rev. Mod. Phys. **81**, 1353–1404 (2009).

[23] S. G. Brush, H. L. Sahlin, and E. Teller, "Monte Carlo Study of a One-Component Plasma. I," J. Chem. Phys. **45**, 2102–2118 (1966).

[24] J. P. Hansen, "Statistical Mechanics of Dense Ionized Matter. I. Equilibrium Properties of the Classical One-Component Plasma," Phys. Rev. A **8**, 3096–3109 (1973).

[25] N. Desbiens, P. Arnault, and J. Clérouin, "Parametrization of pair correlation function and static structure factor of the one component plasma across coupling regimes," Phys. Plasmas **23**, 092120 (2016).

[26] H. E. DeWitt, "Statistical mechanics of dense plasmas: numerical simulation and theory," J. Phys. Colloq. **39**, C1–173–C1–180 (1978).

[27] S. A. Khrapak and A. G. Khrapak, "Simple thermodynamics of strongly coupled one-component-plasma in two and three dimensions," Phys. Plasmas **21**, 104505 (2014).

[28] S. Hamaguchi, R. T. Farouki, and D. H. E. Dubin, "Phase diagram of Yukawa systems near the one-component-plasma limit revisited," J. Chem. Phys. **105**, 7641–7647 (1996).

[29] J. P. Hansen, I. R. McDonald, and E. L. Pollock, "Statistical mechanics of dense ionized matter. III. Dynamical properties of the classical one-component plasma," Phys. Rev. A **11**, 1025–1039 (1975).

[30] I. Korolov, G. J. Kalman, L. Silvestri, and Z. Donkó, "The Dynamical Structure Function of the One-Component Plasma Revisited," Contrib. Plasma Phys. **55**, 421–427 (2015).

[31] J. P. Mithen, J. Daligault, and G. Gregori, "Onset of negative dispersion in the one-component plasma," AIP Conf. Proc. **1421**, 68–72 (2012).

[32] S. A. Khrapak, A. G. Khrapak, N. P. Kryuchkov, and S. O. Yurchenko, "Onset of transverse (shear) waves in strongly-coupled Yukawa fluids," J. Chem. Phys. **150**, 104503 (2019).

[33] J. P. Hansen, "Plasmon dispersion of the strongly coupled one component plasma in two and three dimensions," J. Phys. Lett. **42**, 397–400 (1981).

[34] G. Kalman and K. I. Golden, "Response function and plasmon dispersion for strongly coupled Coulomb liquids," Phys. Rev. A **41**, 5516–5527 (1990).

[35] K. I. Golden and G. J. Kalman, "Quasilocalized charge approximation in strongly coupled plasma physics," Phys. Plasmas **7**, 14–32 (2000).

[36] S. A. Khrapak, B. Klumov, L. Couëdel, and H. M. Thomas, "On the long-waves dispersion in Yukawa systems," Phys. Plasmas **23**, 023702 (2016).

[37] S. A. Khrapak, "Onset of negative dispersion in one-component-plasma revisited," Phys. Plasmas **23**, 104506 (2016).

[38] S. Khrapak and L. Couëdel, "Dispersion relations of Yukawa fluids at weak and moderate coupling," Phys. Rev. E **102**, 033207 (2020).

[39] M. S. Murillo, "Ultrafast Dynamics of Strongly Coupled Plasmas," Phys. Rev. Lett. **96**, 165001 (2006).

[40] M. D. Acciarri, C. Moore, and S. D. Baalrud, "Strong Coulomb coupling influences ion and neutral temperatures in atmospheric pressure plasmas," Plasma Sources Sci. Technol. **31**, 125005 (2022).

[41] M. S. Murillo, "Static local field correction description of acoustic waves in strongly coupling dusty plasmas," Phys. Plasmas **5**, 3116–3121 (1998).

[42] P. K. Kaw and A. Sen, "Low frequency modes in strongly coupled dusty plasmas," Phys. Plasmas **5**, 3552–3559 (1998).

[43] A. Diaw and M. S. Murillo, "Generalized hydrodynamics model for strongly coupled plasmas," Phys. Rev. E **92**, 013107 (2015).

[44] D. Jou, C. Pérez-García, L. S. García-Colín, M. López de Haro, and R. F. Rodríguez, "Generalized hydrodynamics and extended irreversible thermodynamics," Phys. Rev. A **31**, 2502–2508 (1985).

[45] J. W. Herivel, "The derivation of the equations of motion of an ideal fluid by Hamilton's principle," Math. Proc. Camb. Philos. Soc. **51**, 344–349 (1955).

[46] R. L. Seliger and G. B. Whitham, "Variational principles in continuum mechanics," Proc. R. Soc. A **305**, 1–25 (1968).

[47] C. C. Lin, in *Liquid helium: Proceedings of the international school of physics "Enrico Fermi"*, Course XXI (Academic Press, 1963) pp. 93–146.

[48] S. Putterman, "Comments on the variational principle and superfluid mechanics," Phys. Lett. A **89**, 146–148 (1982).

[49] H. Goldstein, C. Poole, and J. Safko, *Classical Mechanics*, 3rd ed. (Pearson, 2001).

[50] V. B. Berestetskii, E. M. Lifshitz, and L. P. Pitaevskii, *Quantum Electrodynamics: Volume 4 (Course of Theoretical Physics)*, 2nd ed. (Pergamon, 1982).

[51] L. D. Landau and E. M. Lifshitz, *Statistical Physics: Volume 5 (Course of Theoretical Physics)*, 3rd ed. (Butterworth-Heinemann, 1980).

[52] I. Fairushin, S. Khrapak, and A. Mokshin, "Direct evaluation of the physical characteristics of Yukawa fluids based on a simple approximation for the radial distribution function," Results Phys. **19**, 103359 (2020).

[53] A. J. Chorin and J. E. Marsden, *A Mathematical Introduction to Fluid Mechanics*, 3rd ed. (Springer, 1993).

[54] C. P. Frahm, "Some novel delta-function identities," Am. J. Phys. **51**, 826–829 (1983).

[55] J. R. Blake and D. C. Gibson, "Cavitation Bubbles Near Boundaries," Annu. Rev. Fluid Mech. **19**, 99–123 (1987).

[56] P. Kumar and R. Saini, "Study of cavitation in hydro turbines—A review," Renew. Sustain. Energy Rev. **14**, 374–383 (2010).

[57] A. J. Walton and G. T. Reynolds, "Sonoluminescence," Adv. Phys. **33**, 595–660 (1984).

[58] L. Rayleigh, "On the pressure developed in a liquid during the collapse of a spherical cavity," Philos. Mag. **34**, 94–98 (1917).

[59] B. P. Barber and S. J. Putterman, "Observation of synchronous picosecond sonoluminescence," Nature **352**, 318–320 (1991).

[60] R. H. Cole, *Underwater explosions* (Princeton Univ. Press, Princeton, 1948).

[61] C. Hunter, "On the collapse of an empty cavity in water," J. Fluid Mech. **8**, 241–263 (1960).

[62] M. Tanaka, G. Girard, R. Davis, A. Peuto, and N. Bignell, "Recommended table for the density of water between 0 °C and 40 °C based on recent experimental reports," Metrologia **38**, 301 (2001).

[63] G. Vazquez, C. Camara, S. Putterman, and K. Weninger, "Sonoluminescence: nature's smallest blackbody," Opt. Lett. **26**, 575–577 (2001).

[64] M. C. Ramsey and R. W. Pitz, "Energetic Cavitation Collapse Generates 3.2 Mbar Plasma with a 1.4 J Driver," Phys. Rev. Lett. **110**, 154301 (2013).

[65] R. Garcia and F. G. Hammitt, "Cavitation Damage and Correlations With Material and Fluid Properties," J. Basic Eng. **89**, 753–763 (1967).

[66] Y. Toriyabe, E. Yoshida, J. Kasagi, and M. Fukuhara, "Acceleration of the $d+d$ reaction in metal lithium acoustic cavitation with deuteron bombardment from 30 to 70 keV," Phys. Rev. C **85**, 054620 (2012).

[67] K. V. Khishchenko, "Equation of state for lithium in shock waves," Math. Montis. **41**, 91–98 (2018).

[68] H. W. Davison, "Compilation of thermophysical properties of liquid lithium," (1968).

[69] C. C. Wu and P. H. Roberts, "Shock-wave propagation in a sonoluminescing gas bubble," Phys. Rev. Lett. **70**, 3424–3427 (1993).

[70] D. Fuster, C. Dopazo, and G. Hauke, "Liquid compressibility effects during the collapse of a single cavitating bubble," J. Acoust. Soc. Am. **129**, 122–131 (2011).

[71] D. Fuster and S. Popinet, "An all-Mach method for the simulation of bubble dynamics problems in the presence of surface tension," J. Comput. Phys. **374**, 752–768 (2018).

[72] Y. Saade, D. Lohse, and D. Fuster, "A multigrid solver for the coupled pressure-temperature equations in an all-Mach solver with VoF," J. Comput. Phys. **476**, 111865 (2023).

[73] S. Popinet, "A quadtree-adaptive multigrid solver for the Serre–Green–Naghdi equations," J. Comput. Phys. **302**, 336–358 (2015).

[74] R. Klein, "Semi-Implicit Extension of a Godunov-Type Scheme Based on Low Mach Number Asymptotics I: One-Dimensional Flow," J. Comput. Phys. **121**, 213–237 (1995).

[75] S. Noelle, G. Bispen, K. R. Arun, M. Lukáčová-Medvi̇dová, and C.-D. Munz, "A Weakly Asymptotic Preserving Low Mach Number Scheme for the Euler Equations of Gas Dynamics," SIAM J. Sci. Comput. **36**, B989–B1024 (2014).